Development of Non-Hallucinogenic Psychoplastogens

By

LEE DUNLAP

DISSERTATION

Submitted in partial satisfaction of the requirements for the degree of

DOCTOR OF PHILOSOPHY

in

Chemistry

in the

OFFICE OF GRADUATE STUDIES

of the

UNIVERSITY OF CALIFORNIA

DAVIS

Approved:

David E. Olson, Chair

Dean J. Tantillo

Michael A. Rogawski

Committee in Charge

2022

Abstract

The ability of psychedelics to treat a myriad of brain disorders has made them appealing drug targets. Many of the psychedelics known belong to a class of compounds we have deemed psychoplastogens, compounds capable of rapidly promoting structural and functional neuroplasticity. Despite the beneficial properties psychedelics hold for treating neuropsychiatric disorders, they are far from ideal drug candidates. The ability to produce hallucinations not only poses hazards to the user but also limits the use of these drugs to controlled clinical settings, hindering their widespread application. By leveraging medicinal chemistry, I was able to determine key aspects of the psychedelic scaffold that give rise to their hallucinogenic and psychoplastogenic effects. Using this knowledge, we were able to design next-generation therapeutics, based on psychedelics, that lack the hallucinogenic effects.

Acknowledgments

First, I would like to thank my friends and family for all of their support during this journey. I would not have made it this far without you all. Daniel, your guidance and support really made this possible. I don't know if I would have believed in myself if you had not been there to show me this was possible and show me the way. Mom and Dad, thanks for never giving up on me. I know I made a lot of mistakes and squandered many opportunities, but I think in the end this has all worked out the way it was supposed to and that wouldn't have happened without your help.

Josh, none of this would have been possible without you. Its crazy looking back at how far we've come in the past 10 years. Without you, Steve, Chris, Larry, Sam, and Amber I'd still be squandering my life away at Café 4. To the night shift and Davis group, you all know what you did, and I am grateful every day for your help keeping me who I am. GI and Calvin, you all have been like a second family. You were there for the good times, but you also helped me through one of the hardest times of my life and I will always remember that. Arya, my man, mentoring you was definitely a highlight of my time here at Davis. I hope you learned some useful stuff for your future but either way we got to have a lot of fun and do some cool chemistry.

To the Olson Lab, you all are the best lab mates anyone could ask for. All of the work that went into my Ph.D. was only possible with your help. RJ you always kept me going with the late night phish jams, Paige side rage side, and your sense of morality has always served as example for all of us. Winston and Favela, you all are genuinely some of the best people I know and were always there to help, no matter the ask. Calvin I owe all of my cell culture success to your awesome mentorship. Lindsay, thanks for always being my go-to for neuroscience questions and for all the shenanigans. Max, you are one of the best people in lab to collaborate with. You also have the best work life balance of anyone in lab and consistently nail all of your experiments. Lastly, I want to thank David Olson. David, you took a chance on a first-year student with a less than impressive transcript and I will never forget that. Your enthusiasm and guidance over the years has inspired me to work hard and make the most out of this opportunity. You have done so much, not just for me, but the entire lab. You have worked hard to make this lab a place we will be proud to graduate from and you've made it fun while also pushing us to do our best work. Thanks for everything.

In Loving Memory:

Chris Wharton, Larry Ward, Eric Kudlow, Will Minnich,

Ray Kennedy, Daniel Geros, Tyler Cameron,

and all the others we have lost along the way.

Contents

Chapter 1. Understanding the Hallucinogenic and Therapeutic Potential of LSD

Chapter 1.1 Introduction

The psychedelic lysergic acid diethylamide (LSD) is arguably the most famous hallucinogen, often being referenced in the media and cinema. It was originally discovered in 1938 by the Swiss chemist, Albert Hofmann. However, its psychoactive properties weren't discovered until 1943 when Hofmann accidentally ingested LSD. Since then, there has been a growing body of evidence to support the idea that psychedelics have potential benefits for treating neuropsychiatric disorders. This chapter will focus on some of the work towards elucidating both the therapeutic and hallucinogenic mechanisms of psychedelics using LSD.

Chapter 1.2 Structure-Activity Relationship Studies

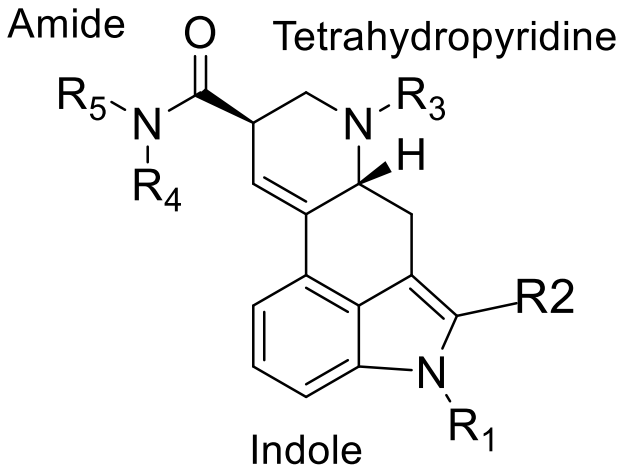

Figure 1.1. Structure of LSD depicting areas that have been subjected to SAR studies.

One of the biggest complications to the structure-activity relationship (SAR) studies of LSD is the lack of an efficient total synthesis. A comprehensive review has already been written on efforts toward the total synthesis of lysergic acid.[1] Importantly, most of the syntheses to date start from an appropriately

[1]Tasker, N.R.; Wipf, P. Biosynthesis, total synthesis, and biological profiles of Ergot alkaloids. *Alkaloids Chem Biol.* **2021**, 85, 1-112.

modified indole. This has made modifications to the benzene ring of the indole moiety difficult. As a result, the majority of SAR studies of LSD have focused on modifications to the amide group, the indole nitrogen, and the tetrahydropyridine **(FIG 1.1)**. Substitution to the indole ring of tryptamine drastically alters the pharmacology of psychedelic tryptamines as well as impacts their hallucinogenic and therapeutic effects.[2,3,4,5] This suggests a need for a facile synthesis of LSD that will enable SAR of the indole moiety.

Early syntheses of LSD were performed starting from lysergic acid which was obtained by hydrolysis of ergotamine.[6] As a result, modifications to the amide functional group were some of the easiest changes to make. The diethylamide is a highly conserved moiety as modifications drastically reduce hallucinogenic effects and serotonin receptor activity.[7,8] Conversion of the diethylamide to dimethyl, morpholine, pyrrolidine, or monoethyl resulted in a 10 fold reduction in hallucinogenic efficacy.[7] Nichols et. al. synthesized a series of LSD analogs with conformationally restrained, chiral azetidines.[9] They found that of the three azetidines synthesized, only the S,S azetidine produced effects comparable to LSD in drug discrimination studies and beta-arrestin recruitment.[10] In another study, Nichols et. al. tested a series of non-restrained, chiral alkyl groups. While all the alkyl amides tested displayed a nanomolar affinity for 5-HT2ARs, the *R*-enantiomers were 17-fold more potent than their *S*-enantiomers in phosphoinositide hydrolysis and 4x as potent in drug discrimination studies in rats.[11,12] This work provided evidence that the

---

[2] Blair, J. B.; Kurrasch-Orbaugh, D.; Marona-Lewicka, D.; Cumbay, M. G.; Watts, V. J.; Barker, E. L.; Nichols, D. E. Effect of ring fluorination on the pharmacology of hallucinogenic tryptamines. *J. Med. Chem*. **2000**, 43, 4701-4710.

[3] Glennon, R. A.; Young, R. l.; Jacyno, J. M.; Slusher, M.; Rosecrans, J. A. DOM-Stimulus Generalization to LSD and other Hallucinogenic Indolealkylamines. *Eur. J. Pharmacol.* **1983**, 86, 453– 459.

[4] Dunlap, L. E., Azinfar, A., Ly, C., Cameron, L. P., Viswanathan, J., Tombari, R. J., Myers-Turnbull, D., Taylor, J. C., Grodzki, A.C., Lein, P. J., Kokel, D.; Olson, D. E. Identification of Psychoplastogenic N,N-Dimethylaminoisotryptamine (isoDMT) Analogues through Structure-Activity Relationship Studies*. J. Med. Chem.* **2020**, 63, 1142–1155.

[5] Dong, C.; Ly, C.; Dunlap, L. E.; Vargas, M. V.; Sun, J.; Hwang, I.-W.; Azinfar, A.; Oh, W. C.; Wetsel, W. C.; Olson, D. E.; Tian, L. Psychedelic-Inspired Drug Discovery Using an Engineered Biosensor. *Cell* **2021**, 184, 2779– 2792.

[6] Nichols, D. E. Dark Classics in Chemical Neuroscience: Lysergic Acid Diethylamide (LSD). *ACS Chem. Neurosci*. **2018**, 9, 2331-2343.

[7] Isbell, H.; Miner, E. J.; Logan, C. R.; Relationships of psychotomimetic to anti-serotonin potencies of congeners of lysergic acid diethylamide (LSD-25). *Psychopharmacologia.* **1959,** 1, 20-8. N

[8] Cerletti, A.; Doepfner, W. J Comparative study on the serotonin antagonism of amide derivatives of lysergic acid and of ergot alkaloids. *Pharmacol. Exp. Ther.* **1958**, 122, 124-136.

[9] Nichols, D. E.; Frescas, S.; Marona-Lewicka, D.; Kurrasch-Orbaugh, D. M. . Lysergamides of isomeric 2,4-dimethylazetidines map the binding orientation of the diethylamide moiety in the potent hallucinogenic agent *N,N*-diethyllysergamide (LSD). *J. Med. Chem.* **2002**, 45, 4344-4349.

[10] Wacker, D.; Wang. S.; McCorvy, J. D.; Betz, R. M.; Venkatakrishnan, A. J.; Levit, A.; Lansu, K.; Schools, Z. L.; Che, T.; Nichols, D. E.; Shoichet, B. K.; Dror, R. O.; Roth, B. L. Crystal Structure of an LSD-Bound Human Serotonin Receptor. *Cell* **2017,** 168, 377-389.

[11] Nichols, D. E. Structure-activity relationships of serotonin 5-HT2A agonists. *Wiley Interdiscip. Rev. Membr. Transp. Signal*. **2012**, 1, 559-579.

[12] Oberlender, R.; Pfaff, R. C.; Johnson, M. P.; Huang, X. M.; Nichols, D. E. Stereoselective LSD-like activity in d-lysergic acid amides of (R)- and (S)-2-aminobutane. *J. Med. Chem*. **1992** ,35, 203-211.

confirmation of the alkylamine plays a critical role in the biological activity of LSD. It was later discovered that upon binding to 5-HT2Rs, LSD forms strong interactions with the extracellular loop 2 which forms a "lid" on the binding pocket.[10]

Conversion of the methyl group on the tetrahydropyridine to a propyl group was equipotent to LSD. Conversion of the methyl group to a benzyl group or removal of the methyl group to yield nor-lysergic acid produced no generalization to LSD in drug discrimination studies. However, the ethyl (ETH-LAD) and allyl (AL-LAD) substituted tetrahydropyridines were found to be 2-3x more potent than LSD in drug discrimination studies.[13] This was in agreement with human studies showing that ETH-LAD was slightly more potent than LSD.[14,15]

Other notable modifications to the LSD scaffold include halogenation of the indole moiety at the C-2 position. 2-Bromo-LSD, BOL-148, has nanomolar affinity at 5-HT2A and 5-HT2C and acts as an antagonist.[16,17,18] BOL-148 is generally believed to be non-hallucinogenic, however there have been case reports of BOL-148 causing psychoactive effects in humans.[19] In other studies, it was found that pretreatment with BOL-148 blocked the hallucinogenic effects of LSD in humans.[20] 2-[I^{125}]-LSD, a 5-HT2AR antagonist, has been used to label 5-HT2 receptors.[21,22]

Acylation of the indole nitrogen has also been examined. Acetyl (ALD-52), propanoyl (1P-LSD), and butanoyl (1B-LSD) groups on the indole nitrogen resulted in decreased affinity for 5-HT2Rs.[23] Brandt

---

[13] Hoffman, A. J.; Nichols, D. E. Synthesis and LSD-like discriminative stimulus properties in a series of N(6)-alkyl norlysergic acid N,N-diethylamide derivatives. *J. Med. Chem.* **1985** ,28, 1252-1255. s

[14] Shulgin, A. T.; Shulgin, A. Tihkal: The continuation. **1997**, Berkeley, CA: Transform Press.

[15] Halberstadt, A. L.; Chatha, M.; Klein, A. K.; Wallach, J.; Brandt, S. D. Correlation between the potency of hallucinogens in the mouse head-twitch response assay and their behavioral and subjective effects in other species *Neuropharmacology*. **2020** .167, 107933.

[16] Wainscott, D. B.; Lucaites, V. L.; Kursar, J. D.; Baez, M.; Nelson, D. L. Pharmacologic characterization of the human 5-hydroxytryptamine2B receptor: evidence for species differences. *J. Pharmacol. Exp. Ther*. **1996**, 276, 720-727.

[17] Abramson, H. A. Antiserotonin action of LSD-25 and other lysergic acid derivatives: fact and fiction. *Asthma Res*. **1964**, 1, 207-211.

[18] Sollero, L.; Page, I. H.; Salmoiraghi, G. C. Brom-lysergic acid diethylamide: a highly potent serotonin antagonist. *J Pharmacol Exp Ther*. **1956**, 117, 10-15.

[19] Richards, N.; Chapman, L. F.; Goodell, H.; Wolff, H. G. LSD-like delirium following ingestion of a small amount of its brom analog (BOL-148). *Annals of internal medicine*. **1958**, https://doi.org/10.7326/0003-4819-48-5-1078.

[20] Ginzel, K. H.; Mayer-Gross, W. Prevention of Psychological Effects of d-Lysergic Acid Diethylamide (LSD 25) by its 2-Brom Derivative (BOL 148). *Nature* **1956**, 178, 210.

[21] Nakada, M. T..; Wieczorek, C. M.; Rainboe, T. C. Localization and characterization by quantitative autoradiography of [125I]LSD binding sites in rat brain. *Neurosci. Lett*. **1984** ,49, 13-18.

[22] Engel, G.; Muller-Schweinitzer, E.; Palacios, J. M. 2-[125Iodo]LSD, a new ligand for the characterisation and localisation of 5-HT2 receptors. *Naunyn Schmiedebergs Arch Pharmacol*. **1984**, 325, 328-336.

[23] Halberstadt, A. L.; Chatha, M.; Klein, A. K.; McCorvy, J. D.; Meyer, M. R.; Wagmann, L.; Stratford, A.; Brandt, S. D. Pharmacological and biotransformation studies of 1-acyl-substituted derivatives of d-lysergic acid diethylamide (LSD). *Neuropharmacology* **2020** ,172, doi: 10.1016/j.neuropharm.2019.107856.

et. al found that acylation of the indole nitrogen also had effects on the activity of LSD at 5-HT2Rs.[23] While LSD has potent agonist activity, the acyl-LSD analogs displayed weak agonistic or antagonistic activity in Gq mediated calcium flux. While these studies demonstrate the importance of the indole nitrogen in the function of LSD at 5-HT2Rs, these acylLSDs would likely produce effects similar to LSD, in humans. In the head twitch response assay (HTR), ALD-52 produced a significant number of head twitches in mice, albeit to a lesser degree than LSD. This is likely due to the prodrug-like actions of ALD-52. The acyl group is readily hydrolyzed in vivo resulting in appreciable concentrations of LSD in the plasma of rats treated with ALD-52.[23]

Chapter 1.3 Pharmacology

The primary effects of LSD are mediated via the 5-HT2AR. However, LSD also has nanomolar affinity at other receptors, including dopamine receptors, D1 and D2.[24,25,9] The reported psychostimulant effects of LSD may be attributed to the amphetamine scaffold located in the core of the LSD scaffold **(FIG 1.2).** The psychoactive effects of LSD are separated into two distinct phases: an initial hallucinogenic phase that is 5HT2AR-mediated, coinciding with a second paranoia phase that is mediated by dopamine receptors.[26,27,28]

[24] Watts, V. J.; Lawler, C. P.; Fox, D. R.; Neve, K. A.; Nichols, D. E.; Mailman, R. B. LSD and structural analogs: pharmacological evaluation at D1 dopamine receptors. *Psychopharmacology (Berl)* **1995**, 118, 401-409.
[25] Giacomelli, S.; Palmery, M.; Romanlli, L.; Cheng, C. Y.; Silvestrini, B. Lysergic acid diethylamide (LSD) is a partial agonist of D2 dopaminergic receptors and it potentiates dopamine-mediated prolactin secretion in lactotrophs in vitro. *Life Sci.* **1998**, 63, 215-222.
[26] Marona-Lewicka, D.; Thisted, R. A.; Nichols, D. E. Distinct temporal phases in the behavioral pharmacology of LSD: dopamine D2 receptor-mediated effects in the rat and implications for psychosis. *Psychopharmacology (Berl*) **2005**,180, 427-435.
[27] Marona-Lewicka, D.; Nichols, D. E. Further evidence that the delayed temporal dopaminergic effects of LSD are mediated by a mechanism different than the first temporal phase of action. *Pharmacol Biochem Behav*. 2007, 87, 453-461.
[28] Marona-Lewicka, D.; Chemel, B. R.; Nichols, D. E. Dopamine D4 receptor involvement in the discriminative stimulus effects in rats of LSD, but not the phenethylamine hallucinogen DOI. *Psychopharmacology (Berl)* **2009**, 203, 265-277.

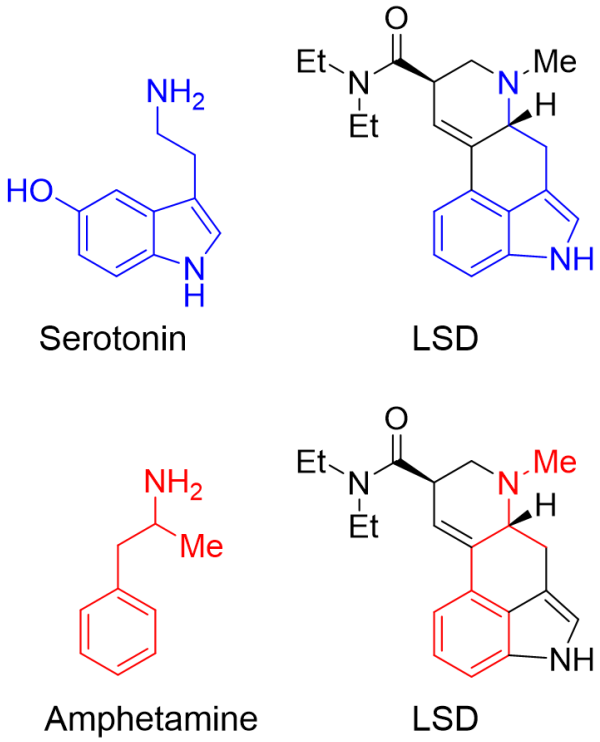

Figure 1.2. Structures of amphetamine and serotonin superimposed on the structure of LSD.

Even though the mechanism of LSD-induced hallucinations has not been fully established, activation of the 5HT2AR has been strongly correlated to hallucinations in animal and human studies.[29] Common measures of 5-HT2A receptor activation have not been able to distinguish hallucinogenic from non-hallucinogenic 5-HT2A ligands. LSD and the non-hallucinogenic analog, lisuride, have been shown to have similar potencies for PLA2 mediated arachidonic acid release and PLC mediated inositol phosphate accumulation **(FIG 1.3)**.[30] Lisuride exhibits minimal activity for β-arrestin2 recruitment whereas LSD potently recruits β-arrestin2.[31] There is mixed evidence however for β-arrestin2s involvement in the hallucinogenic effects of psychedelics. In β-arrestin2 knockout mice, several behavioral effects including the head twitch

[29] Vollenweider, F. X.; Vollenweider-Scherpenhuyzen, M. F; Bäbler A.; Vogel, H.; Hell, D. Psilocybin induces schizophrenia-like psychosis in humans via a serotonin-2 agonist action. *Neuroreport.* **1998**, 9, 3897-3902.
[30] Kurrasch-Orbaugh, D. M.; Watts, V. J.; Barker, E. L.; Nichols, D. E. Serotonin 5-hydroxytryptamine 2A receptor-coupled phospholipase C and phospholipase A2 signaling pathways have different receptor reserves. *J. Pharmacol Exp Ther.* **2003**, 304, 229-237.
[31] Cao, D.; Yu, J.; Wang, H.; Luo, Z.; Liu, X.; He, L.; Qi, J.; Fan, L.; Tang, L.; Chen, Z.; Li, J.;Cheng. J.; Wang. S. Structure-based discovery of nonhallucinogenic psychedelic analogs. *Science* **2022**, 375, 403-411.

response (HTR) induced by LSD and 5-hydroxytryptophan (5-HTP) were significantly reduced.[32,33] However, β-arrestin knockout had no effects on the DOI-elicited head twitch response.[32]

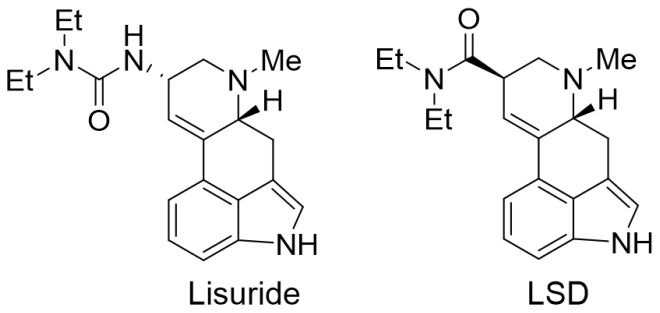

Figure 1.3. Structures of lisuride and LSD.

Another possible mechanism for the hallucinogenic effects of psychedelics is the activation of a metabotropic glutamate receptor (mGlu2R)/5-HT2AR heterodimer.[34] Glutamate is believed to play an important role in schizophrenia via excessive glutamatergic neurotransmission.[35] Since hallucinations are a key symptom of schizophrenia it was believed that mGluRs may play a role in the mechanism of hallucinogens. There have been several reports of using mGLu2/3 receptor agonists for treating the positive symptoms of schizophrenia.[36] In mice, the mGlu2/3 receptor agonists LY354740 and LY379268 blocked the head twitch response caused by DOI and 25CN-NBOH.[37,38] An effect that was also seen in mGlu2 knock-out mice.[39] In cortical neurons, both lisuride and LSD signal through 5-HT2ARs resulting in induction

[32] Backstrom, J. R.; Chang, M. S.; Chu, H.; Niswender, C. M.; Sanders-Bush, E. Agonist-Directed Signaling of Serotonin 5-HT2C Receptors: Differences Between Serotonin and Lysergic Acid Diethylamide (LSD) *Neuropsychopharmacology* **1999**, 21, 77–81.
[33] Rodriguiz, R. M.; Nadkarni, V.; Means, C. R.; Pogorelov, V. M.; Chiu, T. Y.; Roth, B. L.; Wetsel, W. C. LSD-stimulated behaviors in mice require β-arrestin 2 but not β-arrestin 1. *Sci Rep*. **2021**, 11, 176907.
[34] Gonzalez-Maeso, J.; Ang, R.; Yuen, T.; Chan, P.; Weisstaub, N. V.; Lopez-Gimenez, J. F.; Zhou, M.; Okawa, Y.; Callado, L. F.; Graeme, M.; Gingrich, J. A.; Filizola, M.; Meana, J.; Sealfon, S. C. Identification of a Novel Serotonin/Glutamate Receptor Complex Implicated in Psychosis. *Nature.* **2008**, 452, 93–97.
[35] Krivov, A.; Fischel, T.; Weizman, A. The possible involvement of metabotropic glutamate receptors in schizophrenia. *Eur Neuropsychopharmacol*. **2008**, 18, 395-405.
[36] Chaki, S.; Hikichi, H. Targeting of metabotropic glutamate receptors for the treatment of schizophrenia. *Curr Pharm Des*. **2011**, 17, 94-102.
[37] Halberstadt, A. L.; Van Der Zee, J. V. F.; Chatha, M.; Geyer, M. A.; Powell, S. B. Chronic treatment with a metabotropic mGlu2/3 receptor agonist diminishes behavioral response to a phenethylamine hallucinogen *Psychopharmacology (Berl).* **2019**, 236, 821-830.
[38] Klodzinska, A.; Bijak, M.; Tokarski, K.; Pilc, A. Group II mGlu receptor agonists inhibit behavioural and electrophysiological effects of DOI in mice. *Pharmacol Biochem Behav*. **2002**, 73, 327-332.
[39] Moreno, J. L.; Holloway, T.; Albizu, L.; Sealfron, S. C.; Gonzalez-Maeso, J. Metabotropic glutamate mGlu2 receptor is necessary for the pharmacological and behavioral effects induced by hallucinogenic 5-HT2A receptor agonists *Neurosci Lett.* **2011**, 493, 76-79.

of c-*fos* expression, however only LSD causes an increase in *egr-2* expression which is blocked by the mGLu2 agonist LY-379,268.[34] This suggests that hallucinogenic signaling requires activation of a mGLu2/5-HT2A heterodimer while non-hallucinogenic ligands may signal through 5-HT2ARs monomer.

In rhesus monkeys administered LSD, it was found that LSD localized in specific brain regions. The highest concentration of LSD were found in the pituitary and pineal glands.[40] However, it was later discovered that in rats, LSD was actually found primarily bound in the cortex and not bound in the pituitary.[41] This distribution of bound LSD is likely the cause of the broad therapeutic potential of psychedelics like LSD as the PFC plays a critical role in the top-down control of areas of the brain implicated in various neuropsychiatric disorders.[42,43]

Chapter 1.4 Therapeutic Potential

Compounds capable of promoting neuroplasticity in the PFC have received a lot of attention for their therapeutic potential. We have recently reported on a class of drugs called psychoplastogens, which are small molecules capable of rapidly promoting structural and functional neuroplasticity.[42] Many psychedelics, like LSD, are some of the most potent psychoplastogens known.[44,45,46] Psychoplastogens bind to the 5-HT2AR, causing a glutamate burst which activates α-amino-3-hydroxy-5-methyl-4-isoxazolepropionic acid (AMPA) receptors resulting in secretion of the brain-derived neurotrophic factor (BDNF).[47,48] In cultured cortical neurons, pretreatment with the 5-HT2R antagonist ketanserin blocked the

[40] Snyder, S. H.; Reivich, M. Regional Localization of Lysergic Acid Diethylamide in Monkey Brain. *Nature* **1996**, 209, 1093–1095.
[41] Diab, L. M.; Freedman, D. X.; Roth, L. J. [^{3}H]lysergic acid diethylamide: cellular autoradiographic localization in rat brain. *Science* **1971**, 173, 1022-1024.
[42] Olson, D. E. Psychoplastogens: A Promising Class of Plasticity-Promoting Neurotherapeutics. *J Exp Neurosci.* **2018**. doi: 10.1177/1179069518800508
[43] Vázquez-Borsetti, P.; Cortes, R.; Artigas, F. Pyramidal neurons in rat prefrontal cortex projecting to ventral tegmental area and dorsal raphe nucleus express 5-HT2A receptors. *Cereb Cortex* . **2009**, 19, 1678-1686.
[44] Ly, C.; Greb, A. C.; Cameron, L. P.; Wong, J. M.; Barragan, E. V.; Wilson, P. C.; Burbach, K. F.; Soltanzadeh Zarandi, S.; Sood, A.; Paddy, M. R.; Duim, W. C.; Dennis, M. Y.; McAllister, A. K.; Ori-McKenney, K. M.; Gray, J. A.; Olson, D. E. Psychedelics Promote Structural and Functional Neural Plasticity. *Cell Reports* **2018**, 23, 3170–3182.
[45] Ly, C.; Greb, C. A.; Vargas, M. V.; Duim, W. C.; Grodzki, A. C. G.; Lein, P. J.; Olson, D. E. Transient Stimulation with Psychoplastogens is Sufficient to Initiate Neuronal Growth. *ACS Pharmacol. Transl. Sci*., **2020**, 4, 452–460
[46] Aghalanian, G. K.; Marek, G. J. Serotonin and Hallucinogens. *Neuropsychopharmacology* **1999**, 21, 16–23.
[47] Olson, D. E. Biochemical Mechanisms Underlying Psychedelic-Induced Neuroplasticity. *Biochemistry* **2022**, 61, 127–136
[48] Jourdi, H.; Hsu, Y. T.; Zhou, M.; Qin, Q.; Bi, X.; Baudry, M. Positive AMPA Receptor Modulation Rapidly Stimulates BDNF Release and Increases Dendritic mRNA Translation. *J. Neurosci*. **2009**, 29, 8688−8697.

effects of LSD on dendritic arborization and increased spine density.[44] Further, pretreatment with the AMPA receptor antagonist, DNQX, was sufficient to block the effects of LSD on neuritogenesis in vitro.[45]

Endogenous growth factors, like the brain-derived neurotrophic factor (BDNF), play a prominent role in regulating plasticity in the brain via activation of tropomyosin receptor kinase B (TrkB).[49] TrkB receptor stimulation results in activation of the mammalian target of rapamycin which leads to the synthesis of proteins necessary for increased plasticity.[50] Pretreatment of embryonic cortical neurons with either the selective TrkB antagonist, ANA-12, or the mTOR antagonist, rapamycin, blocked the ability of LSD to promote neuritogenesis.[45]

In animal models, psychedelics have been shown to produce anti-depressive like behaviors.[51] LSD was found to promote anti-depressive like behaviors in the forced swim test.[52] The antidepressant-like responding of animals administered LSD was blocked using the 5-HT2R antagonist M100907.[31] In mice, psychedelics have been shown to prevent both cocaine and morphine self-administration, as well as decrease alcohol consumption.[53]

In humans, LSD has shown effects in treating heroin and alcohol addiction showing increased abstinence up to 12 months after receiving treatment.[54,55] In addition, LSD has shown positive outcomes in treating anxiety**,** measured using the State-Trait Anxiety Inventory (STAI) in patients with life-threatening diseases. These effects were persistent showing significant improvement 2 months after administration and trending toward positive improvements after one year.[56] Similar effects were seen in patients in measures

[49] Saeger, H. N.; Olson, D. E. Psychedelic-inspired approaches for treating neurodegenerative disorders. *J Neurochem*. **2021** Nov 24. doi: 10.1111/jnc.15544.
[50] Hoeffer, C. A.; Klann, E. MTOR signaling: at the crossroads of plasticity, memory and disease. *Trends Neurosci*. **2010**, 33, 67−75.
[51] Cameron, L. P.; Benson, C. J.; Dunlap, L. E.; Olson, D. E. Effects of *N,N*-dimethyltryptamine (DMT) on rat behaviors relevant to anxiety and depression. *ACS Chem. Neurosci*. **2018**, 9, 1582–1590.
[52] Hibicke, M.; Landry A. N.; Kramer, H. M.; Talman, Z. K.; Nichols, C. D. Psychedelics, but Not Ketamine, Produce Persistent Antidepressant-like Effects in a Rodent Experimental System for the Study of Depression. *ACS Chem. Neurosci.* **2020**, 11, 864–871.
[53] Glick, S. D. Maisonneuve, I. M.; Szumlinski, K. K. 18-Methoxycoronaridine (18-MC) and ibogaine: comparison of antiaddictive efficacy, toxicity, and mechanisms of action. *Ann N Y Acad Sci*. **2000**, 914, 369-386.
[54] Savage, C.; McCabe, O. L. Residential Psychedelic (LSD) Therapy for the Narcotic Addict. *Arch Gen Psychiatry* **1973**, 28, 808.
[55] Tomsovic. M.; Edwards, R. V. Lysergide treatment of schizophrenic and nonschizophrenic alcoholics: a controlled evaluation. *Q J Stud Alcohol* **1970**, 31, 932–939.
[56] Gasser, P.; Holstein, D.; Michel, Y.; Doblin, R.; Yazar-Klosinski, B.; Passie, T.; Brenneisen, R. Safety and efficacy of lysergic acid diethylamide-assisted psychotherapy for anxiety associated with life-threatening diseases. *J Nerv Mental Dis.* **2014,** 202, 513–520.

of depression and anxiety.[57] Acute effects of LSD impair working memory but this is likely due to the acute psychological and hallucinogenic effects of LSD, as microdoses of LSD in humans improved cognition.[58,59]

Chapter 1.5 Safety

Initially, it was reported that LSD causes chromosomal damage in humans. However, this was later disproven, and LSD is generally considered not to produce serious adverse effects.[6,60,61] While LSD may generally be regarded as safe, it is not without the potential for negative effects. LSD has a potent affinity for the 5-HT2B receptor, which has been shown to produce cardiac valvopathy.[62] In addition, other psychedelics have been shown to produce more serious side effects including degeneration of Purkinje cells and inhibition of hERG resulting in cardiac arrhythmia.[63,64]

One of the greatest drawbacks to the use of LSD as a therapeutic is its long-lasting effects. LSD has a plasma half-life of 2.6 hours after administration of 100 and 200 µg LSD. In humans, the psychoactive effects of LSD can persist up to 10 hours depending on the dose.[65,66] In addition, the potential for a "bad trip" cannot be ruled out. While this is not common in the clinical setting, psychedelics have the ability to produce terrifying thoughts and feelings, or potentially harmful flashbacks.[67] The development of non-

[57] Denson. R.; Sydiaha D. A controlled study of LSD treatment in alcoholism and neurosis. *Br J Psychiatry* **1970,** 116, 443–445.
[58] Hutten, N. R. P.; Mason, N. L.; Dolder, P. C.; Theunien, E. L.; Holze, F.; Liechti, M. E.; Fielding, A.; Ramaekers, J. G.; Kuypers, K. P. C. Mood and cognition after administration of low LSD doses in healthy volunteers: A placebo controlled dose-effect finding study. *Eur Neuropsychopharmacol*. **2020,** 41, 81-91.
[59] Pokorny, T.; Duerler, P.; Seifritz, E.; Vollenweider, F. X.; Preller, K. H. LSD acutely impairs working memory, executive functions, and cognitive flexibility, but not risk-based decision-making. *Psychol Med*. **2020**, 50, 2255-2264.
[60] Robinson, J. T.; Chitham, R. G.; Greenwood, R. M.; Taylor, J. W.; .Chromosome aberrations and LSD. *Br J Psychiatry* **1974**, 125, 238–244.
[61] Cohen, M. M.; Marinello, M. J.; Back, N. Chromosomaldamage in human leukocytes induced by lysergic aciddiethylamide. *Science* **1967**, 155, 1417–1419
[62] Rothman, R. B.; Baumann, M. H.; Savage, J. E.; Rauser, L.; McBride, A.; Hufeisen, S. J.; Roth, B. L. Evidence for possible involvement of 5-HT(2B) receptors in the cardiac valvulopathy associated with fenfluramine and other serotonergic medications. *Circulation* **2000**, 102, 2836-2841.
[63] O'Hearn, E.; Molliver, M. E. Degeneration of Purkinje cells in parasagittal zones of the cerebellar vermis after treatment with ibogaine or harmaline. *Neuroscience* **1993**, 55, 303–310.
[64] Koenig, X.; Kovar, M.; Boehm, S.; Sandtner, W.; Hilber, K. Anti-addiction drug ibogaine inhibits hERG channels: a cardiac arrhythmia risk. *Addict Biol*. **2014**, 19, 237–239.
[65] Dolder, P. C.; Schmid, Y.; Steuer, A. E.; Kraemer, T.; Rentsch, K. M.; Hammann, F.; Liechti, M. E. Clin Pharmacokinetics and Pharmacodynamics of Lysergic Acid Diethylamide in Healthy Subjects. *Pharmacokinet*. **2017**, 56, 1219-1230. 4
[66] Passie, T.; Halpern, J. H.; Stichtenoth, D. O.; Emrich, H. M.; Hintzen, A. The pharmacology of lysergic acid diethylamide: a review. *CNS Neurosci Ther*. **2008**, 14, 295-314.
[67] Strassman, R. J. Adverse reactions to psychedelic drugs. A review of the literature *J Nerv Ment Dis.* **1984**, 172, 577-595.

hallucinogenic analogs of psychedelics that retain the therapeutic effects may mitigate the possibility of adverse events.

Chapter 2. Structure-Activity Relationship Studies of Psychoplastogens.[1]

Chapter 2.1 Introduction

Psychoplastogens, compounds capable of rapidly promoting structural and functional neural plasticity, represent a promising new class of therapeutics.[2] Psychoplastogens represent a broad class of drugs with both clinical and anecdotal reports that these drugs possess properties for treating numerous neuropsychiatric disorders like depression, post-traumatic stress disorder (PTSD), and addiction. While psychoplastogens, like the classic psychedelics, have been around for decades, the mechanism of their therapeutic effects is still poorly understood. We hypothesize that a key aspect of their action, their ability to promote neural plasticity, is responsible for their broad impact on various brain disorders. The majority of psychoplastogens identified to date belong to the class of serotonergic psychedelics (**FIG 2.1.A**). We have recently shown that DMT has psychoplastogenic effects in vitro and is able to produce an anti-depressive phenotype in vivo.[3,4]

Despite the remarkable success of psychedelics and a few successful advancements to U.S. Food and Drug Administration (FDA) approved clinical trials, these drugs still have limitations. Many of these drugs possess off-target effects like agonism of the serotonin 2B receptor(5-HT2B), inhibition of human Ether-à-go-go-Related Gene (hERG), and hallucinations.[5,6] There have been arguments proposing that the

---

[1] The data in this chapter in (**FIG 2.2-2.7**) can be found in the following publication and were used with the journals consent. Dunlap, L. E.; Azinfar, A.; Ly, C.; Cameron, L. P.; Viswanathan, J.; Tombari, R. J.; Myers-Turnbull, D.; Taylor, J. C.; Grodzki, A. C.; Lein, P. J.; Kokel, D.; Olson, D. E. Identification of Psychoplastogenic N,N-Dimethylaminoisotryptamine (isoDMT) Analogs Through Structure-Activity Relationship Studies. *J. Med. Chem*., **2020**, 63, 1142–1155.

[2] Olson, D. E. Psychoplastogens: A Promising Class of Plasticity-Promoting Neurotherapeutics. *J Exp Neurosci.* **2018**. doi: 10.1177/1179069518800508

[3] Cameron, L. P.; Benson, C. J.; Dunlap, L. E.; Olson, D. E. Effects of *N,N*-dimethyltryptamine (DMT) on rat behaviors relevant to anxiety and depression. *ACS Chem. Neurosci*. **2018**, 9, 1582–1590.

[4] Ly, C.; Greb, A. C.; Cameron, L. P.; Wong, J. M.; Barragan, E. V.; Wilson, P. C.; Burbach, K. F.; Soltanzadeh Zarandi, S.; Sood, A.; Paddy, M. R.; Duim, W. C.; Dennis, M. Y.; McAllister, A. K.; Ori-McKenney, K. M.; Gray, J. A.; Olson, D. E. Psychedelics Promote Structural and Functional Neural Plasticity. *Cell Reports* **2018**, 23, 3170–3182

[5] Rothman, R. B.; Baumann, M. H.; Savage, J. E.; Rauser, L.; McBride, A.; Hufeisen, S. J.; Roth, B. L. Evidence for possible involvement of 5-HT(2B) receptors in the cardiac valvulopathy associated with fenfluramine and other serotonergic medications. *Circulation* **2000**, 102, 2836-2841.

[6] Koenig, X.; Kovar, M.; Boehm, S.; Sandtner, W.; Hilber, K. Anti-addiction drug ibogaine inhibits hERG channels: a cardiac arrhythmia risk. *Addict Biol*. **2014**, 19, 237–239.

hallucinogenic effects are necessary for the therapeutic effects.[7] However, there is growing evidence to suggest that the hallucinogenic effects may not be necessary.[8][9] At the time of this work, there were few papers suggesting that the hallucinogenic effects were not necessary to elicit a therapeutic response. Our lab had shown in rodent models that acute microdoses of the psychedelic DMT elicited antidepressive phenotypes in rodent models comparable to a large, acute dose.[10] Perhaps some of the most compelling evidence to disprove the theory that hallucinations are important was work conducted by Sazra et. al in the 1960s. While studying the effects of the *N,N*-diethyltryptamine (DET), they discovered that the drug 6-fluoro-DET produced no hallucinogenic effects, yet still produced mood changes.[11] To this end, we set out to determine if hallucinogenic effects could be decoupled from the therapeutic effects by synthesizing and screening compounds structurally similar to classic psychedelics that lack hallucinogenic activity.

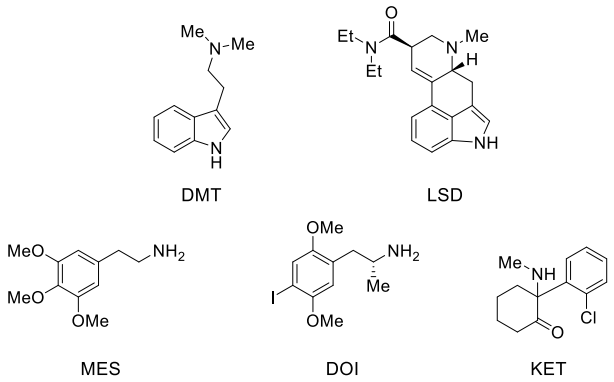

Figure 2.1. Structures of psychedelics. DMT = N,N-dimethyltryptamine, LSD = lysergic acid diethylamide, MES = mescaline, DOI = 2,5-dimethoxy-4-iodoamphetamine, KET = ketamine.

[7] Yarden, D. B.; Griffiths, R. R. The Subjective Effects of Psychedelics Are Necessary for Their Enduring Therapeutic Effects. *ACS Pharmacol Transl Sci* . **2020,** 4, 568-572.

[8] Olson, D. E. The Subjective Effects of Psychedelics May Not Be Necessary for Their Enduring Therapeutic Effects. *ACS Pharmacol. Transl. Sci.* **2020**, 4, 563–567.

[9] Cameron, L. P.; Nazarian, A.; Olson, D. E. Psychedelic Microdosing: Prevalence and Subjective Effects. *J. Psychoactive Drugs*, **2020**, 52, 113–122.

[10] Cameron, L. P.; Benson, C. J.; DeFelice, B. C.; Fiehn, O.; Olson, D. E. "Chronic, Intermittent Microdoses of the Psychedelic N,N-Dimethyltryptamine (DMT) Produce Positive Effects on Mood and Anxiety in Rodents. *ACS Chem. Neurosci*. **2019**, 10, 3261−3270.

[11] Kalir, A.; Szara, S. Synthesis and pharmacological activity of fluorinated tryptamine derivatives. *J Med Chem*. **1963**, 6, 716-719.

Chapter 2.2 IsoDMTs as Potential Non-Hallucinogenic Analogs of DMT

Through our literature search, we discovered that a class of DMT analogs, isoDMTs, had previously been shown to lack hallucinogenic effects in drug discrimination studies.[12] IsoDMTs are similar to DMTs but the alkyl chain linking the dimethylamine to the indole moiety has been transposed from the C3 position to the N1 on the indole ring (**FIG. 2.2.A**). It should be noted that these differences result in an improved central nervous system multiparameter optimization (CNS MPO) score.

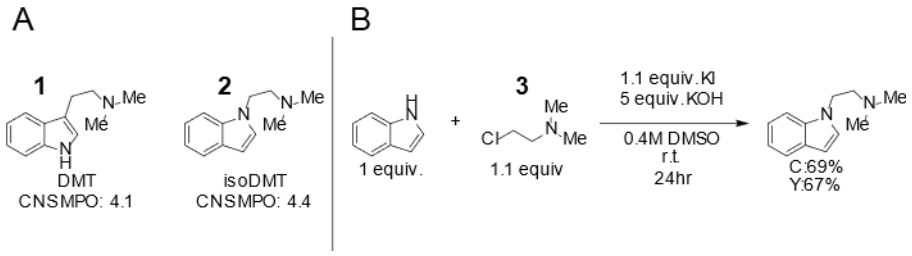

Figure 2.2. (**A**) Structures of DMT and isoDMT with respective CNS MPO scores. (**B**) Synthesis of isoDMT. C = conversion measured using ^{1}HNMR with 6-fluoroindole as the internal standard. Y = yield of the fumarate salt.

Using a simple, one-step method (**FIG 2.2 B**) we were able to synthesize isoDMT as the fumarate salt without extensive purification. This provides an advantage for structure-activity relationship (SAR) studies, as the current methods of synthesizing DMTs are multiple steps and involve harsh conditions. For comparison, we can synthesize 5-F-isoDMT (**13**) in one step with a yield of 53%, whereas using the Speeter method, synthesis of the analogous 6-F-DMT (**29**) can be achieved in 3 steps with an overall yield of 21%.[13,14] This simple one-step method allowed for the rapid synthesis of a wide range of isoDMTs (**FIG. 2.3.**)

[12] Glennon, R. A.; Jacyno, J. M.; Young, R.; McKenney, J. D.; Nelson, D. Synthesis and Evaluation of a Novel Series of *N,N*-dimethylisotryptamines. *J. Med. Chem*. **1984**, 27, 41– 45,
[13] Tombari, R. J.; Saunders, C. M.; Wu, C.-Y.; Dunlap, L. E.; Tantillo, D. J.; Olson, D. E. Ex Vivo Analysis of Tryptophan Metabolism Using 19F NMR. *ACS Chem. Biol.* **2019**, 14, 1866-1873.
[14] Speeter, M. E.; Anthony, W. C. The Action of Oxalyl Chloride on Indoles: A New Approach to Tryptamines. *J. Am. Chem. Soc.* **1954**, 76, 6208– 6210.

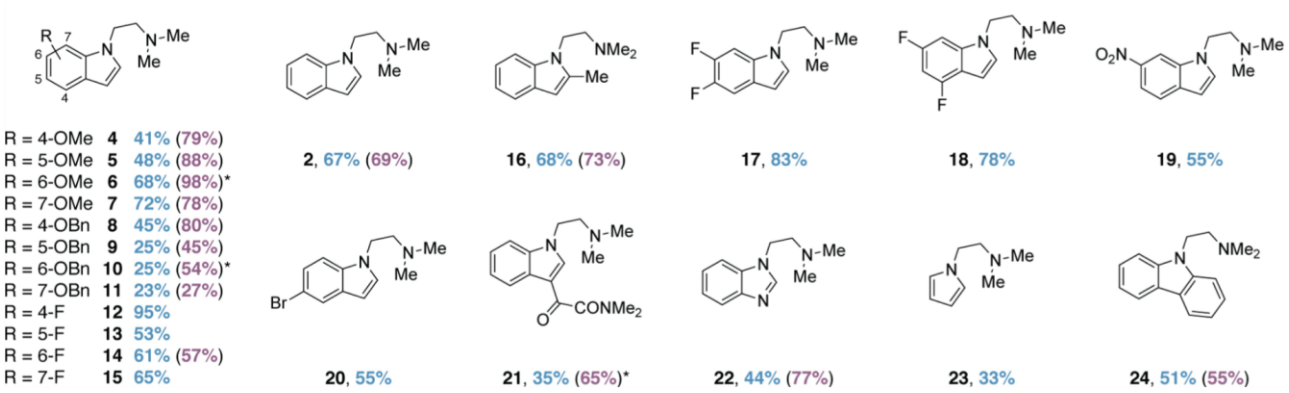

Figure 2.3. Structures of synthesized isoDMTS. Yields following crystallization as the fumarate in blue. Brackets denote yield based on ^{1}HNMR. Asterisk denotes compounds purified via column chromatography.

Chapter 2.3 IsoDMTs Promote Neuritogenesis Comparable to DMT

With this library of compounds in hand, our first step was to investigate whether isoDMT retained the plasticity-promoting properties that DMT possesses. Recently published crystal structures of the 5-HT2A and 5-HT2B receptors show a key interaction between the indole N-H bond and a serine residue S242$^{5.46}$ and glycine G221$^{5.42}$ respectively.[15,16] As we have previously shown that psychedelics, like DMT, promote plasticity via a 5-HT2A dependent mechanism, we needed to assess if this key interaction was crucial to the psychoplastogenic phenotype. To this end, we tested isoDMT and DMT for their ability to promote neuritogenesis in primary cortical neurons using Sholl analysis. We also prepared the DMT analog 1-Me-DMT, a compound lacking the N-H indole bond. We were delighted to observe that both isoDMT and 1-Me-DMT were able to promote neuritogenesis comparable to DMT in rat cortical neurons (**FIG 2.4**).[17]

[15] Kim, K.; Che, T.; Panova, O.; DiBerto, J. F.; Lyu, J.; Krumm, B. E.; Wacker, D.; Robertson, M. J.; Seven, A. B.; Nichols, D. E.; Shoichet, B. K.; Skiniotis, G.; Rother, B. L. Structure of a Hallucinogen-Activated Gq-Coupled 5-HT 2A Serotonin Receptor. *Cell*. **2020**, 182,1574-1588.
[16] Wacker, D.; Wang. S.; McCorvy, J. D.; Betz, R. M.; Venkatakrishnan, A. J.; Levit, A.; Lansu, K.; Schools, Z. L.; Che, T.; Nichols, D. E.; Shoichet, B. K.; Dror, R. O.; Roth, B. L. Crystal Structure of an LSD-Bound Human Serotonin Receptor. *Cell* **2017,** 168, 377-389.
[17] Figures in this chapter were taken, with permission from J. Med. Chem, from Dunlap, L. E.; Azinfar, A.; Ly, C.; Cameron, L. P.; Viswanathan, J.; Tombari, R. J.; Myers-Turnbull, D.; Taylor, J. C.; Grodzki, A. C.; Lein, P. J.; Kokel, D.; Olson, D. E. Identification of Psychoplastogenic N,N-Dimethylaminoisotryptamine (isoDMT) Analogs Through Structure-Activity Relationship Studies. J. Med. Chem., 2020, 63, 1142–1155.

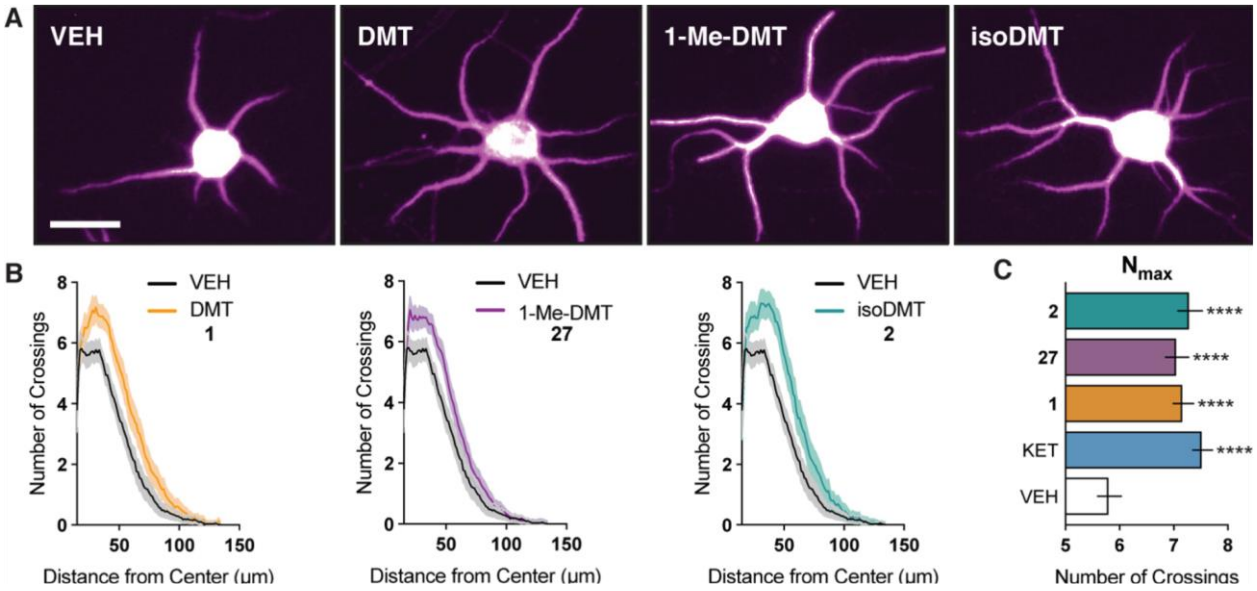

Figure 2.4. (A) Representative images of cortical neurons (DIV6) post-treatment (1 h) with compounds. **(B)** Sholl analysis plots showing that compounds lacking an N-H hydrogen bond are capable of increasing dendritic arbor complexity (n = 46–79 neurons). **(C)** The maximum number of crossings (Nmax) of the Sholl plots in B. Data are represented as mean ± standard error of the mean (SEM). *p < 0.05, **p < 0.01, ***p < 0.001, ****p < 0.0001, as compared to the vehicle control following a one-way analysis of variance (ANOVA) with Dunnett's post hoc test (F = 9.702; DFn = 4; DFd = 304; p-value < 0.0001). VEH = vehicle, KET = ketamine. Scale bar = 20 µm.

Chapter 2.4 Structure-Activity Relationship (SAR) Studies of the isoDMT Scaffold

Having shown that a number of isoDMTs promote neuronal growth comparable to DMT, we set out to study other key areas of the DMT and isoDMT scaffold in an attempt to elucidate a psychoplastogen pharmacophore. Modification of the *N,N*-dimethylamino group to an amide (**31**) or removing the nitrogen (**25**) abolished the plasticity promoting effects (**FIG. 2.5 A, B**).[17] Modifications to the indole ring resulted in minimal decreases in psychoplastogenic effects (**FIG 2.5 C**), with the benzimidazole based analog (**22**) showing the greatest reduction in efficacy. Taken together these data suggest that the essential psychoplastogen pharmacophore consists of an aromatic ring, a short carbon chain, and a basic amine group.

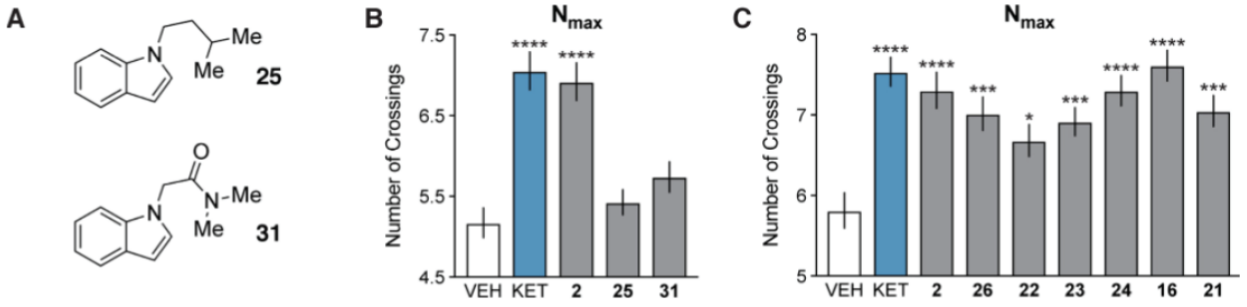

Figure 2.5. (A) Structures of nonbasic isoDMT analogs. **(B, C)** Nmax values post-treatment (1 h) with compound. (n = 46–85 neurons). Data are represented as mean ± SEM. *p < 0.05, **p < 0.01, ***p < 0.001, ****p < 0.0001, as compared to the vehicle control following a one-way ANOVA with Dunnett's post hoc test. [For B: F = 19.03; DFn = 4; DFd = 273; p-value < 0.0001. For C: F = 6.933; DFn = 8; DFd = 599; p-value < 0.0001.] VEH = vehicle, KET = ketamine.

Glennon and coworkers had previously shown that substituents on the aromatic ring of isoDMTs can alter binding affinity at the 5-HT2A receptor and impact hallucinogenic effects.[12] These trends are also apparent in the respective isomeric DMT counterparts. Substitution of a methoxy group at the C5 position of the indole ring on DMT, 5-MeO-DMT (**28**), results in increased hallucinogenic potency. However, its isomer, 6-MeO-DMT, is a non-hallucinogenic analog.[18] To determine if the same substitution patterns bear any effects on the plasticity-promoting properties, we screened a series of isoDMTs with different functional groups at varying positions on the indole ring (**FIG. 2.6**).[17] To our surprise, we did not discover any differences between 5- and 6- substituted isoDMTs, however, we observed that substituents at the 4-position, corresponding to 7- substituted DMTs, abolished all activity. This result was shocking as that position seems sensitive to any substitution.

[18] Glennon, R. A.; Young, R. I.; Jacyno, J. M.; Slusher, M.; Rosecrans, J. A. DOM-Stimulus Generalization to LSD and other Hallucinogenic Indolealkylamines. *Eur. J. Pharmacol.* **1983**, 86, 453– 459.

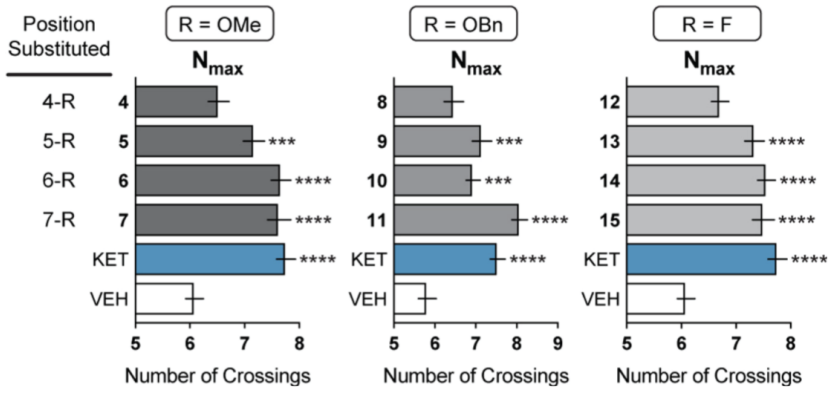

Figure 2.5. Nmax values post-treatment (1 h) with compound (n = 39–93 neurons). Data are represented as mean ± SEM. *p < 0.05, **p < 0.01, ***p < 0.001, ****p < 0.0001, as compared to the vehicle control following a one-way ANOVA with Dunnett's post hoc test. (For R = OMe: F = 13.85; DFn = 5; DFd = 493; p-value < 0.0001. For R = OBn: F = 15.44; DFn = 5; DFd = 372; p-value < 0.0001. For R = F: F = 13.24; DFn = 5; DFd = 506; p-value < 0.0001.) VEH = vehicle, KET = ketamine.

Chapter 2.5 IsoDMTs Promote Neuritogenesis Via a 5-HT2R Mediated Mechanism

Having established that isoDMTs are capable of promoting increases in dendritic arbor complexity, we wanted to further assess their similarities to DMT. We have previously shown that psychedelics promote their psychoplastogenic effects via a 5-HT2R mediated mechanism. We first completed a 4-point dose-response with 2 sets of DMTs and their isomers (**FIG 2.6 A, B**) We found that like their DMT counterparts, both 6-MeO-isoDMT(**6**) and isoDMT(**2**) were effective at promoting neuritogenesis at doses as low as 1nM. Further, we found that the effects on neurite outgrowth were blocked by the 5-HT2R antagonist ketanserin (**FIG 2.6 C**).

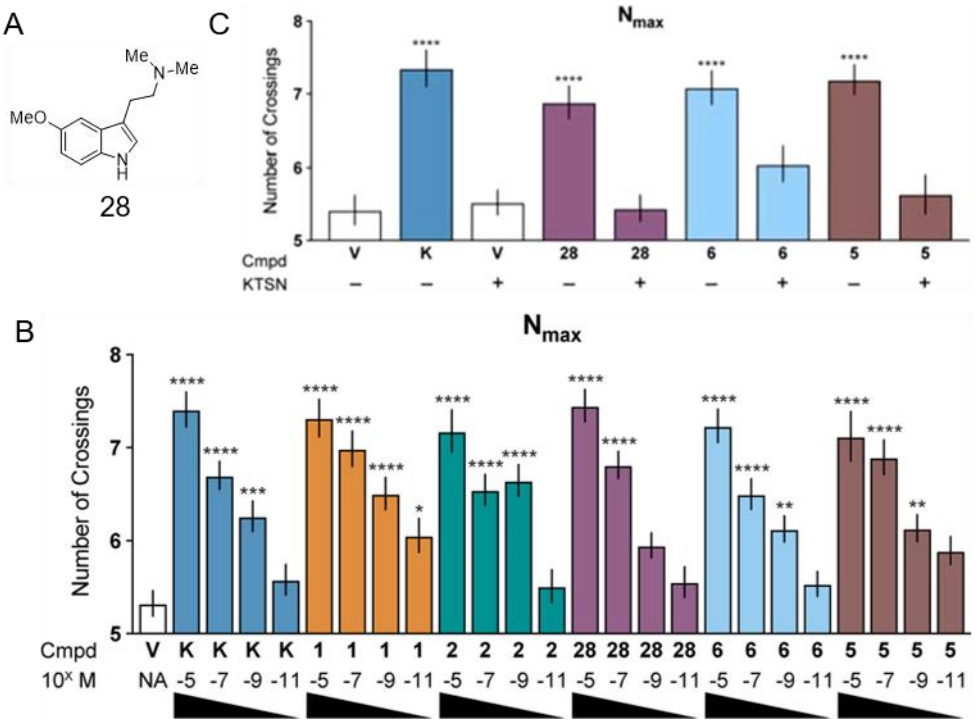

Figure 2.6. (**A**) Structures of DMT(**1**), 5-MeO-DMT(**28**) and their isoDMT(**2**,**6**) analogs. (**B**) Nmax values post-treatment (1 h) with compounds at concentrations ranging from 10 μM to 10 pM (n = 66–123 neurons). (**C**) (n = 45–63 neurons) in the presence (+) or absence (−) of the 5-HT2A antagonist ketanserin. Data are represented as mean ± SEM. *p < 0.05, **p < 0.01, ***p < 0.001, ****p < 0.0001, as compared to the vehicle control following a one-way ANOVA with Dunnett's post hoc test (F = 15.40; DFn = 24; DFd = 2,276; p-value < 0.0001). V = vehicle, K = ketamine, KTSN = ketanserin.

Chapter 2.6 IsoDMTs do not Elicit a Hallucinogenic Response

Having established that isoDMTs exert similar effects on plasticity via a 5-HT2R mediated mechanism, we next tested the hallucinogenic potential of isoDMTs. Serotonergic psychedelics like DMT are known to cause a phenotypic head twitch response (HTR) in mice.[19] Measuring the number of head twitches a drug causes is well validated and the potency in the HTR assay has been shown to correlate

[19] Hanks, J. B.; González-Maeso, J. Animal models of serotonergic psychedelics. *ACS Chem Neurosci*. **2013**, 4, 33-42.

well with reported human potencies for hallucinogens.[20] Using this assay we tested a series of DMT and isoDMTs to determine if isoDMTs possess reduced hallucinogenic potential (**FIG 2.7**). We tested a small series of DMTs and their respective isoDMT analogs in the HTR assay. We observed that of the 2 DMTs tested, 5-MeO-DMT (**28**) produced a significant HTR while its structural analog 6-MeO-isoDMT (**6**) produced a much weaker response. We also observed that both 6-MeO-DMT (**30**) and 5-MeO-isoDMT (**5**) produced no HTR suggesting that both of these compounds are non-hallucinogenic. It is worth noting that while 6-MeO-isoDMT produced a reduced HTR compared to 5-MeO-DMT, this data suggests that isoDMTs may exhibit similar responses as their isosteric DMT analogs in animal models making them useful tools for studying the SAR of DMTs.

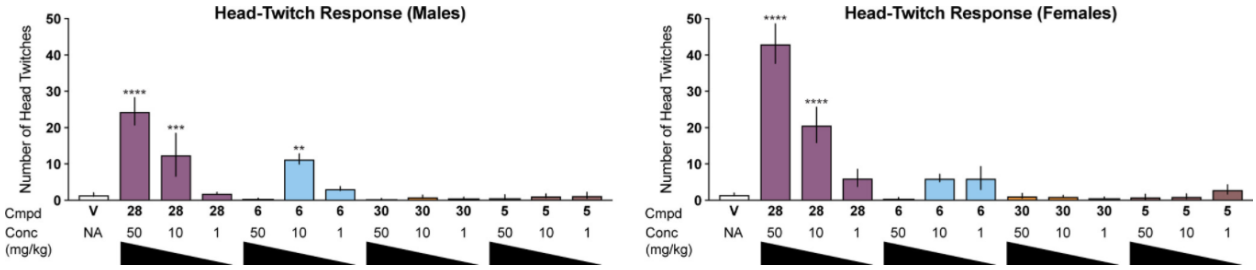

Figure 2.7. Head twitch response assay performed in mice. The number of head-twitches was recorded over a 20 min period post intraperitoneal (IP) injection of test drug (n = 3–8 mice per condition). Data are represented as mean ± SEM. *p < 0.05, **p < 0.01, ***p < 0.001, ****p < 0.0001, as compared to the vehicle control following a one-way ANOVA with Dunnett's post hoc test. V = vehicle.

Chapter 2.7 SAR of the Basic Amine

We established that the basic amine on the isoDMT scaffold plays a key role in regulating the ability of these compounds to promote neuroplasticity. We next sought to expand our understanding of the role of this key functional group. In 2020, Roth et al. solved the crystal structure of the 5-HT2A receptor with an agonist, partial agonist, and inverse agonist bound.[15] While these compounds exhibit different conformations in the binding pocket, they all share a similar interaction; a hydrogen bond that exists between the basic amine and an aspartic acid residue D155$^{3.32}$.[15] Among the different classes of

[20] Halberstadt, A. L.; Chatha, M.; Klein, A. K.; Wallach, J.; Brandt, S. D. Correlation between the potency of hallucinogens in the mouse head-twitch response assay and their behavioral and subjective effects in other species. *Neuropharmacology* **2020**, 167, 107933.

psychedelics, there are varying degrees of methylation on the basic amine. As the majority of the psychedelics tested up to this point (**FIG 2.8**) were mostly tertiary amines, we wanted to investigate if substitution around the basic amine was necessary for the psychoplastogenic effects.[4] As serotonin is the endogenous ligand for the 5-HT2Rs and it is also an agonist at these receptors, like the classic psychedelics, we theorized that it would exhibit similar effects as psychedelics.

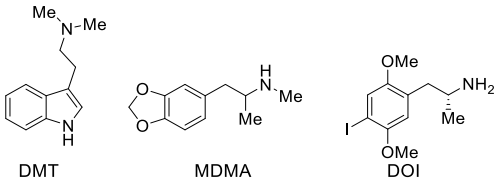

Figure 2.8. Structures of psychedelics with varying degrees of methylation. DMT = N,N-dimethyltryptamine, MDMA = 3,4-Methylenedioxymethamphetamine, DOI = 2,5-Dimethoxy-4-iodoamphetamine, KET = ketamine.

We began our investigation by synthesizing a series of methylated tryptamines (**FIG 2.9**). We chose tryptamine, serotonin, and 5-MeO-tryptamine as they have comparable affinities for the 5-HT2A receptor.[21] We tested these compounds and their methylated analogs using Sholl analysis (**FIG 2.10**). To our surprise, we observed that serotonin and the other primary amines had little to no effect on neurite outgrowth, but the methylated amines caused an increase in outgrowth.

[21] McKenna, D. J.; Peroutka, S. J. Differentiation of 5-Hydroxytryptamine, Receptor Subtypes Using 125I-R-(-)2,5-Dimethoxy-4-iodo-phenylisopropylamine and 3H-Ketanserin. *J. Neuroscience*. **1989**, 9, 3482–3490.

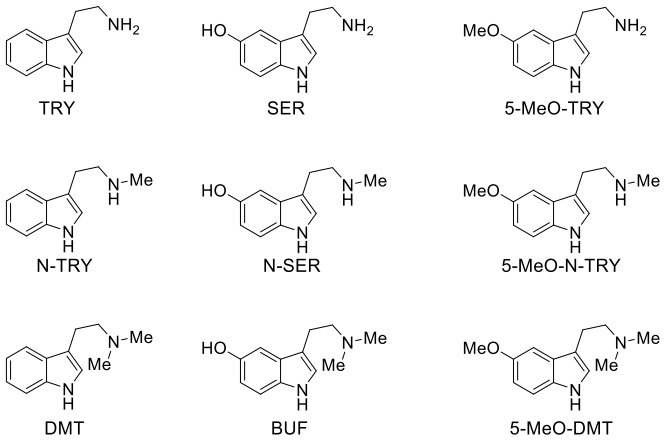

Figure 2.9. Structures of methylated tryptamines. TRY = Tryptamine, N-TRY = N-Methyltryptamine, DMT = N,N-Dimethyltryptamine, SER = Serotonin, N-SER = N-Methylserotonin, BUF = N,N-Dimethylserotonin, 5-MeO-TRY = 5-MeO-tryptamine, 5-MeO-N-TRY = 5-MeO-N-Methyltryptamine, 5-MeO-DMT = 5-MeO-N,N-Dimethyltryptamine.

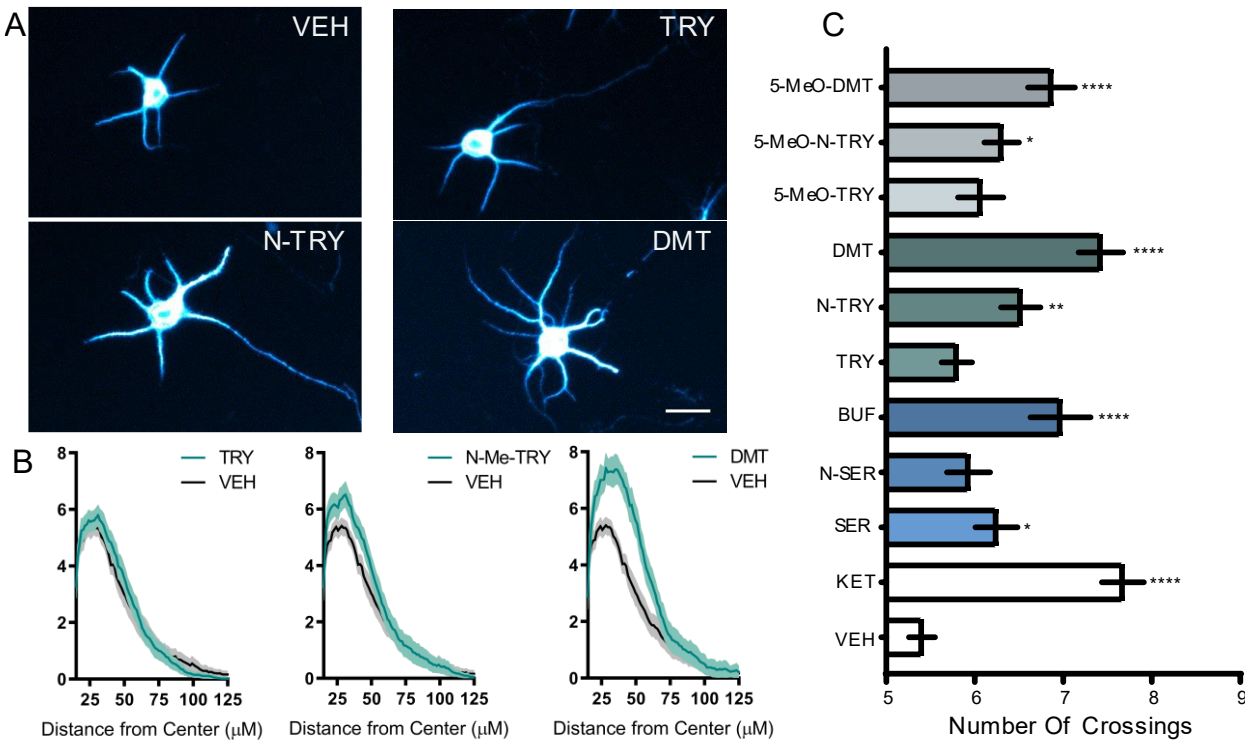

Figure 2.10. (**A**) Representative images of cortical neurons treated with VEH, TRY, N-TRY, and DMT. Scale bar 20 μm. (**B**) Sholl plots (n = 40–64 neurons). (**C**) Nmax values of tryptamine series (n = 32–64 neurons). Data are represented as mean ± SEM. *p < 0.05, **p < 0.01, ***p < 0.001, ****p < 0.0001, as compared to the vehicle control following a one-way ANOVA with Dunnett's post hoc test (F = 15.40; DFn = 24; DFd = 2,276; p-value < 0.0001). V = vehicle, K = ketamine, TRY = Tryptamine, N-TRY = N-Methyltryptamine, DMT = N,N-Dimethyltryptamine, SER = Serotonin, N-SER = N-Methylserotonin, BUF = N,N-Dimethylserotonin, 5-MeO-TRY = 5-MeO-tryptamine, 5-MeO-N-TRY = 5-MeO-N-Methyltryptamine, 5-MeO-DMT = 5-MeO-N,N-Dimethyltryptamine.

Chapter 2.8 Psychoplastogens Promote Plasticity Via an Inside-Out Mechanism

We hypothesized that the increased lipophilicity of the alkylated amines may be the reason for their efficacy. As the 5-HT2AR is primarily expressed intracellularly, the increased lipophilicity may make these compounds more accessible to their intracellular target. To prove this theory, we tested a series of compounds known to promote plasticity alongside membrane-impermeable analogs (**FIG 2.11**). Salts with a permanent charge are known to have poor membrane permeability, so we synthesized two compounds,

N,N,N-trimethyltryptamine iodide (TMT), and *N*-Me-ketanserin (MKETSN). In addition to these two charged molecules, we included psilocybin, which bears a charged phosphate moiety.

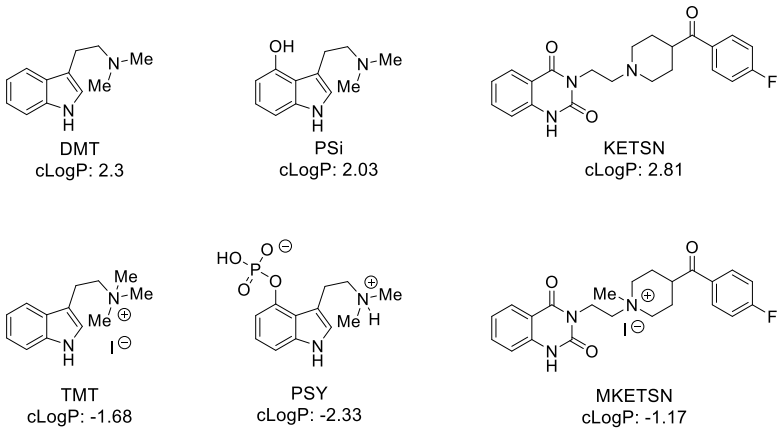

Figure 2.11. Structures of membrane permeable and impermeable psychoplastogens DMT = N,N-dimethyltryptamine, TMT = N,N,N-trimethyltryptamine iodide, PSI = psilocin, PSY = psilocybin, KETSN = ketanserin, MKETSN = N-Me-ketanserin.

We began by running neurite outgrowth assays and found that both DMT and psilocin were able to increase neuritogenesis, however, the salt forms, TMT and psilocybin, were not able to promote growth relative to the vehicle control (define) (**FIG 2.12 A**). Further, when we attempted to block the effects of DMT using KETSN or its methylated salt form (MKETSN), only KETSN was able to block the effects. We conducted a similar experiment, but this time we examined the number of dendritic spines (**FIG 2.12 B, C**). As with the neurite outgrowth assay, only DMT and psilocin were able to elicit an increase in the number of spines and only KETSN was able to block the effects of DMT (**FIG 2.12 D**). To prove this phenomenon was a result of membrane penetrance and not lack of activity, we repeated the experiments from (**FIG 2.12 A**) except we electroporated the cells in the presence of drugs. Electroporation causes the cells to form pores on the membrane, allowing the salt forms of our test compounds to enter the intracellular space. Cells that were electroporated with either TMT or psilocybin were able to increase neurite outgrowth after electroporation (**FIG 2.12 E**). Further, the membrane-impermeable form of ketanserin was able to block the effects of DMT when both drugs were electroporated.

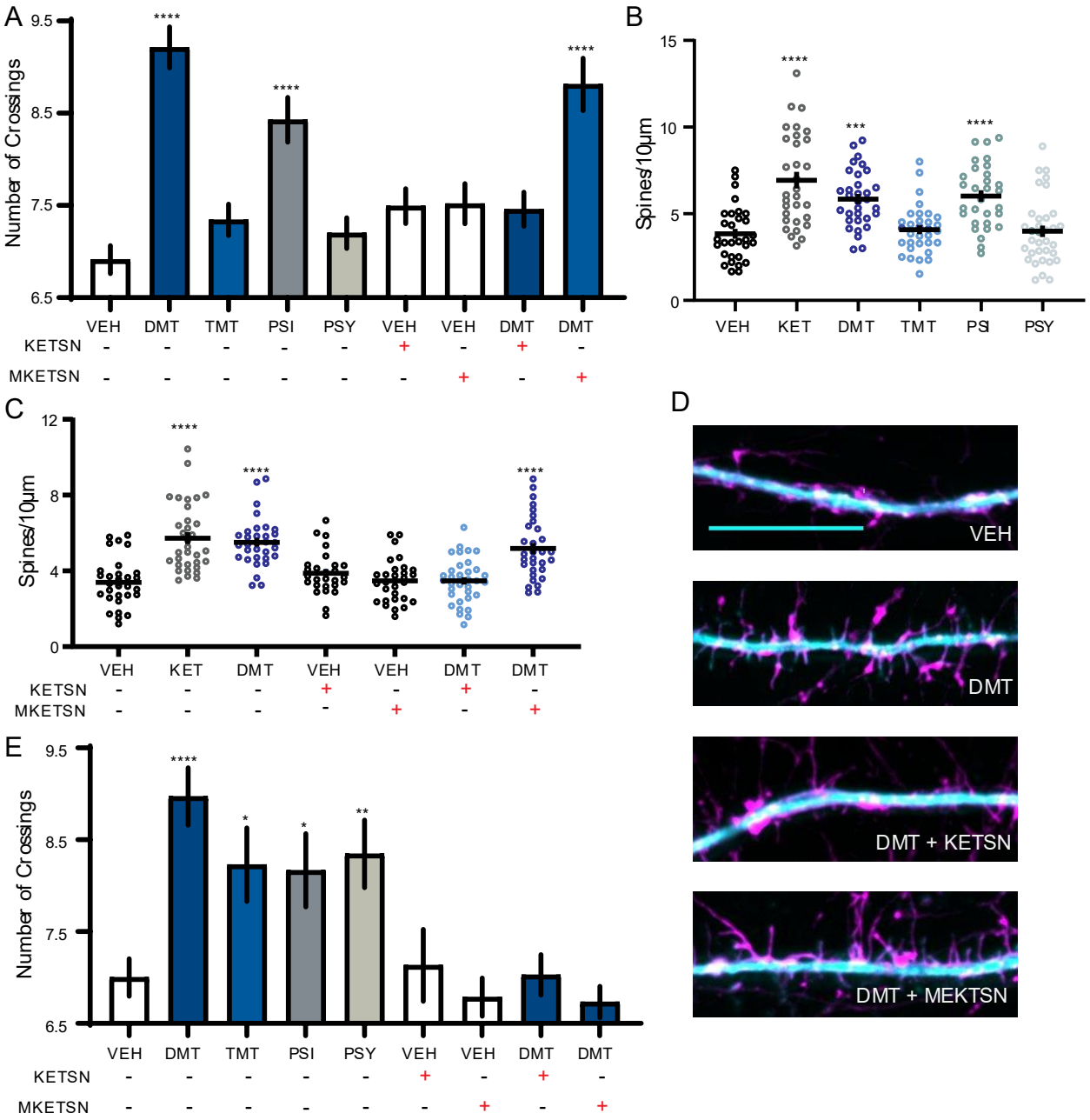

Figure 2.12. Psychoplastogens mediate plasticity via an intracellular 5-HT2R mechanism. (**A,B**) DMT and PSI but not their membrane impermeable analogs PSY and TMT are able to promote neuritogenesis (n = 64–110 neurons) and spineogenesis (n = 30–34 neurons). **(C)** DMTs effects were blocked by KETSN but not MKETSN (n = 29–35 neurons). **(D)** Representative images of spines treated with PSI, PSY, and VEH. Spines stained with MAP2 (cyan) and F-actin (magenta). (**E**) Electroporation of neurons with membrane impermeable compounds exhibit growth (n = 35–86 neurons). Data are represented as mean ± SEM. *p <

0.05, **p < 0.01, ***p < 0.001, ****p < 0.0001, as compared to the vehicle control following a one-way ANOVA with Dunnett's post hoc test (F = 15.40; DFn = 24; DFd = 2,276; p-value < 0.0001). VEH = vehicle, KET = ketamine, DMT = N,N-dimethyltryptamine, TMT = N,N,N-trimethyltryptamine iodide, PSI = psilocin, PSY = psilocybin, KETSN = ketanserin, MKETSN = N-Mel-ketanserin.

Serotonin is the endogenous ligand for numerous receptors including the 5-HT2A receptor, a receptor believed to be important in the plasticity-promoting properties of psychedelics. However, we have found that the administration of serotonin causes minimal changes to dendritic arborization or spinogenesis (**FIG 2.13 A, B**). This could be explained by the low membrane permeability of serotonin coupled with the limited lack of serotonin transporter (SERT) expression in cortical neurons.[22] To support this theory, we expressed SERT in cortical neurons to allow serotonin to cross the membrane to activate intracellular receptor targets (**FIG 2.13 A,B**). Serotonin had no effect in SERT-negative neurons but was able to promote growth in SERT-positive neurons. Further expression of SERT had no effects on DMT and ketamine-treated neurons.

[22] Fujita, M.; Shimada, S.; Maeno, H.; Nishimura, T.; Tohyama, M.; Cellular localization of serotonin transporter mRNA in the rat brain. *Neurosci Lett*. **1993**,162, 59-62.

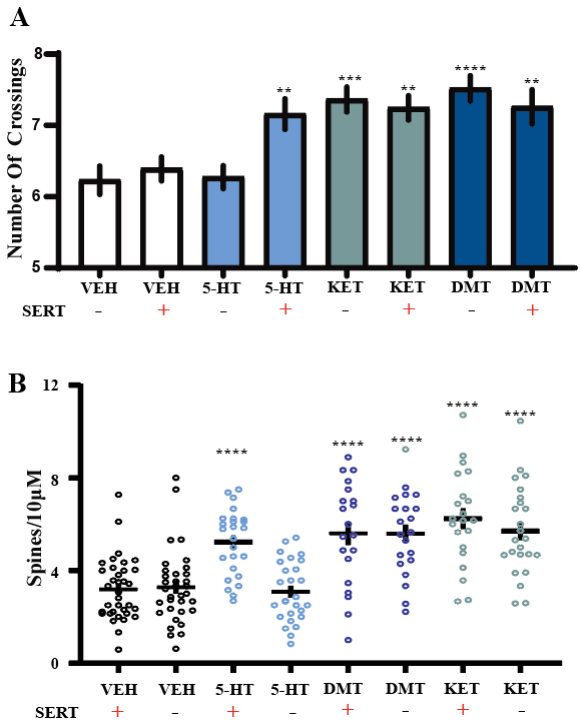

Figure 2.13. Serotonin can promote structural plasticity in SERT + neurons. (**A,B**) Serotonin promotes neuritogenesis (n = 57–93 neurons)and spineogenesis (n = 20–35 neurons) in SERT + but not SERT – neurons. The presence of SERT has no effect on DMT or ketamine. Data are represented as mean ± SEM. *p < 0.05, **p < 0.01, ***p < 0.001, ****p < 0.0001, as compared to the vehicle control following a one-way ANOVA with Dunnett's post hoc test (F = 15.40; DFn = 24; DFd = 2,276; p-value < 0.0001). VEH = vehicle, KET = ketamine, DMT = N,N-Dimethyltryptamine, 5-HT = serotonin.

Having demonstrated that expression of SERT is sufficient to induce changes in structural plasticity in neurons treated with serotonin, we wanted to determine if serotonin was working via SERT mediated 5-HT2R activation. Serotonin's effects on neuritogenesis were blocked via pretreatment with the 5-HT2AR antagonist ketanserin (KTSN) and the SERT inhibitor citalopram (CIT) (**FIG. 2.14 C**). We also showed that blocking SERT had no effect on DMT's ability to promote plasticity (**FIG. 2.14 D**).

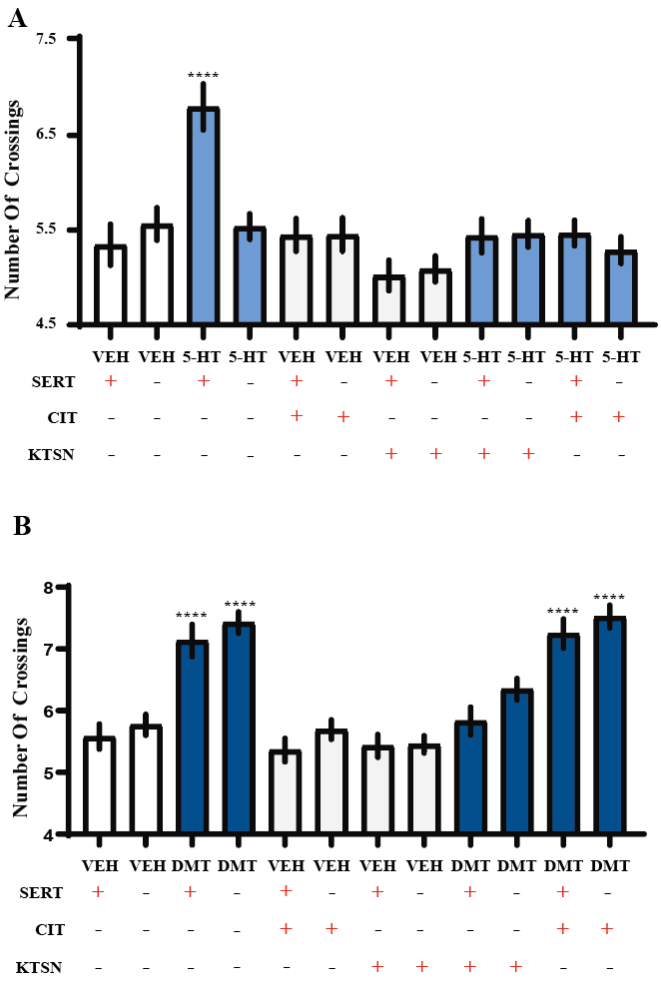

Figure 2.14. Citalopram inhibits the effects of serotonin (5-HT) in SERT + neurons but not the psychoplastogen DMT. (**A**) Citalopram and ketanserin inhibit the ability of 5-HT to promote neuritogenesis in SERT + neurons(n = 76–121 neurons). (**B**) Citalopram had no effect on DMT treated neurons but the 5-HT2R antagonist ketanserin blocked the effects(n = 59–109 neurons). Data are represented as mean ± SEM. *p < 0.05, **p < 0.01, ***p < 0.001, ****p < 0.0001, as compared to the vehicle control following a one-way ANOVA with Dunnett's post hoc test (F = 15.40; DFn = 24; DFd = 2,276; p-value < 0.0001). VEH = vehicle, KET = ketamine, DMT = N,N-dimethyltryptamine, 5-HT = serotonin, CIT = citalopram, KTSN = ketanserin.

Chapter 2.9 Conclusion

Psychedelics have received a lot of attention for their ability to promote rapid and long-lasting therapeutic effects. Despite the recent advances in the field, we still know little about the structural characteristics that give rise to their therapeutic and hallucinogenic effects. Further, our understanding of the mechanism of the therapeutic effects of these drugs is still limited.

We have demonstrated here that isoDMTs, structural analogs of DMTs, have potential therapeutic effects, i.e the ability to promote neuroplasticity. In addition to providing proof of concept that the hallucinogenic and therapeutic effects of psychedelics can be decoupled, we have identified key structural characteristics that are necessary for their therapeutic effects. Modification of the basic amine to either the amide or a neopentyl group renders these compounds ineffective. Modifications to the aromatic ring (i.e the 4- and 5- positions) attenuate the plasticity promoting properties of isoDMTs. We believe that not only will the results of these findings translate to other tryptamine-based scaffolds, i.e ergolines, and iboga alkaloids, but we can use this information to design new, second-generation therapeutics that retain the efficacy of their parent psychedelic compounds, without the hallucinogenic effects.

To date little was known about the therapeutic action of psychedelics. Our lab has recently discovered that the plasticity-promoting properties are mediated via a 5-HT2R, tropomyosin receptor kinase B (TrkB), α-amino-3-hydroxy-5-methyl-4-isoxazolepropionic acid receptor (AMPAR), and the mechanistic target of rapamycin (mTOR).[4,23] In light of these results we believed that serotonin, the endogenous ligand would be the ideal psychoplastogen. However, we discovered that methylation of the primary amine is essential for the therapeutic effects. Our SAR work led to insights into the mechanism of these drugs, i.e that psychoplastogens operate via an inside-out mediated mechanism.

It is well known that 5-HT2A is a primarily intracellular receptor expressed in layer V pyramidal neurons in the medial prefrontal cortex (mPFC).[24] Serotonin does not readily cross cell membranes and needs a transporter (SERT) to help shuttle it across membranes from the extracellular to intracellular space. SERT is not heavily expressed in the mPFC which suggests that serotonin may not function as the

[23] Ly, C.; Greb, C. A.; Vargas, M. V.; Duim, W. C.; Grodzki, A. C. G.; Lein, P. J.; Olson, D. E. Transient Stimulation with Psychoplastogens is Sufficient to Initiate Neuronal Growth. *ACS Pharmacol. Transl. Sci*. **2020**, 4, 452–460.
[24] Cornea-Hebert, V.; Riad, M.; Wu, C.; Singh, S. K.; Descarries, L. Cellular and subcellular distribution of the serotonin 5-HT2A receptor in the central nervous system of adult rat. J Comp Neurol. 1999, 409, 187-209.

endogenous ligand of intracellular 5-HT2ARs.[25] It has recently been reported that endogenous DMT can reach levels comparable to other neurotransmitters in the brain.[26] DMT's role as an endogenous monoamine remains unclear, however, our results, coupled with the fact that DMT has a nanomolar affinity for the 5HT2AR, suggest that DMT may play a role as an endogenous ligand of 5-HT2Rs and act as a biogenic plasticity modulator.[27] More work is needed to confirm this theory. For example, studies using indole(ethyl)amine-N-methyl transferase (INMT) knockout animals would lack the ability to produce DMT. By studying the effects of knocking out INMT on plasticity and behavior may shine a light on the role of endogenous DMT.

We have provided proof of concept that the hallucinogenic effects of psychedelics like DMT may not be necessary for their therapeutic effects, as isoDMT analogs with reduced hallucinogenic potential compared to DMTs are still efficacious in a number of our cell outgrowth assays. Further, we have discovered key features of the tryptamine core scaffold that give rise to their therapeutic effects. Through our SAR work, we have also identified that psychedelics exert their plasticity-promoting properties via an inside-out 5-HT2AR mediated mechanism. This work has also pointed to a possible role for endogenous DMT

Acknowledgments

I would like to acknowledge Max Vargas for performing the experiments in figures 2.11-2.13. I would also like to thank Calvin Ly for all of his help performing the cellular assays in this chapter and Lindsay Cameron and Jayashri Viswanathan for performing the HTR assay.

[25] Fujita, M.; Shimada, S.; Maeno, H.; Nishimura, T.; Tohyama, M.; Cellular localization of serotonin transporter mRNA in the rat brain. *Neurosci Lett*. **1993**,162, 59-62.
[26] Dean, J. G.; Liu, T.; Huff, S.; Sheler, B.; Barker, S. A.; Strassman, R. J.; Wang, M. M.; Borjigin, J.; Biosynthesis and Extracellular Concentrations of N,N-dimethyltryptamine (DMT) in Mammalian Brain. *Scientific Reports* **2019**, 9, 9333.
[27] McKenna, D. J.; Peroutka, S. J. Differentiation of 5-Hydroxytryptamine, Receptor Subtypes Using ^{125}I-R-(-)2,5 Dimethoxy-4-iodo-phenylisopropylamine and ^{3}H-Ketanserin. *J. Neuroscience*, **1989**, 9, 3482-3490.

Chapter 2.10 Methods

Drugs

The NIH Drug Supply Program provided psilocin (PSI) and psilocybin (PSY). Other chemicals were purchased from commercial, ketamine hydrochloride (KET, Fagron), serotonin hydrochloride (5HT, Alfa Aesar), ketanserin (KETSN, ApexBio), tryptamine(ACROS).

Chemistry (General)

All reagents were obtained from commercial sources and were used without purification unless otherwise noted. DMSO was purified by passage under 12 psi N_2 through activated alumina columns. Reactions were performed using glassware that was flame-dried under reduced pressure (~1 Torr). Chromatography was performed using Fisher Chemical Silica Gel Sorbent (230−400 mesh, grade 60). Compounds purified by chromatography were dissolved in a minimal amount of chloroform for loading. Thin-layer chromatography (TLC) was performed on Millipore silica gel 60 F254 plates. Visualization of the developed chromatogram was accomplished by fluorescence quenching or by staining with ninhydrin.

Nuclear magnetic resonance (NMR) spectra were acquired on either a Bruker 400 operating at 400 and 100 MHz, a Varian 600 operating at 600 and 150 MHz, or a Bruker 800 operating at 800 and 200 MHz for 1H and 13C, respectively, and are referenced internally according to residual solvent signals. Data for ^{1}H NMR are recorded as follows: chemical shift (δ, ppm), multiplicity (s, singlet; d, doublet; t, triplet; q, quartet; m, multiplet), integration, coupling constants (Hz). Data for ^{13}C NMR are reported in terms of chemical shift (δ, ppm). Infrared spectra were recorded using a Thermo Nicolet iS10 Fourier transform infrared (FT-IR) spectrometer with a Smart iTX Accessory [diamond attenuated total reflection (ATR)] and are reported in the frequency of absorption (v, cm^{-1}). Liquid chromatography−mass spectrometry (LC−MS) was performed using a Waters LC−MS with an ACQUITY Arc QDa detector. Ketamine was purchased from Fagron. DMT (**1**) and 6-F-DMT (**29**) were synthesized using previously published methods [purity >99% as determined by ultra-high-performance liquid chromatography (UHPLC)]. For cellular plasticity assays (i.e., dendritogenesis), all compounds were dissolved in DMSO and stored as 10 mM stock solutions in the dark at −20 °C.

All compounds tested in cellular assays were confirmed to be of >95% purity based on UHPLC analysis (Waters ACQUITY Arc) measuring absorbance at 254 and 280 nm. Mobile phase A consisted of 0.01% formic acid in water, and mobile phase B consisted of 0.01% formic acid in acetonitrile. All samples were injected at a volume of 5 µL, and the column temperature was maintained at 40 °C. One of the three methods was used depending on the specific compound. Method A utilized a CORTECS C18, 2.7 µm, 4.6 × 50 mm2 column, a flow rate of 0.6 mL/min, and a gradient from 10 to 90% mobile phase B over 3 min, which was maintained for an additional 2 min. Method B utilized an XBridge BEH C18 2.5 µm, 2.1 × 100 mm2 column, a flow rate of 0.6 mL/min, and a gradient from 10 to 90% mobile phase B over 0.5 min, which was maintained for an additional 4.5 min. Method C utilized a CORTECS C18, 2.7 µm, 4.6 × 50 mm^2 column, a flow rate of 0.2 mL/min, and a gradient from 10 to 90% mobile phase B over 4 min, which was maintained for an additional 2 min. As most compounds reported in this study were isolated as the fumarate salts, peaks in UHPLC traces corresponding to fumaric acid were not included in the calculation of purity.

Synthesis of isoDMTs. To a solution of respective indole or related heterocycle in DMSO (0.4 M) were added 2-chloro-N, Ndimethylethylamine hydrochloride (1.1 equiv), potassium iodide (1.1 equiv), and potassium hydroxide pellets (5.0 equiv). The reaction was stirred at room temperature for 24 h before being diluted with 1.0 M $NaOH_{(aq)}$. The aqueous phase was extracted three times with dichloromethane (DCM). The organic extracts were combined, dried over Na_2SO_4, filtered, and concentrated under reduced pressure to yield an oil. The unpurified oil was dissolved in a minimal amount of acetone and added dropwise to a boiling solution of fumaric acid (1.0 equiv) in acetone. In most cases, a precipitate formed immediately, which was stored at −20 °C overnight. The resulting crystals were filtered and washed with several portions of ice-cold acetone to yield the desired product. In cases where the desired product did not readily crystalize as the fumarate salt, the oil was subjected to column chromatography (9:1 CH_2Cl_2/MeOH/1% $NH_4OH_{(aq)}$) unless noted otherwise.

2-(1H-Indol-1-yl)-*N,N*-dimethylethan-1-amine Fumarate Salt (1:1) (2). Reaction performed using indole (100 mg, 0.85 mmol) and purified via crystallization. Yield = 175 mg, 67%. Purity >99%. TLC R_f (free base) = 0.66 (9:1 CH_2Cl_2/MeOH/ 1% $NH_4OH_{(aq)}$); ^{1}H NMR (600 MHz, DMSO-d_6) δ 7.54 (d, 1H, J = 7.6 Hz), 7.48 (d, 1H, J = 7.6 Hz), 7.38 (d, 1H, J = 3.1 Hz), 7.13 (ddd, 1H, J = 7.6, 1.0 Hz), 7.01 (dd, 1H, J = 7.6, 1.0 Hz),

6.61 (s, 2H), 6.42 (d, 1H J = 3.1 Hz), 4.29 (t, 2H, J = 6.7 Hz), 2.70 (t, 2H, J = 6.7 Hz), 2.26 (s, 6H) ppm; ^{13}C NMR (150 MHz, DMSO-d_6) δ 166.32, 135.66, 134.20, 128.82, 128.06, 120.96, 120.38, 118.88, 109.68, 100.54, 58.09, 44.83, 43.11 ppm; IR (diamond, ATR) v 3100, 2923, 2393, 1705 cm^{-1} ; low-resolution mass spectrometry (LRMS) (ES+) calcd for C12H16N2 + 188.13, found 189.38 (MH+); mp = 147−149 °C.

2-(4-Methoxy-1H-indol-1-yl)-*N,N*-dimethylethan-1-amine Fumarate Salt (1:1) (4). Reaction performed using 4-methoxyindole (100 mg, 0.68 mmol) and purified via crystallization. Yield = 95 mg, 42%. Purity = 96%. TLC R_f (free base) = 0.35 (9:1 CH_2Cl_2/MeOH/ 1% $NH_4OH_{(aq)}$); ^{1}H NMR (600 MHz, DMSO-d_6) δ 7.26 (d, 1H, J = 3.1 Hz), 7.10 (d, 1H, J = 7.8 Hz), 6.90 (t, 1H, J = 7.8 Hz), 6.66 (d, 1H, J = 7.8 Hz), 6.60 (s, 2H), 6.35 (d, 1H, J = 3.1 Hz), 4.49 (t, 2H, J = 7.0 Hz), 3.89 (s, 3H), 2.76 (t, 2H, J = 7.0 Hz), 2.32 (s, 6H) ppm; ^{13}C NMR (150 MHz, DMSO-d_6) δ 166.30, 146.96, 134.17, 130.46, 129.79, 124.94, 119.64, 113.33, 102.42, 100.93, 59.61, 55.32, 45.63, 44.63 ppm; IR (diamond, ATR) v 2929, 2455, 1712, 1644 cm^{-1}. LRMS (ES+) calcd for $C_{13}H_{18}N_2O^+$ 219.15, found 220.33 (MH^+); mp = 140−145 °C.

2-(5-Methoxy-1H-indol-1-yl)-*N,N*-dimethylethan-1-amine Fumarate Salt (1:1) (5). Reaction performed using 5-methoxyindole (100 mg, 0.68 mmol) and purified via crystallization. Yield = 111 mg, 49%. Purity = 98%. TLC R_f (free base) = 0.66 (9:1 CH_2Cl_2/MeOH/ 1% $NH_4OH_{(aq)}$); ^{1}H NMR (600 MHz, DMSO-d_6) δ 7.38 (d, 1H, J = 8.9 Hz), 7.33 (d, 1H, J = 3.0 Hz), 7.04 (d, 1H, J = 2.4 Hz), 6.77 (dd, 1H, J = 8.9, 2.4 Hz), 6.6 (s, 2H), 6.33 (d, 1H, J = 3.0 Hz), 4.29 (t, 2H, J = 6.8 Hz), 3.74 (s, 3H), 2.79 (t, 2H, J = 6.8 Hz), 2.30 (s, 6H) ppm; ^{13}C NMR (150 MHz, DMSO-d_6) δ 166.58, 153.42, 134.32, 130.90, 129.20, 128.48, 111.12, 110.39, 102.13, 100.34, 57.68, 55.30, 44.44, 42.91 ppm; IR (diamond, ATR) v 3035, 2923, 2446, 1715 cm^{-1}. LRMS (ES+) calcd for $C_{13}H_{18}N_2O^+$ 219.15, found 220.19 (MH^+); mp = 140−142 °C.

2-(6-Methoxy-1H-indol-1-yl)-*N,N*-dimethylethan-1-amine (6). Reaction performed using 6-methoxyindole (147 mg, 1.0 mmol) and purified via chromatography. Yield = 148 mg, 68%. Purity >99%. TLC Rf (free base) = 0.32 (9:1 CH_2Cl_2/MeOH/ 1% $NH_4OH_{(aq)}$); ^{1}H NMR (600 MHz, $CDCl_3$) δ 7.49 (d, 1H, J = 7.8 Hz), 7.02 (d, 1H, J = 8.2 Hz), 6.82 (s, 2H), 6.78 (dd, 1H, J = 7.5 Hz), 6.42 (d, 1H, J = 7.8 Hz), 4.17 (t, 2H, J = 7.0 Hz), 2.31 (s, 3H), 2.69 (t, 2H, J = 7.0 Hz), 2.31 (s, 6H) ppm; ^{13}C NMR (150 MHz, $CDCl_3$) δ

156.30, 136.77, 127.04, 123.00, 121.67, 109.22, 101.31, 93.14, 59.00, 55.91, 45.94, 44.91 ppm; IR (diamond, ATR) *v* 2940, 2859, 2769, 1602 cm^{-1}. LRMS (ES+) calcd for $C_{13}H_{18}N_2O^+$ 219.15, found 220.33 (MH^+). The free base was used for dendritogenesis assays.

2-(6-Methoxy-1H-indol-1-yl)-*N,N*-dimethylethan-1-amine Oxalate (6). Reaction performed using 6-methoxyindole (250 mg, 1.7 mmol) and purified via crystallization. Yield = 221 mg, 42%. Purity = 98%. ^1H NMR (600 MHz, CD_3OD) δ 7.42 (d, 1H, *J* = 8.5 Hz), 7.16 (d, 1H, *J* = 2.9 Hz), 7.02 (s, 2H), 6.74 (d, 1H, *J* = 8.5 Hz), 6.44 (d, 1H, *J* = 2.9 Hz), 4.58 (t, 2H, *J* = 6.8 Hz), 3.87 (s, 3H), 3.56 (t, 2H, *J* = 7.0 Hz), 2.86 (s, 6H) ppm; ^{13}C NMR (150 MHz, CD_3OD) δ 166.72, 158.20, 138.02, 127.52, 124.45, 122.61, 111.06, 103.58, 93.83, 57.22, 56.19, 44.04, 42.17 ppm; IR (diamond, ATR) *v* 3129, 3014, 2641, 1727 cm^{-1}. LRMS (ES+) calcd for $C_{13}H_{18}N_2O^+$ 219.15, found 220.05 (MH^+); mp = 165−167 °C. The oxalate salt was used for HTR assays.

2-(7-Methoxy-1H-indol-1-yl)-*N,N*-dimethylethan-1-amine Fumarate Salt (1:1) (7). Reaction performed using 7-methoxyindole (100 mg, 0.68 mmol) and purified via crystallization. Yield = 162 mg, 72%. Purity >99%. TLC R_f (free base) = 0.44 (9:1 CH_2Cl_2/MeOH/ 1% $NH_4OH_{(aq)}$); ^1H NMR (600 MHz, DMSO-d_6) δ 7.26 (d, 1H, *J* = 3.1 Hz), 7.09−7.03 (m, 2H), 6.60 (s, 2H), 6.52 (dd, 1H, *J* = 6.1, 1.3 Hz), 6.41 (dd, 1H, *J* = 3.0, 0.7 Hz), 4.29 (t, 2H, *J* = 6.8 Hz), 3.86 (s, 3H), 2.75 (t, 2H, *J* = 6.8 Hz), 2.29 (s, 6H) ppm; ^{13}C NMR (150 MHz, DMSO-d_6) δ 166.46, 152.80, 137.02, 134.24, 127.14, 121.98, 118.38, 103.09, 99.16, 97.88, 57.83, 54.89, 44.60, 43.15 ppm; IR (diamond, ATR) *v* 3435, 3034, 2653, 1705 cm^{-1}. LRMS (ES+) calcd for $C_{13}H_{18}N_2O^+$ 219.15, found 220.40 (MH^+); mp 120−123 °C.

Benzyloxy Indoles. The 4-, 5-, 6-, and 7-OBn indoles were synthesized using methods published previously.[28]

[28] Buemi, M. R.; De Luca, L.; Chimirri, A.; Ferro, S.; Gitto, R.; Alvarez-Builla, J.; Alajarin, R. Indole Derivatives as Dual-Effective Agents for the Treatment of Neurodegenerative Diseases: Synthesis, Biological Evaluation, and Molecular Modeling Studies. Bioorg. Med. Chem. 2013, 21, 4575−4580

2-(4-(Benzyloxy)-1H-indol-1-yl)-*N,N*-dimethylethan-1- amine Fumarate Salt (1:1) (8). Reaction performed using 4- benzyloxyindole (200 mg, 0.89 mmol) and purified via crystallization. Yield = 120 mg, 46%. Purity >99%. TLC R_f (free base) = 0.42 (9:1 CH_2Cl_2/MeOH/1% $NH_4OH_{(aq)}$); ^{1}H NMR (400 MHz, CD_3OD) δ 7.49 (d, 2H, *J* = 7.5 Hz), 7.37 (t, 2H, *J* = 7.5 Hz), 7.31 (t, 1H, *J* = 7.5 Hz), 7.20 (d, 1H, *J* = 3.26 Hz), 7.12 (m, 2H), 6.72 (s, 1H), 6.66 (m, 1H), 5.22 (s, 2H), 4.57 (t, 2H, J = 6.7 Hz), 3.50 (t, 2H, *J* = 6.7 Hz), 2.81 (s, 6H) ppm; ^{13}C NMR (100 MHz, CD_3OD) δ 169.90, 153.99, 139.05, 138.85, 135.75, 129.47, 128.78, 128.47, 127.21, 124.18, 121.16, 103.87, 102.67, 101.07, 70.95, 57.32, 43.90, 42.46 ppm; IR (diamond, ATR) *v* 2918, 2493, 1701, 1639 cm^{-1}. LRMS (ES+) calcd for $C_{19}H_{22}N_2O^+$ 294.17, found 295.24 (MH^+); mp = 145−150 °C.

2-(5-(Benzyloxy)-1H-indol-1-yl)-*N,N*-dimethylethan-1- amine Fumarate Salt (1:1) (9). Reaction performed using 5- benzyloxyindole (287 mg, 1.3 mmol) and purified via crystallization. Yield = 133 mg, 25%. Purity >99%. TLC R_f (free base) = 0.47 (9:1 CH_2Cl_2/MeOH/1% $NH_4OH_{(aq)}$); ^{1}H NMR (400 MHz, CD_3OD) δ 7.44 (d, 2H, *J* = 7.5 Hz), 7.36 (m, 3H), 7.29 (d, 2H, *J* = 7.5 Hz), 7.24 (d, 1H, *J* = 3.2 Hz), 7.15 (d, 1H, *J* = 2.4 Hz), 6.95 (dd, 1H, *J* = 2.4, 8.9 Hz), 6.72 (s, 2H), 6.43 (d, 1H, *J* = 3.2 Hz), 5.07 (s, 2H), 4.54 (t, 2H, *J* = 6.8 Hz), 3.45 (t, 2H, *J* = 6.8 Hz), 2.78 (s, 6H) ppm; ^{13}C NMR (200 MHz, CD_3OD) δ 171.06, 154.78, 139.26, 136.11, 132.77, 130.89, 130.81, 129.44, 128.73, 128.61, 113.97, 110.95, 105.71, 103.24, 71.86, 57.66, 44.16, 42.77 ppm; IR (diamond, ATR) *v* 2916, 2516, 1698, 1639 cm^{-1}. LRMS (ES+) calcd for $C_{19}H_{22}N_2O^+$ 294.17, found 295.17 (MH^+); mp = 133−135 °C.

2-(6-(Benzyloxy)-1H-indol-1-yl)-*N,N*-dimethylethan-1- amine (10). Reaction performed using 6-benzyloxyindole (370 mg, 1.7 mmol) and purified via chromatography. Yield = 184 mg, 38%. Purity >97%. TLC R_f (free base) = 0.45 (9:1 CH_2Cl_2/MeOH/1% $NH_4OH_{(aq)}$); ^{1}H NMR (600 MHz, CD_3OD) δ 7.47 (d, 2H, *J* = 7.4 Hz), 7.40 (d, 2H, *J* = 8.6 Hz), 7.37 (t, 1H *J* = 7.4 Hz), 7.30 (t, 1H, *J* = 7.4 Hz), 7.08 (d, 1H, *J* = 3.8 Hz), 6.96 (s, 1H), 6.78 (d, 1H, *J* = 8.6 Hz), 6.35 (d, 1H, *J* = 3.8 Hz), 5.15 (s, 2H), 4.22 (t, 2H, *J* = 7.3 Hz), 2.66 (t, 2H, *J* = 7.3 Hz), 2.26 (s, 6H) ppm; ^{13}C NMR (150 MHz, $CDCl_3$) δ 156.39, 137.60, 136.66, 128.69, 127.97, 127.67, 127.22, 123.24, 121.68, 109.95, 101.31, 94.71, 70.87, 58.92, 45.91, 44.90 ppm; IR (diamond, ATR) *v* 3030, 2952, 2768, 1621 cm^{-1}. LRMS (ES+) calcd for $C_{19}H_{22}N_2O^+$ 294.17, found 295.10 (MH^+).

2-(7-(Benzyloxy)-1H-indol-1-yl)-*N,N*-dimethylethan-1- amine (11). Reaction performed using 7-benzyloxyindole (119 mg, 0.53 mmol) and purified via chromatography. Yield = 51 mg, 23%. Purity >99%. TLC R_f (free base) = 0.48 (9:1 CH_2Cl_2/MeOH/1% $NH_4OH_{(aq)}$); ^{1}H NMR (600 MHz, $CDCl_3$) δ 7.49 (d, 2H, *J* = 7.4 Hz), 7.40 (t, 2H, *J* = 7.4 Hz), 7.34 (t, 1H, *J* = 7.4 Hz), 7.22 (d, 1H, *J* = 7.9 Hz), 7.01 (d, 1H, *J* = 3.0 Hz), 6.97 (t, 1H, *J* = 7.8 Hz), 6.70 (d, 1H, *J* = 7.8 Hz), 5.19 (s, 2H), 4.45 (t, 2H, *J* = 7.4 Hz), 2.62 (t, 2H, *J* = 7.4 Hz), 2.09 (s, 6H) ppm; ^{13}C NMR (150 MHz, $CDCl_3$) δ 150.59, 146.71, 137.11, 131.25, 129.45, 128.75, 128.24, 128.15, 119.82, 114.16, 103.35, 101.60, 70.55, 61.02, 47.54, 45.64 ppm; IR (diamond, ATR) *v* 2940, 2821, 1575, 1439 cm^{-1}. LRMS (ES+) calcd for $C_{19}H_{22}N_2O^+$ 294.17, found 295.24 (MH^+).

2-(4-Fluoro-1H-indol-1-yl)-*N,N*-dimethylethan-1-amine Fumarate Salt (1:1) (12). Reaction performed using 4-fluoroindole (135 mg, 1.0 mmol) and purified via crystallization. Yield = 164 mg, 51%. Purity >99%. TLC R_f (free base) = 0.39 (9:1 CH_2Cl_2/MeOH/ 1% $NH_4OH_{(aq)}$); ^{1}H NMR (400 MHz, DMSO-d_6) δ 7.44 (d, 1H, *J* = 2.3 Hz), 7.35 (d, 2H, *J* = 8.3 Hz), 7.10 (dd, 2H, *J* = 7.4, 7.25 Hz), 6.79 (t, 2H, *J* = 9.5 Hz), 6.60 (s, 2H), 6.49 (d, 2H, *J* = 2.3 Hz), 4.32 (t, 2H, *J* = 6.7 Hz), 2.74 (t, 2H, *J* = 6.8 Hz), 2.28 (s, 6H) ppm; ^{13}C NMR (150 MHz, DMSO-d_6) δ 166.37, 156.67, 154.34, 138.56, 138.44, 134.21, 129.35, 121.63, 121.55, 116.74, 116.51, 106.48, 106.45, 103.70, 103.51, 96.24, 57.90, 44.73, 43.40 ppm; IR (diamond, ATR) *v* 3123, 2389, 1702, 1660 cm^{-1}. LRMS (ES+) calcd for $C_{12}H_{16}FN_2^+$ 207.13, found 208.32 (MH^+); mp = 145−149 °C.

2-(5-Fluoro-1H-indol-1-yl)-*N,N*-dimethylethan-1-amine Fumarate Salt (1:1) (13). Reaction performed using 5-fluoroindole (135 mg, 1.0 mmol) and purified via crystallization. Yield = 145 mg, 45%. Purity >99%. TLC R_f (free base) = 0.35 (9:1 CH_2Cl_2/MeOH/ 1% $NH_4OH_{(aq)}$); ^{1}H NMR (400 MHz, DMSO-d_6) δ 7.50 (dd, 1H, *J* = 4.5, 4.3 Hz), 7.46 (d, 1H, *J* = 2.1 Hz), 7.29 (d, 1H, *J* = 9.5 Hz), 6.97 (t, 1H, *J* = 9.5 Hz), 6.60 (s, 2H), 6.41 (d, 1H, *J* = 2.1 Hz), 4.32 (t, 2H, *J* = 6.7 Hz), 2.79 (t, 2H, *J* = 6.7 Hz), 2.31 (s, 6H) ppm; ^{13}C NMR (150 MHz, DMSO-d_6) δ 166.59, 159.61, 158.06, 135.77, 135.69, 134.33, 129.54, 129.51, 124.72, 121.39, 121.32, 107.48, 107.32, 100.97, 96.32, 96.15, 57.66, 44.58, 43.00 ppm; IR (diamond, ATR) *v* 3036, 2049, 1723, 1663 cm^{-1}. LRMS (ES+) calcd for $C_{12}H_{16}FN_2^+$ 207.13, found 207.40 (MH^+); mp = 145−148 °C.

2-(6-Fluoro-1H-indol-1-yl)-*N,N*-dimethylethan-1-amine Fumarate Salt (1:1) (14). Reaction performed using 6-fluoroindole (100 mg, 0.739 mmol) and purified via crystallization. Yield = 145 mg, 61%. Purity = 97%. TLC R_f (free base) = 0.45 (9:1 CH_2Cl_2/ MeOH/1% $NH_4OH_{(aq)}$); ^{1}H NMR (600 MHz, DMSO-d_6) δ 7.52 (dd, 1H, *J* = 7.0, 3.0 Hz), 7.39−7.37 (m, 2H), 6.88−6.85 (m, 1H), 6.59 (s, 2H), 6.44 (d, 1H, *J* = 3.1 Hz), 4.29 (t, 2H, *J* = 6.8 Hz), 2.77 (t, 2H, *J* = 6.8 Hz), 2.30 (s, 6H) ppm; ^{13}C NMR (150 MHz, DMSO-d_6) δ 166.59, 159.61, 158.06, 136.16, 134.75, 129.95, 125.14, 121.78, 107.91, 107.74, 101.39, 96.74, 96.57, 57.66, 44.58, 43.00 ppm; IR (diamond, ATR) *v* 3058, 2385, 1698, 1634 cm^{-1}. LRMS (ES+) calcd for $C_{12}H_{16}FN_2^+$ 207.13, found 208.39 (MH^+); mp = 141−147 °C.

2-(7-Fluoro-1H-indol-1-yl)-*N,N*-dimethylethan-1-amine Fumarate Salt (1:1) (15). Reaction performed using 7-fluoroindole (135 mg, 1.0 mmol) and purified via crystallization. Yield = 172 mg, 53%. Purity = 98%. TLC R_f (free base) = 0.45 (9:1 CH_2Cl_2/MeOH/ 1% $NH_4OH_{(aq)}$); ^{1}H NMR (400 MHz, DMSO-d_6) δ 7.41 (s, 1H), 7.35 (d, 1H, *J* = 7.6 Hz), 6.98−6.88 (m, 2H), 6.61 (s, 2H), 6.48 (s, 1H,), 4.37 (t, 2H, *J* = 6.7 Hz), 2.69 (t, 2H, *J* = 6.7 Hz), 2.23 (s, 6H) ppm; ^{13}C NMR (100 MHz, CD_3OD) δ 169.37, 134.60, 133.26, 129.51, 119.90, 119.46, 116.82, 116.79, 107.06, 106.88, 102.78, 57.61, 57.61, 43.71, 43.67, 42.90 ppm; IR (diamond, ATR) *v* 3040, 2429, 1718, 1661 cm^{-1}. LRMS (ES+) calcd for $C_{12}H_{16}FN_2^+$ 207.13, found 207.33 (MH^+); mp = 168−170 °C.

***N,N*-Dimethyl-2-(2-methyl-1H-indol-1-yl)ethan-1-amine Fumarate Salt (1:1) (16).** Reaction performed using 2-methylindole (100 mg, 0.76 mmol) and purified via crystallization. Yield (172 mg, 71%). Purity >99%. TLC R_f (free base) = 0.47 (9:1 CH_2Cl_2/MeOH/ 1% $NH_4OH_{(aq)}$); ^{1}H NMR (400 MHz, DMSO-d_6) δ 7.41 (d, 1H, *J* = 7.8 Hz), 7.37 (d, 1H, *J* = 7.8 Hz), 7.06 (t, 1H, *J* = 7.8 Hz), 6.96 (t, 1H, *J* = 7.8 Hz), 6.61 (s, 2H), 6.20 (d, *J* = 1.3 Hz, 1H), 4.24 (t, 2H, *J* = 7.0 Hz), 2.65 (t, 2H, *J* = 7.0 Hz), 2.42 (s, 3H), 2.31 (s, 6H) ppm; ^{13}C NMR (150 MHz, DMSO-d_6) δ 167.03, 137.08, 136.72, 134.75, 128.09, 120.58, 119.65, 119.62, 119.40, 109.61, 100.14, 57.82, 45.18, 12.76 ppm; IR (diamond, ATR) *v* 3040, 2489, 1700, 1606 cm^{-1}. LRMS (ES+) calcd for $C_{13}H_{18}N_2^+$ 203.15, found 204.43 (MH^+); mp = 131−133 °C.

2-(5,6-Difluoro-1H-indol-1-yl)-*N,N*-dimethylethan-1-amine Fumarate Salt (1:1) (17). Reaction performed using 5,6- difluoroindole (153 mg, 1.0 mmol) and purified via crystallization. Yield = 147 mg, 43%. Purity = 98%. TLC R_f (free base) = 0.35 (9:1 CH_2Cl_2/MeOH/1% $NH_4OH_{(aq)}$); ^{1}H NMR (400 MHz, DMSO-d_6) δ 7.64 (dd, 1H, *J* = 7.0, 4.7 Hz), 7.51 (dd, 1H, *J* = 8.5, 2.1 Hz), 7.45 (d, 1H, *J* = 2.1 Hz), 6.60 (s, 2H), 6.43 (d, 1H, *J* = 2.1 Hz), 4.28 (t, 2H, *J* = 6.5 Hz), 2.73 (t, 2H, *J* = 6.5 Hz), 2.27 (s, 6H) ppm; ^{13}C NMR (150 MHz, DMSO-d_6) δ 166.37, 134.21, 131.09, 130.99, 134.70, 130.67, 123.21, 123.12, 106.86, 106.67, 100.98, 100.94, 98.30, 98.08, 57.86, 44.71, 43.36 ppm; IR (diamond, ATR) *v* 3051, 2392, 1712, 1658 cm−1 . LRMS (ES+) calcd for $C_{12}H_{16}F_2N_2^+$ 224.11, found 225.28 (MH^+); mp = 162−165 °C.

2-(4,6-Difluoro-1H-indol-1-yl)-*N,N*-dimethylethan-1-amine Fumarate Salt (1:1) (18). Reaction performed using 4,6- difluoroindole (153 mg, 1.0 mmol) and purified via crystallization. Yield = 265 mg, 78%. Purity >99%. TLC R_f (free base) = 0.35 (9:1 CH_2Cl_2/MeOH/1% $NH_4OH_{(aq)}$); ^{1}H NMR (400 MHz, DMSO-d_6) δ 7.44 (d, 1H, *J* = 2.8 Hz), 7.32 (d, 1H, *J* = 10.1 Hz), 6.83 (t, 1H, *J* = 10.1 Hz), 6.60 (s, 2H), 6.49 (d, 1H, *J* = 2.8 Hz), 4.31 (t, 2H, *J* = 6.6 Hz), 2.78 (t, 2H, *J* = 6.6 Hz), 2.31 (s, 6H) ppm; ^{13}C NMR (150 MHz, DMSO-d_6) δ 166.55, 159.33, 159.21, 156.99, 156.87, 156.03, 155.88, 153.58, 153.43, 137.50, 137.36, 137.22, 134.29, 129.82, 129.79, 113.42, 113.20, 96.61, 94.53, 94.30, 94.24, 94.00, 93.32, 93.28, 93.06, 93.02, 57.49, 44.49, 43.23 ppm; IR (diamond, ATR) *v* 3026, 2398, 1706, 1640 cm^{-1}. LRMS (ES+) calcd for $C_{12}H_{16}F_2N_2^+$ 224.11, found 225.28 (MH^+); mp = 141−145 °C.

***N,N*-Dimethyl-2-(6-nitro-1H-indol-1-yl)ethan-1-amine Fumarate Salt (1:1) (19).** Reaction performed using 6-nitroindole (43.6 mg, 0.269 mmol) and purified via crystallization. Yield = 52 mg, 55%. Purity >96%. TLC R_f (free base) = 0.48 (9:1 CH_2Cl_2/MeOH/ 1% $NH_4OH_{(aq)}$); ^{1}H NMR (400 MHz, DMSO-d_6) δ 8.54 (d, 1H, *J* = 2.0 Hz), 7.90 (dd, 1H, *J* = 8.8, 2.0 Hz), 7.82 (d, 1H, *J* = 3.0 Hz), 7.72 (d, 1H, *J* = 8.8 Hz), 7.74 (s, 1H), 6.65 (d, 1H, *J* = 3.0 Hz), 6.60 (s, 2H), 4.44 (t, 2H, *J* = 6.3 Hz), 2.68 (t, 2H, *J* = 6.3 Hz), 2.23 (s, 6H) ppm; ^{13}C NMR (600 MHz, DMSO-d_6) δ 166.66, 136.18, 134.76, 134.59, 133.41, 121.04, 114.52, 107.53, 102.25, 58.98, 45.50, 44.18 ppm; IR (diamond, ATR) *v* 3048, 2922, 1704, 1607 cm^{-1}. LRMS (ES +) calcd for $C_{12}H_{16}N_3O_2^+$ 233.12, found 234.25 (MH^+); mp = 159− 164 °C.

2-(5-Bromo-1H-indol-1-yl)-*N,N*-dimethylethan-1-amine Fumarate Salt (1:1) (20). Reaction performed using 5-bromoindole (56.1 mg, 0.281 mmol) and purified via crystallization. Yield = 60 mg, 55%. Purity >99%. TLC R_f (free base) = 0.49 (9:1 CH_2Cl_2/MeOH/ 1% $NH_4OH_{(aq)}$); ^{1}H NMR (600 MHz, DMSO-d_6) δ 7.72 (d, *J* = 1.9 Hz, 1H), 7.48 (d, 1H, *J* = 8.7 Hz), 7.44 (d, 1H, *J* = 3.1 Hz), 7.23 (dd, 1H, *J* = 8.7, 1.9 Hz), 6.60 (s, 3H), 6.41 (d, 1H, *J* = 3.1 Hz), 4.27 (t, 2H, *J* = 6.6 Hz), 2.67 (t, 2H, *J* = 6.6 Hz), 2.22 (s, 6H) ppm; ^{13}C NMR (600 MHz, DMSO-d_6) δ 166.24, 134.47, 134.15, 130.46, 129.89, 123.81, 122.54, 111.87, 111.56, 100.28, 58.09, 44.86, 43.32 ppm; IR (diamond, ATR) *v* 2959, 2443, 1705, 1661 cm^{-1}. LRMS (ES+) calcd for $C_{12}H_{16}BrN_2^+$ 266.04, found 267.26 (MH^+); mp = 140−142 °C.

2-(1-(2-(Dimethylamino)ethyl)-1H-indol-3-yl)-*N,N*-dimethyl2-oxoacetamide (21). Reaction performed using 2-(1H-indol-3-yl)- N,N-dimethyl-2-oxoacetamide (synthesized using the method developed by Speeter et. al.)18 (200 mg, 0.92 mmol) and purified via chromatography. Yield = 92 mg, 35%. Purity = 98%. TLC R_f (free base) = 0.38 (9:1 CH_2Cl_2/MeOH/1% $NH_4OH_{(aq)}$); ^{1}H NMR (600 MHz, $CDCl_3$) δ 8.32 (s, 1H), 7.92 (s, 1H), 7.37−7.29 (m, 3H), 4.21 (t, 2H, *J* = 7.0 Hz), 3.08 (s, 3H), 3.04 (s, 3H), 2.71 (t, 2H, *J* = 7.0 Hz), 2.27 (s, 6H) ppm; ^{13}C NMR (150 MHz, $CDCl_3$) δ 185.64, 167.70, 138.82, 137.01, 126.36, 124.00, 123.28, 122.48, 113.45, 110.06, 58.40, 45.68 45.42, 37.59, 34.51 ppm; IR (diamond, ATR) *v* 2981, 1734 1631, 1525 cm^{-1}. LRMS (ES+) calcd for $C_{16}H_{21}N_3O_2^+$ 287.16, found 288.25 (MH^+).

2-(1H-Benzo[d]imidazol-1-yl)-*N,N*-dimethylethan-1-amine Fumarate Salt (1:1) (22). Reaction performed using benzimidazole (200 mg, 1.6 mmol) and purified via crystallization. Yield = 218 mg, 45%. Purity = 98%. TLC *Rf* (free base) = 0.42 (9:1 CH_2Cl_2/MeOH/ 1% $NH_4OH_{(aq)}$); ^{1}H NMR (400 MHz, DMSO-d_6) δ 8.23 (s, 1H), 7.71−7.56 (m, 2H), 7.34−7.10 (m, 2H), 6.61 (s, 2H), 4.41 (t, 2H, *J* = 6.5 Hz), 2.83 (dd, 2H, *J* = 7.0, 6.0 Hz), 2.32 (s, 6H) ppm; ^{13}C NMR (100 MHz, CD_3OD) δ 170.14, 144.78, 143.90, 135.81, 134.62, 124.80, 124.04, 120.36, 111.29, 57.46, 44.39, 41.80 ppm; IR (diamond, ATR) *v* 3054, 2384, 1707, 1654 cm^{-1}. LRMS (ES+) calcd for $C_{11}H_{15}N_3^+$ 189.13, found 190.23 (MH^+); mp = 171−178 °C.

***N,N*-Dimethyl-2-(1H-pyrrol-1-yl)ethan-1-amine Fumarate Salt (1:1) (23).** Reaction performed using pyrrole (0.103 mL, 1.5 mmol) and purified via crystallization. Yield = 126 mg, 33%. Purity >99%. TLC R_f

(free base) = 0.45 (9:1 CH_2Cl_2/MeOH/1% $NH_4OH_{(aq)}$); ^{1}H NMR (600 MHz, CD_3OD) δ 6.80 (t, 2H, *J* = 2.2, Hz), 6.72 (s, 2H), 6.14 (t, 2H. *J* = 2.2, Hz), 4.34 (t, 2H, *J* = 6.4 Hz), 3.50 (dd, 2H, *J* = 6.4 Hz), 2.78 (s, 6H) ppm; ^{13}C NMR (100 MHz, CD_3OD) δ 170.26, 136.21, 122.18, 110.89, 59.35, 45.83, 44.45 ppm; IR (diamond, ATR) *v* 2998, 2532, 1662, 1421 cm^{-1}. LRMS (ES+) calcd for $C_8H_{14}N_2^+$ 138.12, found 139.29 (MH^+); mp = 174−180 °C.

2-(9H-Carbazol-9-yl)-*N,N*-dimethylethan-1-amine Fumarate Salt (1:1) (24). Reaction performed using carbazole (100 mg, 0.57 mmol) and purified via crystallization. Yield = 102 mg, 51%. Purity >99%. TLC R_f (free base) = 0.42 (9:1 CH_2Cl_2/MeOH/1% $NH_4OH_{(aq)}$); ^{1}H NMR (600 MHz, DMSO-d_6) δ 8.15 (d, 2H, *J* = 7.8 Hz), 7.61 (d, 2H, *J* = 8.2 Hz), 7.48−7.44 (m, 2H), 7.23−7.19 (m, 2H), 6.61 (s, 2H), 4.52 (t, 2H, *J* = 7.0 Hz), 2.73 (t, 2H, *J* = 7.0 Hz), 2.31 (s, 6H) ppm; ^{13}C NMR (100 MHz, DMSO-d_6) δ 169.78, 139.86, 134.76, 125.83, 123.17, 119.99, 119.39, 108.34, 54.39, 42.61, 37.85 ppm; IR (diamond, ATR) *v* 3053, 2405, 1720, 1660 cm^{-1}. LRMS (ES +) calcd for $C_{16}H_{18}N_2^+$ 238.15, found 239.34 (MH^+); mp = 182−184 °C.

1-Isopentyl-1H-indole (25). Reaction performed using indole (100 mg, 0.85 mmol) and 1-chloro-3-methylbutane (0.11 mL mg, 0.94 mmol, 1.1 equiv) and purified via chromatography (4:1 hexanes/ EtOAc). Yield = 85 mg, 53%. Purity = 97%. TLC R_f = 0.70 (7:3 hexanes/EtOAc); ^{1}H NMR (600 MHz, $CDCl_3$) δ 7.65 (d, 1H, *J* = 8.0 Hz), 7.36 (d, 1H, *J* = 8.0 Hz), 7.22 (t, 1H, *J* = 6.9 Hz), 7.11 (m, 2H), 6.49 (d, 1H, *J* = 3.1 Hz), 4.15 (t, 2H, *J* = 7.5 Hz), 1.74 (dd, 2H, *J* = 6.7 Hz), 1.62 (quint, 2H, *J* = 6.7 Hz), 0.98 (d, 1H, *J* = 6.7 Hz) ppm; ^{13}C NMR (150 MHz, $CDCl_3$) δ 135.78, 128.46, 127.58, 121.20, 120.83, 119.05, 109.28, 100.78, 44.44, 40.72, 38.92, 25.61, 22.37 ppm; IR (diamond, ATR) *v* 3054, 2955, 2927, 2869 cm^{-1}. LRMS (ES+) calcd for $C_{13}H_{17}N^+$ 187.14, found 188.39 (MH^+).

3-(1H-Indol-1-yl)-*N,N*-dimethylpropan-1-amine Fumarate Salt (1:1) (26). Reaction performed using indole (100 mg, 0.85 mmol) and 3-chloro-N,N-dimethylpropan-1-amine (160 mg, 0.98 mmol, 1.1 equiv) and purified via crystallization Yield = 107 mg, 48%. Purity = 98%. TLC R_f (free base) = 0.38 (9:1 CH_2Cl_2/MeOH/1% $NH_4OH_{(aq)}$); ^{1}H NMR (600 MHz, DMSO-d_6) δ 7.54 (d, 1H, *J* = 7.8 Hz), 7.48 (d, 1H, *J* = 7.8 Hz), 7.36 (d, 1H, *J* = 3.1 Hz), 7.13 (td, 1H, *J* = 7.4, 1.0 Hz), 7.01 (td, 1H, *J* = 7.4, 1.0 Hz), 6.55 (s, 2H),

6.43 (dd, 1H, *J* = 3.1, 1.0 Hz), 4.21 (t, 2H, *J* = 6.8 Hz), 2.56 (t, 2H, *J* = 7.4 Hz), 2.40 (s, 6H), 2.00 (tt, 2H, *J* = 7.4, 6.8 Hz) ppm; ^{13}C NMR (150 MHz, DMSO-d_6) δ 167.19, 135.60, 134.62, 128.49, 128.07, 120.99, 120.41, 118.90, 109.67, 100.61, 54.88, 43.41, 43.07, 26.26 ppm; IR (diamond, ATR) *v* 3435, 3034, 2653, 1705 cm^{-1}. LRMS (ES+) calcd for $C_{13}H_{18}N_2^+$ 203.15, found 204.36 (MH^+); mp = 129−131 °C.

tert-Butyl (2-(1H-Indol-3-yl)ethyl)carbamate. To an ice-cold solution of tryptamine (0.50 g, 3.1 mmol) and triethylamine (0.68 mL, 9.4 mmol, 3 equiv) in CH2Cl2 (44 mL) was added Boc_2O (0.77 g, 3.7 mmol, 1.2 equiv). The reaction was warmed to room temperature, stirred overnight, and then quenched with H_2O (200 mL). The organic phase was separated, and the aqueous phase was extracted with CH_2Cl_2 (2 × 50 mL). The organic extracts were combined, dried over Na_2SO_4, filtered, and concentrated under reduced pressure to afford an oil that was purified by chromatography on silica gel (8:2 hexanes/EtOAc); white solid (0.69 g, 85%).

***N*-Methyl-2-(1-methyl-1H-indol-3-yl)ethan-1-amine**. To an ice-cold solution of sodium hydride (0.23 g, 5.8 mmol, 2.2 equiv) in dimethylformamide (DMF) (3 mL) was added tert-butyl (2-(1Hindol-3-yl)ethyl)carbamate (0.69 g, 2.6 mmol) in DMF (3 mL). The reaction mixture was allowed to stir at room temperature before being cooled to 0 °C. Methyl iodide (0.4 mL, 5.8 mmol, 2.2 equiv) was added dropwise. The reaction was stirred at room temperature for 20 h. Next, the reaction was cooled to 0 °C, quenched with trifluoroacetic acid (TFA) (2 mL), and stirred for 30 min. The mixture was diluted with 1.0 M $NaOH_{(aq)}$ (600 mL) and extracted with CH_2Cl_2 (3 × 75 mL). The organic phases were combined, dried over Na_2SO_4, filtered, and concentrated under reduced pressure to afford an oil that was used without further purification (0.45 g, 90%).

***N,N*-Dimethyl-2-(1-methyl-1H-indol-3-yl)ethan-1-amine Fumarate Salt (1:1) (1-Me-DMT, 27).** To an ice-cold solution of Nmethyl-2-(1-methyl-1H-indol-3-yl)ethan-1-amine (0.14 g, 0.70 mmol) and glacial acetic acid (0.22 mL, 11 mmol, 5.0 equiv) in MeOH (12 mL) was added sodium cyanoborohydride (0.10 g, 1.6 mmol, 2.1 equiv) followed by 37% $formaldehyde_{(aq)}$ (0.16 mL, 1.9 mmol, 2.6 equiv). The reaction was stirred at room temperature for 5 h before being concentrated under reduced pressure. The unpurified material

was then diluted with CH_2Cl_2 (50 mL) and 1 M $NaOH_{(aq)}$ (100 mL). The phases were separated, and the aqueous phase was extracted with CH_2Cl_2 (2 × 50 mL). The organic extracts were combined, dried over Na_2SO_4, filtered, and concentrated under reduced pressure. The unpurified material was dissolved in acetone (5 mL) and was added to a boiling solution of fumaric acid (0.088 g, 1 mmol, 1 equiv) in acetone (20 mL). A precipitate formed immediately, and the solution was cooled to room temperature prior to being filtered. The resulting white solid was dried under reduced pressure to yield the pure compound as the fumarate salt (1:1). Yield = 0.108 g, 65%. Purity >99%. TLC R_f (free base) = 0.19 (9:1 CH_2Cl_2/MeOH/1% $NH_4OH_{(aq)}$); ^{1}H NMR (600 MHz, CD_3OD) δ 7.60 (d, 1H, *J* = 8.0 Hz), 7.37 (d, 1H, *J* = 8.0 Hz), 7.20 (t, 1H, *J* = 8.0 Hz), 7.14 (s, 1H), 7.09 (t, 1H, *J* = 8.0 Hz), 6.69 (s, 2H), 3.78 (s, 3H), 3.42 (t, 2H, *J* = 7.8 Hz), 3.20 (t, 2H, *J* = 7.8 Hz), 2.91 (s, 6H) ppm; ^{13}C NMR (150 MHz, CD_3OD) δ 171.44, 138.80, 136.23, 128.67, 128.59, 122.95, 120.20, 119.27, 110.53, 109.11, 59.12, 43.41, 32.77, 21.72 ppm; IR (diamond, ATR) *v* 3435, 3034, 2653, 1705 cm^{-1}. LRMS (ES+) m/z calcd for $C_{13}H_{18}N_2^+$ 202.15, found 203.37 (MH^+); mp = 167−170 °C.

2-(5-Methoxy-1H-indol-3-yl)-*N,N*-dimethylethan-1-amine Fumarate Salt (2:1) (5-MeO-DMT, 28). To an ice-cold solution of 5-methoxytryptamine (0.50 g, 2.2 mmol) and glacial acetic acid (0.60 mL, 11 mmol, 5.0 equiv) in MeOH (44 mL) was added sodium cyanoborohydride (0.305 g, 4.8 mmol, 2.2 equiv) followed by 37% $formaldehyde_{(aq)}$ (0.46 mL, 5.7 mmol, 2.6 equiv). The reaction was stirred at room temperature for 5 h before being concentrated under reduced pressure. The residue was diluted with CH_2Cl_2 (50 mL) and 1 M $NaOH_{(aq)}$ (100 mL). The phases were separated, and the aqueous phase was extracted with CH_2Cl_2 (2 × 50 mL). The organic extracts were combined, dried over Na_2SO_4, filtered, and concentrated under reduced pressure. The unpurified material was dissolved in acetone (5 mL) and was added to a boiling solution of fumaric acid (0.26 g, 2.2 mmol, 0.7 equiv) in acetone (35 mL). A precipitate formed immediately, and the solution was cooled to room temperature prior to being filtered. The resulting white solid was dried under reduced pressure to yield the pure compound as the fumarate salt (2:1). Yield = 0.49 g, 80%. Purity = 98%. TLC R_f (free base) = 0.20 (9:1 CH_2Cl_2/MeOH/1% $NH_4OH_{(aq)}$); ^{1}H NMR (600 MHz, CD_3OD) δ 7.24 (d, 1H, *J* = 8.8 Hz), 7.14 (s, 1H), 7.07 (s, 1H), 6.78 (d, 1H, *J* = 8.8 Hz), 6.70 (s, 1H), 3.83 (s, 3H), 3.29 (m, 2H), 3.13 (t, 2H, *J* = 7.9 Hz), 2.83 (s, 6H) ppm; ^{13}C NMR (150 MHz, CD_3OD) δ 174.36, 155.27, 137.09, 133.44, 128.49, 124.79, 113.20, 112.96, 110.05, 101.05, 59.25, 56.37, 43.56, 22.12 ppm; IR (diamond, ATR) *v*

3436, 3034 2654, 1705 cm^{-1}. LRMS (ES+) m/z calcd for $C_{13}H_{18}N_2O^+$ 218.14, found 219.34 (MH^+); mp = 175−177 °C.

2-(6-Methoxy-1H-indol-3-yl)-*N,N*-dimethylethan-1-amine Fumarate Salt (2:1) (6-MeO-DMT, 30). To an ice-cold solution of 6-methoxytryptamine (0.40 g, 2.1 mmol) and glacial acetic acid (0.60 mL, 10 mmol, 5.0 equiv) in MeOH (42 mL) was added sodium cyanoborohydride (0.29 g, 4.6 mmol, 2.2 equiv) followed by 37% formaldehyde$_{(aq)}$ (0.44 mL, 5.5 mmol, 2.6 equiv). The reaction was stirred at room temperature for 5 h before being concentrated under reduced pressure. The residue was diluted with CH_2Cl_2 (45 mL) and 1 M $NaOH_{(aq)}$ (100 mL). The phases were separated, and the aqueous phase was extracted with CH_2Cl_2 (2 × 45 mL). The organic extracts were combined, dried over Na_2SO_4, filtered, and concentrated under reduced pressure. The unpurified material was dissolved in acetone (5 mL) and was added to a boiling solution of fumaric acid (0.26 g, 2.2 mmol, 0.7 equiv) in acetone (35 mL). A precipitate formed immediately, and the solution was cooled to room temperature prior to being filtered. The resulting white solid was dried under reduced pressure to yield the pure compound as the fumarate salt (2:1). Yield = 0.320 g, 55%. Purity = 95%. TLC R_f (free base) = 0.31 (9:1 CH_2Cl_2/MeOH/1% $NH_4OH_{(aq)}$); ^{1}H NMR (600 MHz, CD_3OD) δ 7.44 (d, 1H, J = 8.6 Hz), 7.04 (s, 1H), 6.88 (s, 1H), 6.70 (m, 2H), 3.78 (s, 3H), 3.32 (t, 2H, J = 7.5 Hz), 3.12 (t, 2H, J = 7.5 Hz), 2.84 (s, 6H) ppm; ^{13}C NMR (150 MHz, CD_3OD) δ 173.79, 157.87, 138.97, 136.93, 122.89, 122.53, 119.64, 110.40, 109.99, 95.62, 59.12, 55.94, 43.36, 21.96 ppm; IR (diamond, ATR) v 2915, 2836, 1691, 1559 cm^{-1}. LRMS (ES+) m/z calcd for $C_{13}H_{18}N_2O^+$ 218.14, found 219.29 (MH^+); mp = 173−176 °C.

2-(1H-Indol-1-yl)-*N,N*-dimethylacetamide (31). To a solution of indole (117 mg, 1.0 mmol) in DMSO (2.5 mL, 0.4 M) were added 2-chloro-N,N-dimethylacetamide (0.11 mL, 1.1 mmol, 1.1 equiv), potassium iodide (182 mg, 1.1 mmol, 1.1 equiv), and potassium hydroxide pellets (280 mg, 5 mmol, 5.0 equiv). The reaction was stirred at room temperature for 24 h before being diluted with 1 M $NaOH_{(aq)}$ (250 mL). The phases were separated, and the aqueous phase was extracted with CH_2Cl_2 (2 × 50 mL). The organic extracts were combined, dried over Na_2SO_4, filtered, and concentrated under reduced pressure to yield an oil. The oil was purified via chromatography (3:2 hexanes/EtOAc). Yield = 175 mg, 57%. Purity = 99%. TLC R_f = 0.15 (3:2 hexanes/EtOAc); ^{1}H NMR (600 MHz, CD_3OD) δ 7.53 (d, 1H, J = 7.9 Hz), 7.27 (d, 1H, J = 7.9 Hz), 7.12

(m, 2H), 7.01 (t, 1H, *J* = 7.5, Hz), 6.46 (d, 1H, *J* = 2.9 Hz), 5.01 (s, 2H), 3.15 (s, 3H), 2.96 (s, 3H) ppm; ^{13}C NMR (150 MHz, $CDCl_3$) δ 167.4, 136.7, 128.7, 128.5, 122.0, 121.2, 119.8, 109.1, 102.4, 48.2, 36.7, 36.1 ppm; IR (diamond, ATR) *v* 3021, 2922, 2877, 1648 cm^{-1}. LRMS (ES+) calcd for $C_{12}H_{14}N_2O^+$ 202.11, found 203.17 (MH^+); mp = 58−61 °C.

Animals

For the dendritogenesis experiments, timed pregnant Sprague Dawley rats were obtained from Charles River Laboratories (Wilmington, MA). For the head-twitch response assay, male and female C57BL/6J mice were obtained from Jackson Laboratory (Sacramento, CA). Mice were housed in a temperature- and humidity-controlled room maintained on a 12 h light/dark cycle in groups of four to five (same-sex cages). Animals weighed between 17 and 30 g at the time of the experiments. All experimental procedures involving rodents were approved by the UC Davis Institutional Animal Care and Use Committee (IACUC) and adhered to principles described in the National Institutes of Health Guide for the Care and Use of Laboratory Animals. The University of California, Davis is accredited by the Association for Assessment and Accreditation of Laboratory Animal Care International (AAALAC).

Dendritogenesis Experiments

Dendritogenesis experiments were performed following a previously published method with slight modifications.[4] Neurons were plated in a 96-well format (200 µL of media per well) at a density of approximately 15 000 cells/well in Neurobasal (Life Technologies) containing 1% penicillin−streptomycin, 10% heat-inactivated fetal bovine serum, and 0.5 mM glutamine. After 24 h, the medium was replaced with Neurobasal containing 1× B27 supplement (Life Technologies), 1% penicillin−streptomycin, 0.5 mM glutamine, and 12.5 µM glutamate. After 3 days in vitro (DIV3), the cells were treated with compounds.

All compounds tested in the dendritogenesis assays were treated at 10 µM unless noted otherwise. Stock solutions of the compounds in DMSO were first diluted 100- fold in Neurobasal before an additional 10-fold dilution into each well (total dilution = 1:1000; 0.1% DMSO concentration). Treatments were randomized. After 1 h, the media was removed and was replaced with new Neurobasal media containing 1× B27 supplement, 1% penicillin−streptomycin, 0.5 mM glutamine, and 12.5 µM glutamate. The cells were

allowed to grow for an additional 71 h. At that time, neurons were fixed by removing 80% of the media and replacing it with a volume of 4% aqueous paraformaldehyde (Alfa Aesar) equal to 50% of the working volume of the well. Then, the cells were incubated at room temperature for 20 min before the fixative was aspirated and each well was washed twice with Dulbecco's phosphate-buffered saline (DPBS).[29]

Cells were permeabilized using 0.2% Triton X-100 (ThermoFisher) in DPBS for 20 min at room temperature without shaking. Plates were blocked with antibody diluting buffer (ADB) containing 2% bovine serum albumin (BSA) in DPBS for 1 h at room temperature. Then, plates were incubated overnight at 4 °C with gentle shaking in ADB containing a chicken anti-MAP2 antibody (1:10 000; EnCor, CPCA-MAP2). The next day, plates were washed three times with DPBS and once with 2% ADB in DPBS. Plates were incubated for 1 h at room temperature in ADB containing an antichicken IgG secondary antibody conjugated to Alexa Fluor 488 (Life Technologies, 1:500) and washed five times with DPBS.

After the final wash, 100 µL of DPBS was added per well and imaged on an ImageXpress Micro XL High-Content Screening System (Molecular Devices, Sunnyvale, CA) with a 20× objective. Images were analyzed using ImageJ Fiji (version 1.51W). First, images corresponding to each treatment were sorted into individual folders that were then blinded for data analysis. Plate controls (both positive and negative) were used to ensure that the assay was working properly as well as to visually determine appropriate numerical values for brightness/ contrast and thresholding to be applied universally to the remainder of the randomized images. Next, the brightness/contrast settings were applied, and approximately 1−2 individual pyramidal-like neurons per image (i.e., no bipolar neurons) were selected using the rectangular selection tool and saved as separate files. Neurons were selected that did not overlap extensively with other cells or extend far beyond the field of view. The threshold settings were then applied to the individual images. The paintbrush tool was used to eliminate artifacts and dendritic processes originating from adjacent neurons (cleanup phase). See Figure S2 for a visual explanation of how neurons were selected and processed for data analysis. Next, the point tool was used to select the center of the neuron, and the images were saved and processed using the following Sholl analysis batch macro: run("Sholl Analysis...", "starting=0 ending=NaN radius_step=2 #_samples=1 integration=Mean enclosing=1 #_primary=4 infer fit linear polynomial=[Best fitting degree] most semi-log normalizer=Area create background=228 save do"); Sholl

[29] If necessary this is a good place to stop if you don't have time to start the staining in the same day.

analysis circle radii = 2 pixel increments = 0.67 μm. All images were taken and analyzed by an experimenter blinded to treatment conditions. The number of crossings for each neuron at each distinct radius was averaged to produce an average Sholl plot for each treatment. The Nmax values were simply determined by identifying the maximum of each plot. For each treatment, neurons were selected from at least six wells spread across two plates (9 sites/ well × 3 wells/plate × 2 plates). Each plate was prepared using neurons obtained from independent pregnant dams.

Blocking Experiments

For the ketanserin blocking experiments (Figure 4.10 – 4.13), a slightly modified method was employed. On DIV3, neurons were first treated with ketanserin (10 μM) for 1 h followed by a 1 h incubation with the drug (1 μM) and ketanserin (10 μM) (final concentration of DMSO = 0.2%). After 1 h, the media was removed and replaced with new Neurobasal media containing 1× B27 supplement, 1% penicillin−streptomycin, 0.5 mM glutamine, and 12.5 μM glutamate. The cells were allowed to grow for an additional 71 h before being fixed, stained, and imaged.

Electroporation experiments

Electroporation experiments were performed by Max Vargas in a 96-well plates using only the center 60 wells. Before plating, cells were electroporated in the presence of a test compound using a Lonza 4D-nucleofector, following the Lonza protocol for electroporation of mammalian cells. Cells were then incubated followed by fixing and staining (DIV 6) using the protocol outlined previously for neurite outgrowth assays.

Spineogenesis Assays

Dendritic spine assays were conducted following a previously described procedure.[4] Briefly, spineogenesis assays were conducted in 24-well plates using only the center 8 wells. To protect against evaporation autoclaved water was added to the remaining wells. Coverslips,12 mm circular 1.5 mm thick coverslips (Fisher Scientific), were washed with 70% ethanol and flame sterilized using an ethanol flame. Coverslips were then autoclaved then one coverslip was added to each well. Plates were then plated at

35,000 cells per well and incubated for 24 hours at which time plating media was removed and replacement media was added. On DIV6 and DIV 13 half of the media was removed and replaced with fresh feeding media. On DIV20 cells were treated with test compounds and incubated for an additional 24 hours with compound on board before being fixed and stained using MAP2 and phalloidin.

Head-Twitch Response Experiments

Mice (9−10 weeks old) were injected intraperitoneally with compound (injection volume 5 mL/kg), placed in an empty cage (8” x 13” x 5”), and filmed for 20 min. Cages were cleaned with 70% ethanol between experiments. Each video was scored for the number of head-twitches by two trained observers blinded to treatment condition (Pearson correlation coefficients = 0.91 and 0.99 for males and females, respectively), and these results were averaged.

Statistical Analysis

Treatments were randomized, and data were analyzed by experimenters blinded to treatment conditions. Statistical analyses were performed using GraphPad Prism (version 8.1.2). The specific tests used, F-statistics, degrees of freedom, and main effect pvalues are indicated in the figure legends where appropriate. All comparisons were planned prior to performing each experiment. For dendritogenesis experiments, a one-way ANOVA with Dunnett’s post hoc test was deemed most appropriate, as our research question focused on determining whether or not a particular treatment promoted neuronal growth to a greater extent than the vehicle control. Ketamine was included as a positive control to ensure that the assay was working properly.

Chapter 3. Using Chirality To Mitigate Side Effects of Psychoplastogens.

Chapter 3.1 Introduction

Psychedelics have received a lot of attention in the past for their ability to treat various neuropsychiatric disorders. In particular, 3,4-methylenedioxymethamphetamine (MDMA) has shown remarkable results in clinical trials for post-traumatic stress disorder (PTSD).[1,2] Unlike other psychedelic drugs, the effects of MDMA lack the vivid hallucinations often associated with classic serotonergic psychedelics.[3] MDMA exhibits pronounced empathic effects in its users which has resulted in MDMA being deemed an entactogen, or capable of *producing a touching within*.[4] Compounds belonging to the class of entactogens lack hallucinogenic activity but are capable of inducing altered states of consciousness akin to having a deeper connection with one's feelings and emotions as well as those of others.

A key structural characteristic that differentiates amphetamine-type psychedelics, like MDMA, is the dual function of these compounds resulting from the different enantiomers. MDMA has a stereocenter alpha to the basic amine resulting in two enantiomers with different bioactivity (**FIG 3.1A**).[3,5] The *S*-enantiomer has been reported to have more amphetamine-like characteristics while the *R*- enantiomer promotes more LSD-like effects in drug discrimination studies.[3] This is likely due to the pharmacological differences between the two enantiomers with the *S*-enantiomer of MDMA being a potent inhibitor of the

[1] Mithoefer, M. C.; Wagner, M. T.; Mithoefer, A. T.; Jerome, L.; Doblin, R. The safety and efficacy of {±}3,4-methylenedioxymethamphetamine-assisted psychotherapy in subjects with chronic, treatment-resistant posttraumatic stress disorder: the first randomized controlled pilot study. *J. Psychopharmacol.* **2011**, *25*, 439– 452.
[2] Mitchell, J. M.; Bogenschutz, M.; Lilienstein, A. et al. MDMA-assisted therapy for severe PTSD: a randomized, double-blind, placebo-controlled phase 3 study. *Nat Med* **2021**, 27,1025–1033.
[3] Baker, L. E.; Taylor, M. M. Assessment of the MDA and MDMA optical isomers in a stimulant-hallucinogen discrimination. *Pharmacol., Biochem. Behav.* **1997**, *57*, 737– 748.
[4] Nichols, D. E. Differences between the mechanism of action of MDMA, MBDB, and the classic hallucinogens. Identification of a new therapeutic class: entactogens. *J Psychoactive Drugs* 1986, 18, 305-313.
[5] Curry, D. W.; Young, M. B.; Tran, A. N.; Daoud, G. E.; Howell, L. L. Separating the agony from ecstasy: R(−)-3,4-methylenedioxymethamphetamine has prosocial and therapeutic-like effects without signs of neurotoxicity in mice. *Neuropharmacology* **2018**, *128*, 196– 206.

dopamine transporter DAT while the *R*-enantiomer has a greater affinity for 5-HT2 receptors.[6,7,8] It has previously been reported that the psychostimulant side effects of MDMA are dissociable from the therapeutic effects of MDMA. Howell et al. have shown that *R*-MDMA does not produce any psychostimulant-like effects but still facilitates fear extinction learning and increased sociability.[5][9] Our lab previously demonstrated that racemic MDMA is capable of robustly promoting structural neuroplasticity.[10] Nothing is known about which enantiomer is responsible for these effects. To determine this we tested both enantiomers of MDMA as well as the enantiomers of the lesser-known 3,4-Methylenedioxy-*N,N*-dimethylamphetamine (MDDMA).

Little is known about MDDMA however Shulgin reported that it possessed no psychotomimetic activity.[11,12] We theorized that MDDMA may be a more potent psychoplastogen as we have demonstrated that methylation plays an important role in the ability of tryptamines to promote structural plasticity.[13] MDDMA's lack of psychotomimetic effects made it of particular interest to us as a potentially non-hallucinogenic entactogen. Here we report the synthesis of the enantiomers of MDMA and MDDMA and assess the therapeutic potential of R-MDDMA which we have dubbed LED.

---

[6] Toll, L.; Berzetei-Gurske, I. P.; Polgar, W. E.; Brandt, S. R.; Adapa, I. D.; Rodriguez, L.; Schwartz, R. W.; Haggart, D.; O'Brien, A.; White, A.; Kennedy, J. M.; Craymer, K.; Farrington, L.; Auh, J. S. Standard binding and functional assays related to medications development division testing for potential cocaine and opiate narcotic treatment medications. *NIDA Res. Monogr*. **1998**, 178, 440−466.

[7] Hiramatsu, M.' Cho, A. K. Enantiomeric differences in the effects of 3,4-methylenedioxymethamphetamine on extracellular mono- amines and metabolites in the striatum of freely-moving rats: an in vivo microdialysis study. *Neuropharmacology* **1990**, 29, 269– 275,

[8] Acquas, E.; Pisanu, A.; Spiga, S.; Plumitallo, A.; Zernig, G.; Di Chiara, G. Differential effects of intravenous R,S-(±)-3,4- methylenedioxymethamphetamine (MDMA, ecstasy) and its S(+)- and R(−)-enantiomers on dopamine transmission and extracellular signal regulated kinase phosphorylation (pERK) in the rat nucleus accumbens shell. *J. Neurochem.* **2007**, 102, 121– 132,

[9] Brown, P. L.; Kiyatkin, E. A. Brain hyperthermia induced by MDMA (ecstasy): modulation by environmental conditions. *Eur. J. Neurosci*. **2004**, 20, 51−58.

[10] Ly, C.; Greb, A. C.; Cameron, L. P.; Wong, J. M.; Barragan, E. V.; Wilson, P. C.; Burbach, K. F.; Soltanzadeh Zarandi, S.; Sood, A.; Paddy, M. R.; Duim, W. C.; Dennis, M. Y.; McAllister, A. K.; Ori-McKenney, K. M.; Gray, J. A.; Olson, D. E. Psychedelics Promote Structural and Functional Neural Plasticity. *Cell Reports* **2018**, 23, 3170–3182.

[11] Braun, U.; Shulgin, A. T.; Braun, G. Centrally active N-substituted analogs of 3,4 methylenedioxyphenylisopropylamine (3,4-methylenedioxyamphetamine). *J. Pharm. Sci*. **1980**, 69, 192– 195,

[12] Sandtner, W.; Stockner, T.; Hasenhuetl, P. S.; Partilla, J. S.; Seddik, A.; Zhang, Y. W.; Cao, J.; Holy, M.; Steinkellner, T.; Rudnick, G.; Baumann, M. H.; Ecker, G. F.; Newman, A. H.; Sitte, H. H. Binding mode selection determines the action of ecstasy homologs at monoamine transporters. *Mol. Pharmacol.* **2016**, 89, 165– 175,

[13] See chapter 2 for results pertaining to the methylation of the basic amine.

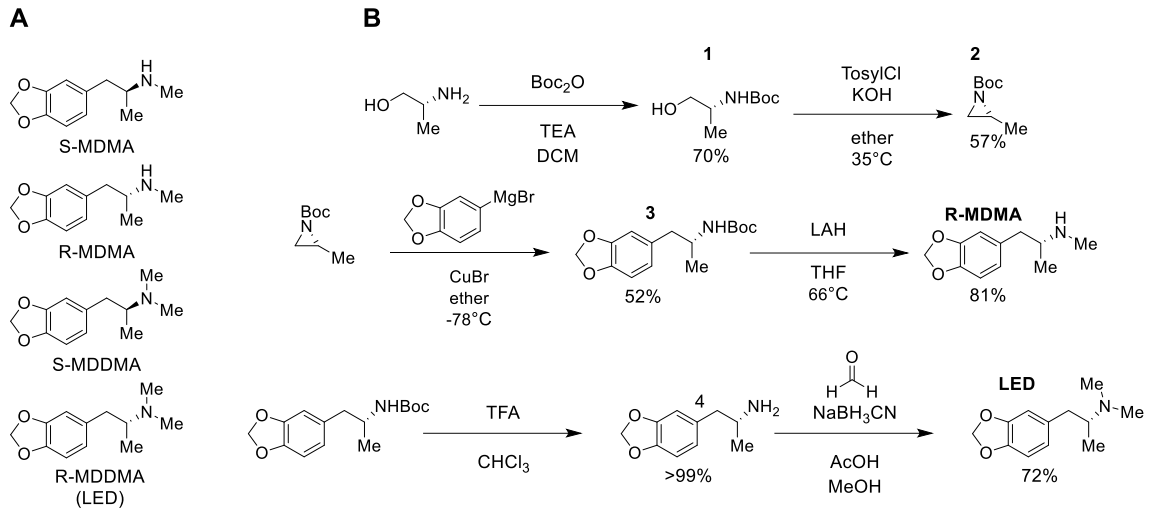

Figure 3.1 (**A**) Enantiomers of MDMA and MDDMA. (**B**) Synthetic scheme to produce enantiopure MDMA and MDDMAs.

Chapter 3.2 Enantioselective Synthesis of MDMA Analogs

Despite numerous attempts to separate the enantiomers of racemic MDA using various methods, we were unable to achieve sufficient ee in acceptable yields. We decided to start from the chiral pool using a previously developed methodology (**FIG 3.1B**).[14] Starting from *R*- or *S*-alaninol, we were able to efficiently Boc protect the primary amine **1**. A one-step tosylation of the alcohol followed by displacement by the Boc protected amine afforded the aziridine intermediate **2**. The aziridine was opened via copper bromide-assisted Grignard to afford the enantiopure Boc protected MDA **3** which upon reduction with lithium aluminum hydride afford enantiopure MDMA.

The synthesis of enantiopure MDDMA followed a similar procedure. After the aziridine ring opening to form intermediate **3** we were able to deprotect the boc group and subsequent reductive amination yielded the desired enantiopure MDDMA.

[14] Nenajdenko, V.G.; Karpov, A.S.; Balenkova, E.S. A new convenient approach to chiral b aryl(heteroaryl)alkylamines. *Tetrahedron Asymmetry* **2001**, 12, 2517–2527.

Chapter 3.3 Effect of Chirality on Neuroplasticity

We have previously shown that MDMA has robust effects on promoting neural plasticity in cortical neurons.[10] This is theorized to be where the therapeutic effects of classic psychedelics come from. The atrophy of cortical neurons is prevalent in stress-related disorders with the medial prefrontal cortex (mPFC) exerting top-down control on various brain regions relevant to anxiety, depression, PTSD, and addiction.[15] As the enantiomers of MDMA are known to exert different behavioral effects, we screened both enantiomers of MDMA and MDDMA using Sholl analysis in a 4pt concentration-response to determine if chirality played a role in the psychoplastogenic effects (**FIG 3.2A**). To our surprise, we observed no difference between sets of enantiomers. We found that LED was more potent than R-MDMA exhibiting results at doses as low as 10 pM. Next, we tested both *R*-MDMA and LED in a spinogenesis assay (**FIG 3.2B**). Both R-MDMA and LED caused a robust increase in the number of dendritic spines. This data suggests that LED has potent psychoplastogenic effects comparable to *R*-MDMA.

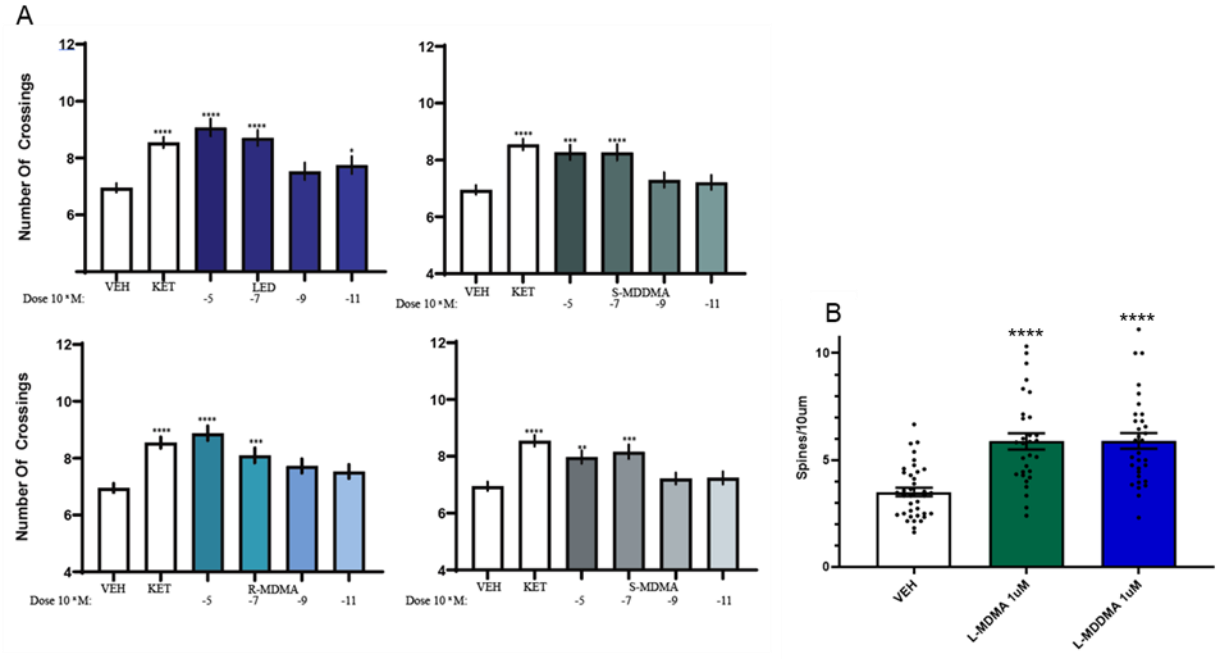

Figure 3.2. (**A**) Maximal number of crossings (Nmax) from Sholl plots (n = 47–103 neurons). ∗∗∗∗p < 0.0001, ∗∗∗p < 0.001, one-way ANOVA with Dunnett's test. (**B**) Both *R*-MDMA and LED increases dendritic

[15] Peters, J.; Olson, D. E. Engineering Safer Psychedelics for Treating Addiction. *Neuroscience Insights* **2021**, 16, https://doi.org/10.1177/26331055211033847.

spine density on rat embryonic cortical neurons after treatment for 24 h (n = 30–37 neurons). ****p < 0.0001, as compared to the vehicle control following a one-way analysis of variance (ANOVA) with Dunnett's post hoc test. Error bars represent SEM.

Chapter 3.4 *R*-MDMA and LED Safety Profiles

One of the biggest limitations to the use of psychoactive compounds for treating neurological disorders is their adverse effects. In Long-Evans rats, MDMA increased body temperature leading to brain hyperthermia lowering the LD_{50}.[9] While most of the adverse effects of MDMA come from the *S*- enantiomer, R-MDMA can also produce subjective effects and has reinforcing properties in animal models.[16,17] We assessed the potential adverse effects of LED to determine if LED could serve as a potentially safer alternative to MDMA. Like *R*-MDMA, LED did not cause an increase in body temperature when measured via an IR thermometer, however, both LED and R-MDMA caused a slight decrease in body temperature at the highest dose **(FIG 3.3A).** Low doses of *R*-MDMA were trending toward a decreased body temperature however these results were not significant. Despite lacking the psychostimulant-like effects of *S*-MDMA, *R*-MDMA caused a dose-dependent increase in locomotion whereas LED caused a decrease in locomotion at the 50mg/kg dose (**FIG 3.3B**).

To assess the anxiolytic or anxiogenic effects of *R*-MDMA and LED we measured the time spent in the center of a novel test arena (**FIG 3.3C**). All doses of *R*-MDMA tested caused an anxiogenic response reducing the amount of time spent in the center which was not correlated with decreased locomotion. In contrast, LED only caused a decrease in locomotion at 50mg/kg. Finally, since *R*-MDMA is known to partially substitute for LSD in animal models we decided to test both compounds in the head twitch response assay (HTR) (**FIG 3.3C**).[3] The HTR is a well-validated mouse model for predicting the hallucinogenic potential of test drugs. Serotonergic psychedelics will cause a rapid back and forth head movement in mice. The potency measured in the HTR assay has been shown to correlate very well with the human potencies

[16] Fantegrossi, W. E.; Ullrich, T.; Rice, K. C.; Woods, J. H.; Winger, G. 3,4-Methylenedioxymethamphetamine (MDMA, "ecstasy") and its stereoisomers as reinforcers in rhesus monkeys: serotonergic involvement. *Psychopharmacology (Berl)* **2002**,161, 356-364.

[17] Dunlap, L. E.; Andrews, A. A.; Olson, D. E. Dark Classics in Chemical Neuroscience: 3,4-Methylenedioxymethamphetamine. *ACS Chem. Neurosci*. **2018**, 9, 2408–2427.

of psychedelics.[18] Neither *R*-MDMA or LED produced any head twitches at all doses tested, suggesting that neither has high hallucinogenic potential.

Chapter 3.5 *R*-MDMA and LED Promote Fear Extinction

Having demonstrated that LED has an improved safety profile compared to *R*-MDMA we next assessed the effects of LED in behavioral models relevant to PTSD. We used a fear extinction paradigm as it has been demonstrated that impairments in the extinction of fear memories is the cause of PTSD.[19] Both doses of *R*-MDMA given 30 minutes prior to extinction training caused substantial reductions in freezing to the conditioned stimuli during the training session (**FIG. 3.4A, B**). The results for the 12.5 mg/kg dose could be attributed to reductions in locomotion caused by the acute effects of R-MDMA. Twenty-four hours later, animals were tested in the extinction context in a drug-free state. *R*-MDMA treated mice still exhibited reductions of conditioned freezing (**FIG. 3.42B**), demonstrating robust fear extinction. LED did not show acute effects during extinction training, however, 24 hours after drug administration the 12.5 mg/kg dose showed a reduction in freezing following the context cue. The results of LED on extinction test day show distinct sex differences. In males the 25 mg/kg dose showed a more robust reduction in freezing, however, in females, the 12.5 mg/kg dose showed the largest effect size. This suggests that females may be more sensitive to the effects of LED. These results are not unsurprising as females in a number of experiments have been shown to be more sensitive to the effects of psychedelics and entactogens.[20,21,22,23]

[18] Halberstadt, A. L.; Chatha, M.; Klein, A. K.; Wallach, J.; Brandt, S. D. Correlation between the potency of hallucinogens in the mouse head-twitch response assay and their behavioral and subjective effects in other species. *Neuropharmacology* **2020,** 167, 107933.

[19] Rothbaum, B. O,.; Davis M. Applying learning principles to the treatment of post-trauma reactions. *Ann N Y Acad Sci.* **2003**,1008, 112-121. 7

[20] Liechti, M. E.; Gamma, A.; Vollenweider, F. X. Gender differences in the subjective effects of MDMA. *Psychopharmacology (Berlin)* **2001**,154, 161−168.

[21] Vizeli, P.; Liechti, M. E. Safety pharmacology of acute MDMA administration in healthy subjects. *J. Psychopharmacol*. **2017**, 31, 576−588

[22] Dunlap, L. E.; Azinfar, A.; Ly, C.; Cameron, L. P.; Viswanathan, J.; Tombari, R. J.; Myers-Turnbull, D.; Taylor, J. C.; Grodzki, A. C.; Lein, P. J.; Kokel, D.; Olson, D. E. Identification of Psychoplastogenic N,N-Dimethylaminoisotryptamine (isoDMT) Analogs Through Structure-Activity Relationship Studies. *J. Med. Chem*. **2020**, 63, 1142–1155.

[23] Shao, L. X.; Liao, C.; Gregg, I.; Davoudian, P. A.; Savalia, N. K.; Delagarza, K.; Kwan, A. C. Psilocybin induces rapid and persistent growth of dendritic spines in frontal cortex in vivo. *Neuron* **2021**, 109, 2535-2544.

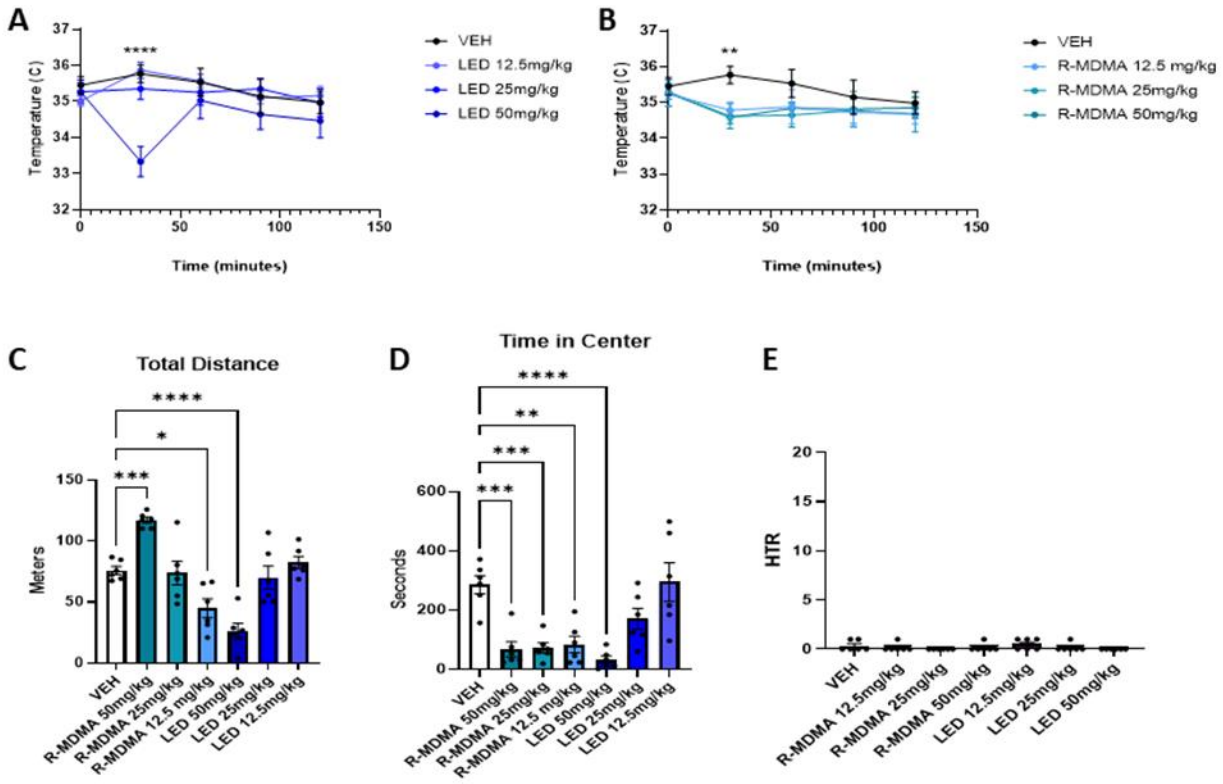

Figure 3.3. (**A**) Only a high dose (50 mg/kg) of LED and *R*-MDMA causes a decrease in body temperature.. N=6 (3 male and 3 female) two-way ANOVA with Dunnett's multiple comparisons test. (**B-D**) N= 6 (3 males and 3 females). (**B**) *R*-MDMA causes a dose-dependent increase in locomotion while LED causes a dose-dependent decrease in locomotion. (**C**) All doses of R-MDMA reduced the amount of time spent in the center whereas only the highest dose of LED reduced the amount of time spent in the center. One-way ANOVA with Dunnett's post hoc. (**D**) None of the doses of R-MDMA and LED caused a HTR. Error bars represent SEM. *p < 0.05, **p < 0.01, ***p < 0.001, ****p < 0.0001.

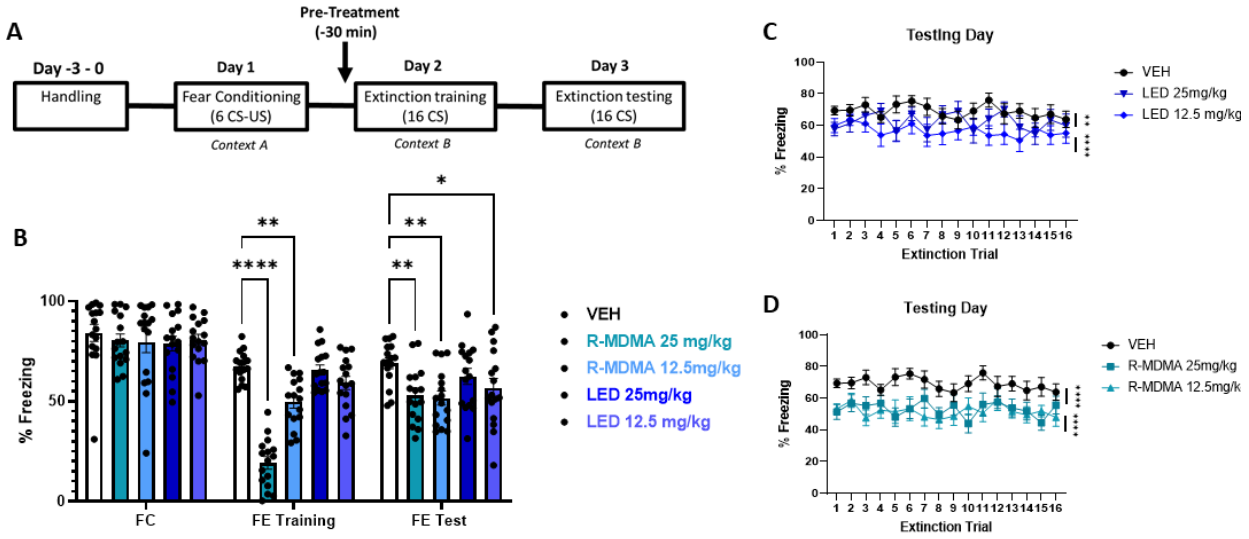

Figure 3.4. (**A**) Fear extinction scheme. (**B-D**) N= 16 (8 males and 8 females). (**B**) When administered 30 min prior to extinction training both doses of *R*-MDMA decreased the percent of freezing. During extinction training, both doses of R-MDMA and the 12.5 mg//kg dose of LED reduced the time spent freezing. (**C,D**) Fear extinction curves show that both doses of LED and R-MDMA caused a reduction in freezing. center. Two-way ANOVA with Dunnett's multiple comparisons test. Error bars represent SEM. *p < 0.05, **p < 0.01, ***p < 0.001, ****p < 0.0001.

It is believed that MDMA primarily exerts its effects by causing the release of monoamines via actions at the serotonin transporter (SERT), dopamine transporter (DAT), and norepinephrine transporter (NET).[24,25,26] There is also compelling evidence to suggest roles for oxytocin and 5-HT1BR in mediating the therapeutic effects.[27] We have demonstrated that the plasticity-promoting properties of psychoplastogens are mediated via a 5-HT2R dependent mechanism.[10] While MDMA does not have a high

[24] Hysek, C. M.; Simmler, L. D.; Nicola, V.; Vischer, N.; Donzelli, M.; Krahenbuhl, S.; Grouzmann, E.; Huwyler, J.; Hoener, M. C.; Liechti, M. E. Duloxetine inhibits effects of MDMA ("ecstasy") in vitro and in humans in a randomized placebocontrolled laboratory study. *PLoS One* **2012**, 7, e36476.
[25] Iversen, L.; Gibbons, S.; Treble, R.; Setola, V.; Huang, X. P.; Roth, B. L. Neurochemical profiles of some novel psychoactive substances. *Eur. J. Pharmacol.* **2013**, 700, 147−151
[26] Jones, D. C.; Lau, S. S.; Monks, T. J. Thioether metabolites of 3,4-methylenedioxyamphetamine and 3,4-methylenedioxymethamphetamine inhibit human serotonin transporter (hSERT) function and simultaneously stimulate dopamine uptake into hSERT-expressing SK-N-MC cells. *J. Pharmacol. Exp. Ther***. 2004**, 311, 298−306.
[27] Nardou, R.; Lewis, E. M.; Rothhaas, R.; Xu, R.; Yang, A.; Boyden, E.; Dolen, G. Oxytocin-dependent reopening of a social reward learning critical period with MDMA. *Nature* **2019**, 569, pages116–120.

affinity for 5-HT2Rs, *R*-MDMA has a micromolar affinity at 5-HT2Rs.[17] It is worth noting though that even though MDMA has a low micromolar affinity for 5-HT2A, the radioligand binding studies were performed using a radiolabeled antagonist. The low affinity for 5-HT2A could be the result of using an antagonist as MDMA's affinity for structurally analogous 5-HT2B receptor was reported to be 500nM when a radiolabeled agonist was used.[17]

Chapter 3.6 R-MDMA and LED Promote Plasticity Via A 5-HT2R Mechanism

To determine if the plasticity-promoting effects of *R*-MDMA and LED are 5-HT2 dependent, we attempted to block the effects of both drugs using the 5-HT2R antagonist ketanserin. We found that pretreatment with ketanserin blocked the effect of both R-MDMA and LED on dendritic arborization and spinogenesis. To confirm if these effects were the result of direct 5-HT2A binding we screened both R-MDMA and MDDMA using psychlight, a genetically encoded fluorescent sensor based on the 5-HT2AR structure.[28,29] To our surprise, neither *R*-MDMA or LED elicited a response in the psychlight assay suggesting neither drug activates 5-HT2ARs. This suggests to us that the target of LED may be the 5-HT2C receptor. Ketanserin is also a potent binder and antagonist of the 5-HT2C receptor and at the doses used in our in vitro plasticity assays, it is possible that the effects we observe arise from the blocking of the 5-HT2C receptor. To test this, we are currently screening LED and *R*-MDMA in a biosensor based on the 5-HT2C receptor ($GRAB_{5\text{-}HT}$) and radioligand binding assays to determine the activity and affinity for 5-HT2CRs.[30]

Lastly, one of the primary mechanisms of MDMA's action is monoamine release. To determine if this could be playing a role in LED's plasticity promoting properties we tested both R-MDMA and LED for

[28] Dong, C.; Ly, C.; Dunlap, L. E.; Vargas, M. V.; Sun, J.; Hwang, I.-W.; Azinfar, A.; Oh, W. C.; Wetsel, W. C.; Olson, D. E.; Tian, L. Psychedelic-Inspired Drug Discovery Using an Engineered Biosensor. *Cell* **2021**, 10, 2779-2792.
[29] For information on psychlight see Chapter 4 of this dissertation
[30] Unger, E. K.; Keller, J. P.; Altermatt, M.; Liang, R.; Yao, Z.; Sun, J.; Matsui, A.; Dong, C. E.; Hon, O. J.; Yao, Z.; Sun, J.; Banala, S.; Flanigan, M. E.; Jaffe, D. A.; Hartanto, S.; Carlen, J.; Mizuno, G. O.; Borden, P. M.; Shivange, A. V.; Cameron, L. P.; Sinning, S.; Underhill, S. M.; Olson, D. E.; Amara, S. G.; Lang, D. T.; Rudnick, G.; Marvin, J.; Lavis, L. D.; Lester, H. A.; Alvarez, V. A.; Fisher, A. J.; Prescher, J. A.; Kash, T. L.; Yarov-Yarovoy, V.; Gradinaru, V.; Looger, L. L.; Tian, L. Directed Evolution of a Selective and Sensitive Serotonin Sensor Via Machine Learning. *Cell* **2020**, 183, 1986–2002

their ability to promote [^{3}H]5-HT release. We used HEK293T cells transiently expressing SERT. We found that at high concentrations *R*-MDMA caused a significant release of [^{3}H]5-HT while LED failed to elicit a response at any of the concentrations tested, this was quite striking as LED is devoid of what is believed to be the primary mechanism of action for MDMA. The high concentration of *R*-MDMA needed to cause this release is not surprising as *R*-MDMA is a weaker monoamine releaser compared to *S*-MDMA.[5]

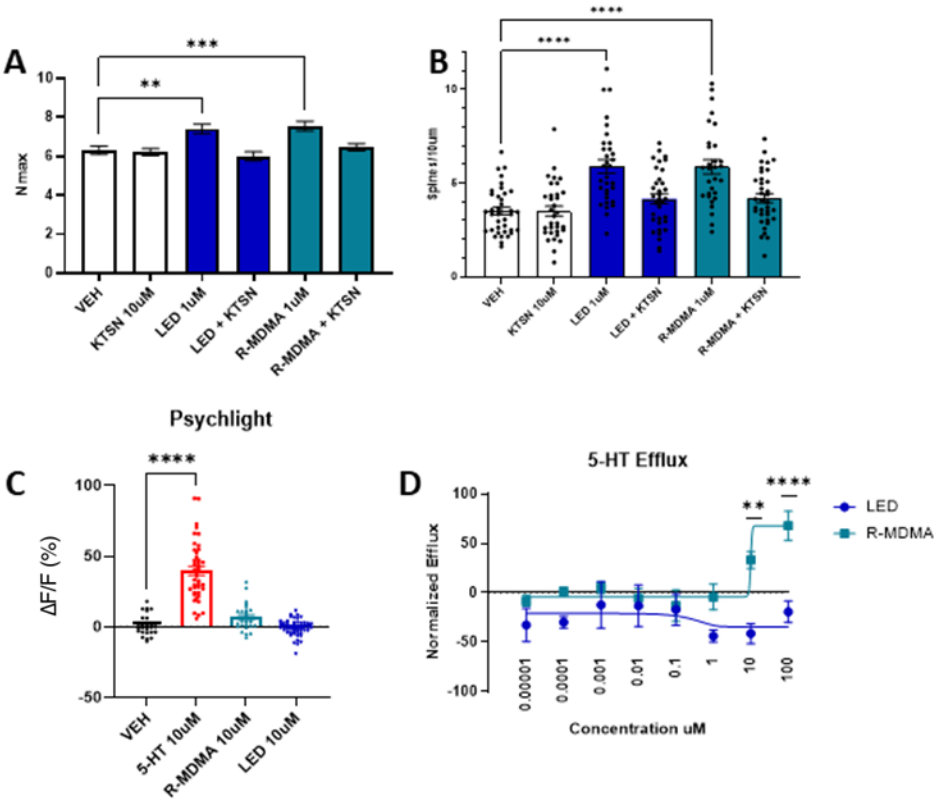

Figure 3.5. (**A**) Maximal number of crossings (Nmax) from Sholl plots (n = 56–74 neurons). Pretreatment with the 5-HT2R antagonist KTSN blocks the effects of LED and *R*-MDMA. ****p < 0.0001, ***p < 0.001, one-way ANOVA with Dunnett's test. (**B**) Pretreatment with KTSN blocks the effects of both *R*-MDMA and LED on spinogenesis after treatment for 24 h (n = 30–37 neurons). (**C**) Neither R-MDMA or LED caused an increase in fluorescence in the 5-HT2A biosensor psychLight2. DIV 10–14 cortical neurons expressing psychLight2 (n = 23–57 neurons). (**D**) *R*-MDMA but not LED caused a dose-dependent increase in [^{3}H]5-HT efflux in HEK293T cells expressing SERT. *p < 0.05, **p < 0.01, ***p < 0.001, ****p < 0.0001, as

compared to the vehicle control following a one-way ANOVA with Dunnett's post hoc test. Error bars represent SEM.

Chapter 3.7 Conclusion

MDMA has received a lot of attention over the years due to its potential for treating neuropsychiatric disorders like PTSD. MDMA is arguably one of the most important compounds for psychedelic research. While there is some debate about whether or not MDMA is a psychedelic or not, its advancement through clinical trials and FDA "breakthrough therapy" status has helped to pave the way for other drugs like psilocybin and LSD. Despite being such an important drug, MDMA is not without drawbacks. The neurotoxic effects and Schedule I status make it a less than ideal drug candidate and a challenging drug to work with and research. We have developed LED, an analog of MDMA with an improved safety profile that has retained the therapeutic effects. We demonstrated that like *R*-MDMA, LED produces robust changes in both neurite outgrowth and spinogenesis assays. Further, we demonstrated that the psychoplastogenic effects can be dissociated from the anxiogenic and hyperlocomotion properties of MDMA.

While the mechanism for the therapeutic effects of MDMA is still unclear, psychoplastogens are known to work through a 5-HT2R mechanism. We show that ketanserin, a 5-HT2R antagonist, blocks the effects of R-MDMA and LED in both neurite outgrowth and spinogenesis assays. We also show that, unlike *R*-MDMA, LED does not affect serotonin release, suggesting that there may be a common underlying mechanism of the therapeutic effects of these drugs that is not dependent on monoamine release. In the future, we hope to use LED as a test drug to better understand the mechanism of psychoplastogens like MDMA.

ACKNOWLEDGEMENTS

I would like to acknowledge Max Vargas for performing all of the *in vitro* and *in vivo* work presented in this chapter. I would also like to thank Robert J. Tombari for his help with the 5-HT efflux experiments. Lastly, I would like to thank Van La for her help determining the dr of MDA.

Chapter 3.8 Methods

Drugs

The NIH Drug Supply Program provided psilocin (PSI) and psilocybin (PSY). Other chemicals were purchased from commercial, ketamine hydrochloride (KET, Fagron), serotonin hydrochloride (5HT, Alfa Aesar), ketanserin (KETSN, ApexBio), tryptamine(ACROS).

Chemistry (General)

All reagents were obtained from commercial sources and were used without purification unless otherwise noted. DMSO was purified by passage under 12 psi N_2 through activated alumina columns. Reactions were performed using glassware that was flame-dried under reduced pressure (~1 Torr). Chromatography was performed using Fisher Chemical Silica Gel Sorbent (230−400 mesh, grade 60). Compounds purified by chromatography were dissolved in a minimal amount of chloroform for loading. Thin-layer chromatography (TLC) was performed on Millipore silica gel 60 F254 plates. Visualization of the developed chromatogram was accomplished by fluorescence quenching or by staining with ninhydrin.

Nuclear magnetic resonance (NMR) spectra were acquired on either a Bruker 400 operating at 400 and 100 MHz or a Varian 600 operating at 600 and 150 MHz respectively, and are referenced internally according to residual solvent signals. Data for ^{1}H NMR are recorded as follows: chemical shift (δ, ppm), multiplicity (s, singlet; d, doublet; t, triplet; q, quartet; m, multiplet), integration, coupling constants (Hz). Data for ^{13}C NMR are reported in terms of chemical shift (δ, ppm). Liquid chromatography−mass spectrometry (LC−MS) was performed using a Waters LC−MS with an ACQUITY Arc QDa detector. Ketamine was purchased from Fagron. For cellular plasticity assays (i.e., dendritogenesis), all compounds were dissolved in DMSO and stored as 10 mM stock solutions in the dark at −20 °C.

All compounds tested in cellular assays were confirmed to be of >95% purity based on UHPLC analysis (Waters ACQUITY Arc) measuring absorbance at 254 and 280 nm. Mobile phase A consisted of 0.01% formic acid in water, and mobile phase B consisted of 0.01% formic acid in acetonitrile. All samples were injected at a volume of 5 µL, and the column temperature was maintained at 40 °C. As most compounds reported in this study were isolated as the fumarate salts, peaks in UHPLC traces corresponding to fumaric acid were not included in the calculation of purity.

Tert-butyl (*R*)-(1-hydroxypropan-2-yl)carbamate. To an ice-cold solution of *(2R)-2-aminopropan-1-ol* (6.7 g, 90.0 mmol) in DCM (180 mL) was added triethylamine (25.2 mL, 180 mmol, 2 equiv.) and Di-tert-butyl dicarbonate (23.5 g, 108.0 mmol, 1.2 equiv.) portion-wise. The reaction was brought to room temperature and stirred overnight before being diluted with DCM (100 mL) and H_2O (300 mL). The phases were separated, and the aqueous phase was extracted with DCM (2 × 100 mL). The organic extracts were combined, dried over Na_2SO_4, filtered, concentrated under reduced pressure, and purified via flash chromatography (7:3 Hexanes/EtOAc) to afford the purified product as a white solid. Yield = 11.0 g, 70%.

Tert-butyl (*R*)-2-methylaziridine-1-carboxylate. To an ice-cold solution of *Tert-butyl (R)-(1-hydroxypropan-2-yl)carbamate* (1.0 g, 5.7 mmol) in diethyl ether (114 mL) was added p-toluenesulfonyl chloride (1.6 g, 8.6 mmol, 1.5 equiv.) then freshly-powdered potassium hydroxide (1.3 g, 23.0 mmol, 4.0 equiv.) portion-wise. The reaction was brought to room temperature and stirred 6 h before being filtered, washing with an ice-cold portion of diethyl ether (30 mL). The filtrate was concentrated under reduced pressure and used without further purification. Yield = 514 mg, 57%.

Tert-butyl (*R*)-(1-(benzo[d][1,3]dioxol-5-yl)propan-2-yl)carbamate. To a -78°C solution of copper(I) bromide dimethyl sulfide (25 mg, 0.12 mmol, 0.3 equiv.) in THF (2.3 mL) was added 3,4-(Methylenedioxy)phenylmagnesium bromide solution(0.8M in toluene:THF 50:50) (1.1 mL, 0.9 mmol, 2.2 equiv.). After 15 min, a solution of tert-butyl (*R*)-2-methylaziridine-1-carboxylate (65 mg, 0.41 mmol) in THF (2 mL) was added drop-wise. The reaction was warmed to room temperature slowly and stirred for 1 h before being diluted with a sat'd solution NH_4Cl (30 mL) and EtOAc (15 mL). The phases were and the aqueous phase was extracted with EtOAc (3x 15 mL). The organic extracts were combined, dried over Na_2SO_4, filtered, concentrated under reduced pressure, and purified via flash chromatography (9:1 Hexanes/EtOAc). The resulting tan solid was dried under reduced pressure to yield the pure compound. Yield = 60 mg, 52%.

(*R*)-1-(benzo[d][1,3]dioxol-5-yl)-N,N-dimethylpropan-2-amine (*R*-MDMA Fumarate 2:1). To an ice-cold solution of *tert-butyl (R)-(1-(benzo[d][1,3]dioxol-5-yl)propan-2-yl)carbamate* (363 mg, 1.3 mmol) in THF (13

mL) was added lithium aluminum hydride (0.4 M) (0.65 mL, 2.6 mmol, 2 equiv.) and stirred for 5 min. The reaction was then heated to 66 °C and stirred for 4 h before being cooled to -10 °C. The reaction was diluted with THF (2 mL) followed by dropwise addition of H_2O (3 mL). The reaction was then diluted into a sat'd solution of Rochelle's salt (100 mL) and EtOAc (40 mL) was added. The phases were separated and the aqueous phase was extracted with EtOAc 3x (40 mL). The organic extracts were combined, dried over Na_2SO_4, filtered, and concentrated under reduced pressure. The resulting solid was taken up in $CHCl_3$ (1 mL) and added to a boiling solution of fumaric acid (151 mg, 1.3 mmol, 1 equiv.) in THF (15 mL). The solution was cooled to room temperature and stored at -20°C overnight. The solid was filtered and washed with ice-cold acetone (1 mL) and dried under reduced pressure to afford the desired product as the 2:1 fumarate salt. Yield = 112 mg, 81%. 1 H NMR (600 MHz, CD_3OD) δ 6.78 (m, 2H), 6.71 (dd, 1H, *J* = 7.8, 1.5 Hz), 6.67 (s, 1H), 5.93 (s, 2H), 3.36 (m, 1H), 3.0 (dd, 1H, *J* = 13.5, 5.2 Hz), 2.67 (m, 4H), 1.21 (d, 3H, *J* = 6.6 Hz), ppm; 13C NMR (150 MHz, CD_3OD) δ 174.42, 149.56, 148.33, 137.11, 130.90, 123.64, 110.45, 109.45, 102.46, 57.71, 40.05, 30.90, 15.79, ppm. LRMS (ES+) m/z calcd for $C_{11}H_{15}NO_2$ + 193.11, found 194.04 (MH+).

(*R*)-1-(benzo[d][1,3]dioxol-5-yl)-N,N-dimethylpropan-2-amine (*R*-MDDMA Fumarate 1:1). To an ice-cold solution of *tert-butyl (R)-(1-(benzo[d][1,3]dioxol-5-yl)propan-2-yl)carbamate* (230 mg, 0.82 mmol) in $CHCl_3$ (2 mL) was added trifluoroacetic acid (0.5 mL) and stirred for 15 min. The reaction was diluted with MeOH (5 mL) and concentrated under reduced pressure. The crude material was taken up in MeOH (21 mL) and cooled to 0°C. Acetic acid (0.24 mL, 4.2 mmol, 5 equiv.) was added to the reaction mixture followed by $NaBH_3CN$ (110 mg, 1.75 mmol, 2.1 equiv.) and the reaction was warmed to room temp. The reaction was stirred overnight before being concentrated under reduced pressure. The resulting crude solid was taken up in 1 M $NaOH_{(aq)}$ (100 mL) and DCM (25 mL). The phases were and the aqueous phase was extracted with DCM (3x 25 mL). The organic extracts were combined, dried over Na_2SO_4, filtered, and concentrated under reduced pressure. The resulting solid was taken up in acetone (1 mL) and added to a boiling solution of fumaric acid (97 mg, 0.84 mmol, 1 equiv.) in acetone (18 mL). The solution was cooled to room temperature and stored at -20°C overnight. The solid was filtered and washed with ice-cold acetone (1 mL) and dried under reduced pressure to afford the desired product as the 1:1 fumarate salt. Yield = 194

mg, 72%. ^{1}H NMR (600 MHz, CD_3OD) δ 6.80 (m, 2H), 6.74 (t, 1H, *J* = 8.08Hz), 6.70 (s, 2H), 5.94 (s, 2H), 3.6 (m, 1H), 3.08 (t, 1H, *J* = 4.34, 8.71 Hz), 2.87 (s, 6H), 2.71 (m, 1H), 1.21 (d, 3H, *J* = 6.71 Hz), ppm; ^{13}C NMR (150 MHz, CD_3OD) δ 170.41, 149.56, 148.33, 135.90, 130.89, 123.61, 110.41, 109.45, 102.47, 64.46, 39.62, 37.79, 12.62, ppm. LRMS (ES+) m/z calcd for $C_{16}H_{21}NO_6$ + 207.13, found 208.26 (MH+).

Tert-butyl (*S*)-(1-hydroxypropan-2-yl)carbamate. To an ice-cold solution of *(2S)-2-aminopropan-1-ol* (3.1 g, 41.0 mmol) in DCM (82 mL) was added triethylamine (11.6 mL, 83 mmol, 2 equiv.) and Di-tert-butyl dicarbonate (11.4 g, 50 mmol, 1.2 equiv.) portion-wise. The reaction was brought to room temperature and stirred overnight before being diluted with DCM (100 mL) and H_2O (250 mL). The phases were separated, and the aqueous phase was extracted with DCM (2 × 100 mL). The organic extracts were combined, dried over Na_2SO_4, filtered, concentrated under reduced pressure, and purified via flash chromatography (7:3 Hexanes/EtOAc) to afford the purified product as a white solid. Yield = 1.9 g, 34.5%.

Tert-butyl (*S*)-2-methylaziridine-1-carboxylate. To an ice-cold solution of *Tert-butyl (S)-(1-hydroxypropan-2-yl)carbamate* (1.0 g, 5.7 mmol) in diethyl ether (19 mL) was added p-toluenesulfonyl chloride (1.6 g, 8.6 mmol, 1.5 equiv.) then freshly-powdered potassium hydroxide (1.3 g, 23.0 mmol, 4.0 equiv.) portion-wise. The reaction was brought to room temperature and stirred 6 h before being filtered, washing with an ice-cold portion of diethyl ether (20 mL). The filtrate was concentrated under reduced pressure and used without further purification. Yield = 513 mg, 57%.

Tert-butyl (*S*)-(1-(benzo[d][1,3]dioxol-5-yl)propan-2-yl)carbamate. To a -78°C solution of copper(I) bromide dimethyl sulfide (20 mg, 0.97 mmol, 0.3 equiv.) in THF (18 mL) was added 3,4-(Methylenedioxy)phenylmagnesium bromide solution(1M in toluene:THF 50:50) (7.2 mL, 7.2 mmol, 2.2 equiv.). After 15 min, a solution of tert-butyl (*S*)-2-methylaziridine-1-carboxylate (513 mg, 3.3 mmol) in THF (10 mL) was added drop-wise. The reaction was warmed to room temperature slowly and stirred for 1 h before being diluted with a sat'd solution NH_4Cl (100 mL) and EtOAc (40 mL). The phases were and the aqueous phase was extracted with EtOAc (3x 40 mL). The organic extracts were combined, dried over Na_2SO_4, filtered, concentrated under reduced pressure, and purified via flash chromatography (9:1

Hexanes/EtOAc). The resulting tan solid was dried under reduced pressure to yield the pure compound. Yield = 500 mg, 91%.

(*S*)-1-(benzo[d][1,3]dioxol-5-yl)-N,N-dimethylpropan-2-amine (*S*-MDMA Fumarate 2:1). To an ice-cold solution of *tert-butyl (R)-(1-(benzo[d][1,3]dioxol-5-yl)propan-2-yl)carbamate* (300 mg, 1.1 mmol) in THF (11 mL) was added lithium aluminum hydride (0.4 M) (0.29 mL, 1.2 mmol, 1.1 equiv.) and stirred for 5 min. The reaction was then heated to 66 °C and stirred for 4 h before being cooled to -10 °C. The reaction was diluted with THF (5 mL) followed by dropwise addition of H_2O (2 mL). The reaction was then diluted into a sat'd solution of Rochelle's salt (150 mL) and EtOAc (40 mL) was added. The phases were separated and the aqueous phase was extracted with EtOAc 3x (40 mL). The organic extracts were combined, dried over Na_2SO_4, filtered, and concentrated under reduced pressure. The resulting solid was taken up in $CHCl_3$ (1 mL) and added to a boiling solution of fumaric acid (125 mg, 1.1 mmol, 1 equiv.) in THF (15 mL). The solution was cooled to room temperature and stored at -20°C overnight. The solid was filtered and washed with ice-cold acetone (1 mL) and dried under reduced pressure to afford the desired product as the 2:1 fumarate salt. Yield = 112 mg, 81%. 1 H NMR (600 MHz, CD_3OD) δ 6.77 (d, 2H, *J* = 8.0 Hz), 6.72 (d, 1H, *J* = 8.0 Hz), 6.66 (s, 1H), 5.92 (s, 2H), 3.35 (m, 1H), 3.04 (dd, 1H, *J* = 13.5, 5.1 Hz), 2.68 (m, 4H), 1.22 (d, 3H, *J* = 6.2 Hz), ppm; 13C NMR (150 MHz, CD_3OD) δ 174.39, 149.55, 148.32, 137.10, 130.90, 123.66, 110.47, 109.45, 102.45, 57.69, 39.89, 30.85, 15.73, ppm. LRMS (ES+) m/z calcd for $C_{11}H_{15}NO_2$ + 193.11, found 194.03 (MH+).

***(S)*-1-(benzo[d][1,3]dioxol-5-yl)-N,N-dimethylpropan-2-amine (*S*-MDDMA Fumarate 1:1).** To an ice-cold solution of *tert-butyl (S)-(1-(benzo[d][1,3]dioxol-5-yl)propan-2-yl)carbamate* (500 mg, 1.8 mmol) in $CHCl_3$ (4 mL) was added trifluoroacetic acid (2 mL) and stirred for 15 min. The reaction was diluted with MeOH (5 mL) and concentrated under reduced pressure. The crude material was taken up in MeOH (24 mL) and cooled to 0°C. Acetic acid (0.44 mL, 7.6 mmol, 5 equiv.) was added to the reaction mixture followed by $NaBH_3CN$ (202 mg, 3.2 mmol, 2.1 equiv.) and the reaction was warmed to room temp. The reaction was stirred overnight before being concentrated under reduced pressure. The resulting crude solid was taken up in 1 M $NaOH_{(aq)}$ (125 mL) and DCM (30 mL). The phases were and the aqueous phase was extracted

with DCM (3x 30 mL). The organic extracts were combined, dried over Na_2SO_4, filtered, and concentrated under reduced pressure. The resulting solid was taken up in acetone (1 mL) and added to a boiling solution of fumaric acid (178 mg, 1.5 mmol, 1 equiv.) in acetone (30 mL). The solution was cooled to room temperature and stored at -20°C overnight. The solid was filtered and washed with ice-cold acetone (1 mL) and dried under reduced pressure to afford the desired product as the 1:1 fumarate salt. Yield = 416 mg, 84%. ^{1}H NMR (600 MHz, CD_3OD) δ 6.79 (m, 2H), 6.74 (m, 1H), 6.70 (s, 2H), 5.94 (s, 2H), 3.6 (m, 1H), 3.06 (t, 1H, *J* = 4.4, 8.9 Hz), 2.85 (s, 6H), 2.71 (dd, 1H, *J* = 2.9, 10.4 Hz), 1.21 (d, 3H, *J* = 7 Hz), ppm; ^{13}C NMR (150 MHz, CD_3OD) δ 169.84, 149.63, 148.41 135.74, 130.73, 123.61, 110.38, 109.50, 102.52, 64.61, 37.77, 12.71, 39.62, 37.79, 12.62, ppm. LRMS (ES+) m/z calcd for $C_{16}H_{21}NO_6$ + 207.13, found 208.01 (MH+).

Enantiopurity

The enantiopurity of MDA was determined by ^{19}F-NMR using a fluorinated chiral auxiliary. The procedures by Wang et al. were adapted as described in the next few steps, respectively.[31] Freshly distilled ethyl trifluoroacetate (4 mL, 33.6 mmol, 1.5 equiv) was added to a solution of l-alanine (2 g, 22.4 mmol) and TEA (3.13 mL, 22.4 mmol, 1 equiv) in MeOH (12.25 mL) after 5 minutes of stirring at room temperature. The liquid mixture was then concentrated under reduced pressure to evaporate the methanol. The concentrated oily mixture was then extracted three times with 2 M HCl (75 mL) and DCM (25 mL). The phases were separated and the aqueous phase was extracted thrice with DCM (25 mL). The organic extracts were combined, dried over Na_2SO_4, filtered, and concentrated under reduced pressure to yield the desired product as a white crystalline solid (3.5 g, 85%). Melting point = 63.0 – 68.5 °C; ^{1}H NMR (400 MHz, DMSO-d_6) δ 9.69 (d,1H), 4.30 (quint, 1H), 1.36 (d, 1H); ^{13}C NMR (400 MHz, DMSO-d_6) δ 172.9, 156.4, 117.7, 48.7, 16.7.

The procedures by Sham et al. were adapted as described in the next few steps, respectively.[32] Briefly, to an ice-cold solution of the TFA-protected l-alanine (0.022 g, 0.12 mmol, 1.1 equiv) in anhydrous DCM (0.54 mL) was added DCC (0.025 g, 0.12 mmol, 1.1 equiv) and then HOBt (0.018 g, 0.12 mmol, 1.1

[31] Wang, K.; Lu, Y.; Ishihara, K.The ortho-substituent on 2, 4-bis (trifluoromethyl) phenylboronic acid catalyzed dehydrative condensation between carboxylic acids and amines. *Chemical Communications*, **2018,** 54, 5410-5413.
[32] Sham, H. L.; Stein, H.; Cohen, J. Novel non-basic bioisostere of histidine synthesized from L-aspartic acid. Journal of the Chemical Society, *Chemical Communications*, **1987**, 23, 1792-1793.

equiv), respectively. *R*-MDA (0.020 g, 0.11 mmol) in anhydrous DCM (0.5 mL) was added into the reaction mixture followed by the addition of pyridine (0.019 mL, 0.24 mmol, 2.2 equiv) and was stirred at 0°C for 15 minutes. The reaction mixture was diluted with water (75 mL) and extracted 3x with DCM (25 mL). The organic extracts were combined, dried over Na_2SO_4, filtered, and concentrated under reduced pressure, and used without further purification.

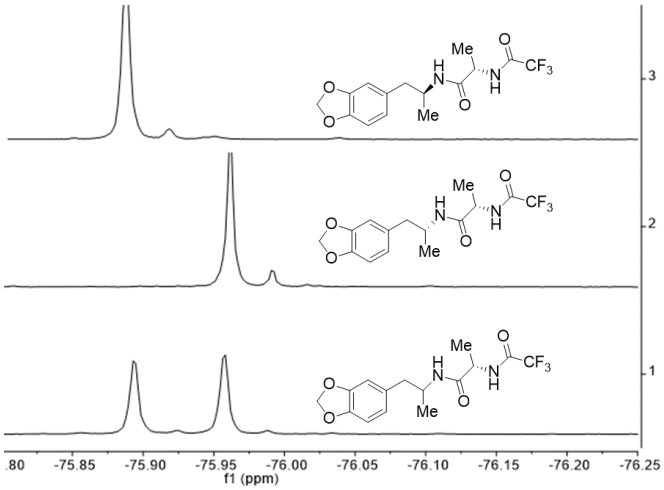

^{19}FNMR spectra of *R*-, *S*-, and racemic MDA.

Animals

All experimental procedures involving animals were approved by the University of California, Davis Institutional Animal Care and Use Committee (IACUC) and adhered to the principles described in the NIH Guide for the Care and Use of Laboratory Animals. E18 timed pregnancy Sprague-Dawley rats were obtained from Charles River Laboratories (Wilmington, MA, USA). C57BL/6J mice were obtained from Jackson Laboratory and were approximately 9-13 weeks old at the time of the experiments.

Dendritogenesis Experiments

For the dendritogenesis experiments conducted using cultured cortical neurons, E18 timed pregnant Sprague Dawley rats were obtained from Charles River Laboratories. Full culturing, staining and analysis experiments were performed as previously described with the exception that there was no media

change during treatments.[33] Dendrites were visualized using a chicken anti-MAP2 antibody (1:10,000; EnCor, CPCA-MAP2). DMSO and ketamine (10 μM) were used as a vehicle and positive controls, respectively. For blocking experiments, ketanserin was added 30-minutes prior to the addition of agonists in 10-fold excess.

Spinogenesis Experiments

Spinogenesis experiments were performed as previously described with the exception that cells were treated at DIV14 instead of DIV18 and then fixed on DIV15.[1033] The images were taken on a Nikon HCA Confocal microscope a with a 100×/NA 1.45 oil objective. DMSO and ketamine (10 μM) were used as a vehicle and positive controls, respectively. For blocking experiments, ketanserin was added 30-minutes prior to the addition of agonists in 10-fold excess.

Head-twitch response, Novelty Induced Locomotion, and Body Temperature Assay

The head-twitch response assay was performed as described previously using both male and female C57BL/6J mice (3 each per treatment). The mice were obtained from Jackson Laboratory and were approximately 9 weeks old at the time of the experiments. Before injecting the mice, their baseline temperature was measured using an IR thermometer as described.[34] Compounds were administered via intraperitoneal (i.p.) injection (5 ml kg−1) using 0.9% saline as the vehicle. Immediately after the animals were placed in an arena (40cm x 40cm) for 30-minutes where their locomotor activity was assessed using AnyMaze automated tracking software. The behavior was also videotaped and later scored by two blind overserves for head-twitch responses, the results were averaged. Upon completion of the novelty-induced locomotion assay, their temperature was measured at the 30-minute mark. The mice were then transferred to a holding cage with their other treatment-matched cage mates and their temperature was measured at the 90 and 120- minute mark.

[33] Ly, C.; Greb, C. A.; Vargas, M. V.; Duim, W. C.; Grodzki, A. C. G.; Lein, P. J.; Olson, D. E. Transient Stimulation with Psychoplastogens is Sufficient to Initiate Neuronal Growth. *ACS Pharmacol. Transl. Sci*. **2020**, 4, 452–460
[34] Kawakami, Y.; Sielski, R.; Kawakami, T. Mouse Body Temperature Measurement Using Infrared Thermometer During Passive Systemic Anaphylaxis and Food Allergy Evaluation. *J Vis Exp.* **2018**, 139, 58391.

Fear Extinction

Mice were exposed to cued fear conditioning on day 1, fear extinction training on day 2, and extinction testing on Day 3. Mice were habituated to handling for 3 days before experimentation. On the day of the experiment, mice were allowed to habituate to the behavior room for 1-hour before beginning the experiment. Mice were separated into individual holding cages 15-minutes before starting the experiment.

Cued fear conditioning consisted of six pairings of a CS auditory cue (80-85 dB white noise, 15 s) and a co-terminating US footshock (0.85 mA and 2 s), each spaced 1.5 minutes apart. The fear conditioning apparatus (Med Associates model # MED-VFC2-SCT-R) consisted of a 30.5 cm × 24.1 cm × 21 cm internal soundproof chamber, with metal grated floors, an infrared camera, a sound generator, and a light source. Mice were initially placed in the conditioning apparatus and the first 1.5 minutes were stimulus-free. After the last shock, the animals remained in the chambers for an additional 2 min before being returned to their home cages. During fear conditioning, the apparatus was illuminated to 100 lx and did not contain any additional odor cues. Freezing responses for fear conditioning (day 1) are presented as the percentage of time spent freezing during the last 1.5 minutes after the last shock. The apparatus was cleaned with 70% EtOH in between trials.

On day 2, animals were separated into individual holding cages and administered either vehicle (0.9% USP saline), R-MDMA (12.5 or 25 mg/kg I.P) or R-MDDMA (12.5 or 25 mg/kg I.P.) 30-minutes prior to being placed in the fear extinction context. Cued fear memory was assessed by exposing the animals to a novel context (lights off, A-frame insert, smooth plastic floor insert, additional vanilla odor) for 2 min prior to 16 presentations of auditory cues (80 dB white noise, 15 s) spaced 15 s apart. Freezing responses for cue testing (day 2 and 3) are presented as the percentage of time spent freezing during the tone presentations. The procedure was repeated on day 3 in the absence of a drug.

Fear conditioning experiments were performed between the hours of 08:00−11:00. Freezing behavior was scored using Med Associates Video Freeze software v2.25 (motion threshold = 100 au, detection method = linear, minimum freeze duration = 15 frames, which is equal to a 0.5 s freeze). The apparatus was cleaned

with 70% EtOH in between trials on day 1 and Sani-cloth gemicidal disposable cloths (PDI, Q89072) were used to clean the apparatus on days 2 and 3.

SERT Efflux Experiments

HEK293T cells were grown in Dulbecco's Modified Eagle Media (DMEM) supplemented with 10% fetal bovine serum (FBS) and 1% penicillin-streptomycin. 24 hours prior to the experiment, cells were plated in 24-well plates at a density of 150,000 cells/well and concurrently transfected using Lipofectamine 3000 according to the manufacturer's protocol. Cells were transfected with hSERT-N1-pEYFP (Addgene #70105) or a GFP control plasmid (Lonza pmaxGFP vector). The next day the wells were washed (1 x 500 µL) with 1X Hank's Balanced Salt Solution supplemented with 2 mM $MgCl_2$ and 2 mM $CaCl_2$ (HBSS) and the plate was placed on a 37 °C water bath for the remainder of the experiment. 250 µL of HBSS containing 10 nM 5-[1,2-^{3}H[N]]-hydroxytryptamine creatinine sulfate (NET498001MC, Lot: 2902700) was added to the wells and incubated for 15 minutes, allowing uptake into SERT expressing HEK cells. Uptake was terminated by aspiration of wells followed by washes (3 x 500 µL) with HBSS. Efflux was initiated by adding 250 µL drug solution (0.02% DMSO as vehicle control, 100 µM DL-*p*-chloroamphetamine (Sigma Aldrich, C9635-1G) as the positive control, 100 µM–10 pM L-MDMA, 100 µM–10 pM L-MDDMA) in HBSS for 15 minutes. 200 µL of media was collected from each well and placed into a scintillation vial containing 1 mL PerkinElmer Ultima Gold™ scintillation cocktail to serve as the efflux fraction. The wells were washed (3 x 500 µL) with HBSS and then cells were lysed for 10 minutes by adding 250 µL radioimmunoprecipitation assay (RIPA) buffer (50 mM Tris HCl, 150 mM NaCl, 1% NP-40, 0.5% sodium deoxycholate, 0.1% SDS, pH 8) to each well. Cells were lysed with a P1000 pipette using the RIPA buffer in the well and all contents of the well were collected into separate scintillation vials containing 1 mL PerkinElmer Ultima Gold™ scintillation cocktail to serve as the intracellular fraction. An additional 250 µL of RIPA buffer was added to each well and then transferred to the intracellular fraction vials. Scintillation vials were mixed by inverting incubated overnight at room temperature. Radioactivity in the form of disintegrations per minute (DPM) was determined the following day with the use of a Beckman LS 6000 liquid scintillation counter. The efflux fraction counts were corrected by a factor of 1.25 to account for the 50 µL remaining in each well (DPM * 250 µL total/ 200 µL collected). Using the DPM for each compound, bar graphs were reported as efflux fraction/(efflux fraction

+ intracellular fraction) and then normalized to the vehicle control and positive control with the vehicle set at 0% and positive control set at 100%. The GFP control cells were checked to ensure radioactivity was below background levels.

Sensor Experiments

E18 rat cortical neurons were plated at 60,000 cells/well in glass 96-well plates (P96-1.5H-N, Cellvis) coated with poly-D-lysine (Sigma, P6407-5MG). At a day in vitro (DIV) 3-7 neurons were infected with AAV9_hSynapsin_psychLight2 (Neurophotonics– Viral Vector Core) or AAV9-hsyn-GRAB_5-HT1.0 (Addgene, 140552-AAV9) at an MOI of 70,000. Neurons were kept in the incubator for one week to allow for viral expression. On imaging day (DIV 10-14), media was aspirated and wells were washed (1 x 200 µL) with HBSS supplemented with 2 mM $MgCl_2$ and 2 mM $CaCl_2$. 50µL HBSS was added to the wells of the assay plate and then imaged on a CellInsight CX7 HCA Platform (Thermo Fisher, CX7A1110) configured with a onstage incubator for live cell imaging (Thermo Fisher, NX7LIVE001) at 40x (N.A. = .60) with 25 regions of interest (ROI) taken per well using an arbitrary ROI pattern for each well with no bias to location and no overlap of the ROIs (exposure = 400 ms, LED power = 100%). Immediately prior to imaging, stock solutions of drugs in DMSO (10 mM) were diluted 1:500 in imaging media (HBSS) and distributed across an empty 96-well treatment plate in triplicate following a randomized plate map. Next, 50 µL from the treatment plate was transferred to the assay plate resulting in a 1:1000 dilution of drug (10 µM as the final concentration in 0.1% DMSO). As a positive and vehicle control, 5-HT (10 µM) and 0.1% DMSO were used, respectively. After a 5-minute incubation, the same sites were re-imaged using the same settings.

Images were then analyzed using ImageJ by selecting ROIs surrounding individual neuronal cell bodies of the post-treatment images and recording the mean fluorescence, the same ROIs were applied to the pretreatment images to record the mean fluorescence. The ΔF/F values were calculated as previously reported.[35]

[35] Dong, C.; Ly, C.; Dunlap, L. E.; Vargas, M. V.; Sun, J.; Hwang, I.-W.; Azinfar, A.; Oh, W. C.; Wetsel, W. C.; Olson, D. E.; Tian, L. Psychedelic-Inspired Drug Discovery Using an Engineered Biosensor. *Cell* **2021**, 10, 2779-2792.

Ketanserin Blocking Experiments

For the ketanserin blocking experiments (Figure 3.5), a slightly modified method was employed. On DIV3, neurons were first treated with ketanserin (10 μM) for 15 min followed by a 24 h incubation with the drug (1 μM) and ketanserin (10 μM) (final concentration of DMSO = 0.2%). The cells were allowed to grow for 72h (sholls) and 24h(spines) before being fixed, stained, and imaged.

Statistical Analysis

Treatments were randomized, and data were analyzed by experimenters blinded to treatment conditions. Statistical analyses were performed using GraphPad Prism (version 8.1.2). The specific tests used, F-statistics, degrees of freedom, and main effect p values are indicated in the figure legends where appropriate. All comparisons were planned prior to performing each experiment. For dendritogenesis experiments, a one-way ANOVA with Dunnett's post hoc test was deemed most appropriate, as our research question focused on determining whether or not a particular treatment promoted neuronal growth to a greater extent than the vehicle control. Ketamine was included as a positive control to ensure that the assay was working properly.

Chapter 4. Using a 5-HT2AR Based Sensor For Drug Discovery

Chapter 4.1 Introduction

A hallmark of depression is the atrophy of neurons in the prefrontal cortex. Compounds that are robustly able to promote the growth of neuronal processes represent valuable drug targets. We have recently reported on a class of drugs that have been coined psychoplastogens, fast-acting therapeutics capable of rapidly promoting structural and functional neural plasticity.[1] These psychoplastogens represent a promising class of therapeutics for the treatment of brain disorders.

Some of the most well-known psychoplastogens like psilocin, the main metabolite of psilocybin and MDMA have shown promising results in clinical studies for depression and PTSD respectively.[2,3] A key aspect of the mechanism of the psychoplastogenic effects of these drugs involves the serotonin 2A receptor (5-HT2AR).[4,5,6] Pretreatment of neuronal cultures with 5-HT2R antagonists blocks the effects of psychoplastogens. While the 5-HT2AR is key for the therapeutic effect of these drugs, it is also responsible for the hallucinogenic side effects of psychedelics-based psychoplastogens, i.e psilocin, LSD, etc. Despite the importance of 5-HT2AR in both mechanisms, we have previously reported that the hallucinogenic effects can be decoupled from their therapeutic effects.[7,8] The exact mechanism of 5-HT2ARs that results in either hallucinations or plasticity-promoting effects is still not clearly understood. Common methods of

[1] Olson, D. E. Psychoplastogens: A Promising Class of Plasticity-Promoting Neurotherapeutics. *J Exp Neurosci.* **2018**. doi: 10.1177/1179069518800508

[2] Mithoefer, M. C.; Wagner, M. T.; Mithoefer, A. T.; Jerome, L.; Doblin, R. The safety and efficacy of {±}3,4-methylenedioxymethamphetamine-assisted psychotherapy in subjects with chronic, treatment-resistant posttraumatic stress disorder: the first randomized controlled pilot study. *J. Psychopharmacol.* **2011**, *25*, 439– 452.

[3] Davis, A. K. Barrett, F. S.; May, D. G.; Cosimano, M. P.; Sepeda, N. D.; Johnson, M. W.; Finan, P. H.; Griffith, R. R. Effects of Psilocybin-Assisted Therapy on Major Depressive Disorder: A Randomized Clinical Trial. *JAMA Psychiatry* **2021**, 78, 481-489

[4] Ly, C.; Greb, A. C.; Cameron, L. P.; Wong, J. M.; Barragan, E. V.; Wilson, P. C.; Burbach, K. F.; Soltanzadeh Zarandi, S.; Sood, A.; Paddy, M. R.; Duim, W. C.; Dennis, M. Y.; McAllister, A. K.; Ori-McKenney, K. M.; Gray, J. A.; Olson, D. E. Psychedelics Promote Structural and Functional Neural Plasticity. *Cell Reports* **2018**, 23, 3170–3182.

[5] Ly, C.; Greb, C. A.; Vargas, M. V.; Duim, W. C.; Grodzki, A. C. G.; Lein, P. J.; Olson, D. E. Transient Stimulation with Psychoplastogens is Sufficient to Initiate Neuronal Growth. *ACS Pharmacol. Transl. Sci*. **2020**, 4, 452–460.

[6] Pitts, E. G.; Minerva, A. R.; Chandler, E. B.; Kohn, J. N.; Logun, M. T.; Sulima, A.; Rice, K. C.; Howell, L. L. 3,4-Methylenedioxymethamphetamine increases affiliative behaviors in squirrel monkeys in a serotonin 2A receptor-dependent manner. Neuropsychopharmacology **2017,** 42, 1962– 1971,

[7] Dunlap, L. E.; Azinfar, A.; Ly, C.; Cameron, L. P.; Viswanathan, J.; Tombari, R. J.; Myers-Turnbull, D.; Taylor, J. C.; Grodzki, A. C.; Lein, P. J.; Kokel, D.; Olson, D. E. Identification of Psychoplastogenic *N,N*-Dimethylaminoisotryptamine (isoDMT) Analogs Through Structure-Activity Relationship Studies. *J. Med. Chem*. **2020**, 63, 1142–1155.

[8] Cameron, L. P.; Tombari, et. al. A Non-Hallucinogenic Psychedelic Analogue with Therapeutic Potential. *Nature* **2021**, 589, 474–479.

determining GPCR activity like phosphoinositide hydrolysis, Gq activation, and calcium flux have proven ineffective in distinguishing hallucinogens from non-hallucinogenic 5-HT2A ligands.[9,10,11] There is evidence to suggest that hallucinogens signal through a 5-HT2AR-mGluR2 heterodimer complex.[12,13] This could explain why non-hallucinogenic 5-HT2AR ligands can display agonist-like activity various assays for determining gpcr activation like inositol phosphate signaling.[14] As such, there currently is not a robust *in vitro* assay to determine whether a molecule is hallucinogenic or not. As my work has focused primarily on developing non-hallucinogenic psychoplastogens, a medium-throughput cell-based assay for predicting hallucinogenic potential was of particular interest to us.

We envisioned that we could engineer a 5-HT2AR with a fluorescent protein tag that could aid in distinguishing between hallucinogenic and non-hallucinogenic compounds. To this end, we developed psychLight—a genetically encoded fluorescent sensor based on the 5-HT2AR structure and characterized its use for predicting hallucinogenic potential.

Chapter 4.2 Development of a PsychlLight[15]

PsychLight was developed in the Tian lab by replacing the third intracellular loop of the human 5-HT2AR with a circularly permuted green fluorescent protein (cpGFP) (**Fig. 4.1A**).[16] The insertion site was screened extensively and the optimal construct was deemed psychLight1. Expression of psychLight1 in

[9] Cussac, D.; Boutet-Robinet, E.; Ailhaud, M. C.; Newman-Tancredi, A.; Martel, J. C.; Danty, N.; Rauly-Lestienne, I. Agonist-directed trafficking of signalling at serotonin 5-HT2A, 5-HT2B and 5-HT2C-VSV receptors mediated Gq/11 activation and calcium mobilisation in CHO cells. *Eur J Pharmacol* **2008**, 594, 32-38.

[10] Rabin, R. A.; Regina, M.; Doat, M.; Winter, J. C. 5-HT2A receptor-stimulated phosphoinositide hydrolysis in the stimulus effects of hallucinogens. *Pharmacol Biochem Behav*. **2002**, 72, 29-37.

[11] Cussac, D.; Boutet-Robinet, E.; Ailhaud, M. C.; Newman-Tancredi, A.; Martel, J. C.; Danty, N.; Rauly-Lestienne, I. Agonist-directed trafficking of signalling at serotonin 5-HT2A, 5-HT2B and 5-HT2C-VSV receptors mediated Gq/11 activation and calcium mobilisation in CHO cells. *Eur J Pharmacol*. **2008**, 594, 32-38.

[12] Moreno, J. L.; Holloway, T.; Albizu, L.; Sealfon, S. C.; Gonzalez-Maeso, J. Metabotropic glutamate mGlu2 receptor is necessary for the pharmacological and behavioral effects induced by hallucinogenic 5-HT2A receptor agonists *Neurosci Lett*. **2011**, 493, 76-79.

[13] Murat, S.; Bigot, M.; Chapron, J.; Konig, G. M.; Kostenis, E.; Battaglia, G.; Nicholetti, F,; Bourinet, E.; Bockaert, J.; Marin, J. Marin, P.; Vandermoere, F. 5-HT 2A receptor-dependent phosphorylation of mGlu 2 receptor at Serine 843 promotes mGlu 2 receptor-operated G i/o signaling. *Mol Psychiatry* **2019**, 24, 1610-1626.

[14] Egan, C. T.; Herrick-Davis, K.; Miller, K.; Glennon, R. A.; Teitler, M. Agonist activity of LSD and lisuride at cloned 5HT2A and 5HT2C receptors. *J Psychopharmacology (Berl).* **1998**, 136, 409-414.

[15] Data in this chapter can also be found in the following paper and is represented here with permission from Cell. Dong, C.; Ly, C.; Dunlap, L. E.; Vargas, M. V.; Sun, J.; Hwang, I.-W.; Azinfar, A.; Oh, W. C.; Wetsel, W. C.; Olson, D. E.; Tian, L. Psychedelic-Inspired Drug Discovery Using an Engineered Biosensor. *Cell*, **2021**, 10, 2779-2792.

[16] Dong, C.; Ly, C.; Dunlap, L. E.; Vargas, M. V.; Sun, J.; Hwang, I.-W.; Azinfar, A.; Oh, W. C.; Wetsel, W. C.; Olson, D. E.; Tian, L. Psychedelic-Inspired Drug Discovery Using an Engineered Biosensor. *Cell* **2021**, 184, 2779– 2792.

human embryonic kidney 293T (HEK293T) cells was predominately located to the cell surface (**Fig. 4.1B**). We then characterized the response of psychLight1 to different ligands of the 5-HT2AR. We found that serotonin (5-HT) gave a dose-dependent increase in fluorescence but the antagonists ketanserin (KETSN) and MDL 100,907 (MDL) gave no response (**FIG. 4.1C**). The EC_{50} of 5-HT measured using psychLight1 was comparable to values obtained using radioligand binding as well as Ca^{+} flux and β-Arrestin2 recruitment.[17,18]

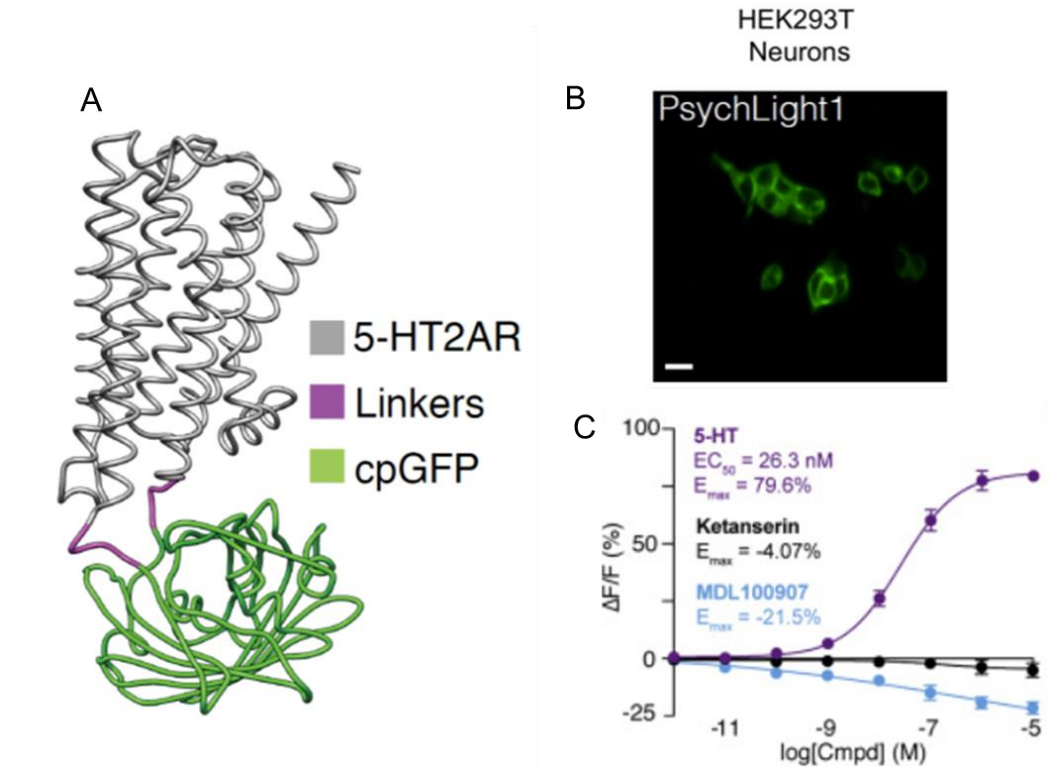

Figure 4.1. (A) Simulated structure of psychLight consisting of 5-HT2AR (gray), a linker (magenta), and a cpGFP (green). **(B)** Representative images of HEK239T cells expressing psychLight1. Scale bar: 20 μm. (**C**) PsychLight1-expressing HEK293T cells respond to ligands in a dose-dependent manner. Serotonin = 5-HT. ΔF/F = change in fluorescence over baseline fluorescence.

[17] Wacker, D.; Wang. S.; McCorvy, J. D.; Betz, R. M.; Venkatakrishnan, A. J.; Levit, A.; Lansu, K.; Schools, Z. L.; Che, T.; Nichols, D. E.; Shoichet, B. K.; Dror, R. O.; Roth, B. L. Crystal Structure of an LSD-Bound Human Serotonin Receptor. *Cell* **2017,** 168, 377-389.
[18] Toro-Sazo, M.; Brea, J.; Loza, M. I.; Cimadevila, M.; Cassels, B. K. 5-HT2 receptor binding, functional activity and selectivity in N-benzyltryptamines. *PLoS One* **2019**, 14, e0209804.

We next validated the potential of psychLight to distinguish between hallucinogenic and non-hallucinogenic compounds. We screened a series of known hallucinogens: *N,N*-dimethyltryptamine (DMT), 5-methoxy-*N,N*-dimethyltryptamine (5-MeO-DMT), lysergic acid diethylamide (LSD), 2,5-Dimethoxy-4-iodoamphetamine (DIO), and their non hallucinogenic analogs 6-fluoro-*N,N*-diethyltryptamine (6-F-DET), 6-methoxy-*N,N*-dimethyltryptamine (6-MeO-DMT), Lisuride, and *R*-3,4-methylenedioxymethamphetamine **(Fig 4.2A)**. We chose these compounds because their hallucinogenic potential has been established in humans or from well-validated animal models.[19,20,21,22,23,24,7] We found that the hallucinogenic compounds robustly activated psychLight while their non-hallucinogenic analogs did not. We also note that the human hallucinogenic potencies correlate well with the EC_{50} values obtained using psychLight **(FIG 4.2.B)**. PsychLight consistently distinguished hallucinogens from non-hallucinogens over traditional measures of 5-HT2AR activity including phosphoinositide hydrolysis, Gq activation, and calcium mobilization **(FIG 4.2C)**.[9,10]

[19] Benes, H.; Deissler, A.; Rodenbeck, A.; Engfer, A.; Kohnen, R. *J. Neural. Transm. (Vienna).* **2006**, 113, 87-92.
[20] Dunlap, L. E.; Andrews, A. A.; Olson, D. E. Dark Classics in Chemical Neuroscience: 3,4-Methylenedioxymethamphetamine. *ACS Chem. Neurosci.* **2018**, 9, 2408–2427.
[21] Halberstadt, A. L.; Chatha, M.; Klein, A. K.; Wallach, J.; Brandt, S. D. Correlation between the potency of hallucinogens in the mouse head-twitch response assay and their behavioral and subjective effects in other species. *Neuropharmacology* **2020**, 167, 107933.
[22] Kalir, A.; Szara, S. Synthesis and pharmacological activity of fluorinated tryptamine derivatives. *J Med Chem.* **1963,** 6, 716-719.
[23]Hanks, J. B.; Gonzalez-Maeso, J. Animal models of serotonergic psychedelics. *ACS Chem Neurosci*. **2013**, 4, 33-42.
[24] Glennon, R. A.; Young, R. l.; Jacyno, J. M.; Slusher, M.; Rosecrans, J. A. DOM-Stimulus Generalization to LSD and other Hallucinogenic Indolealkylamines. *Eur. J. Pharmacol.* **1983**, 86, 453– 459.

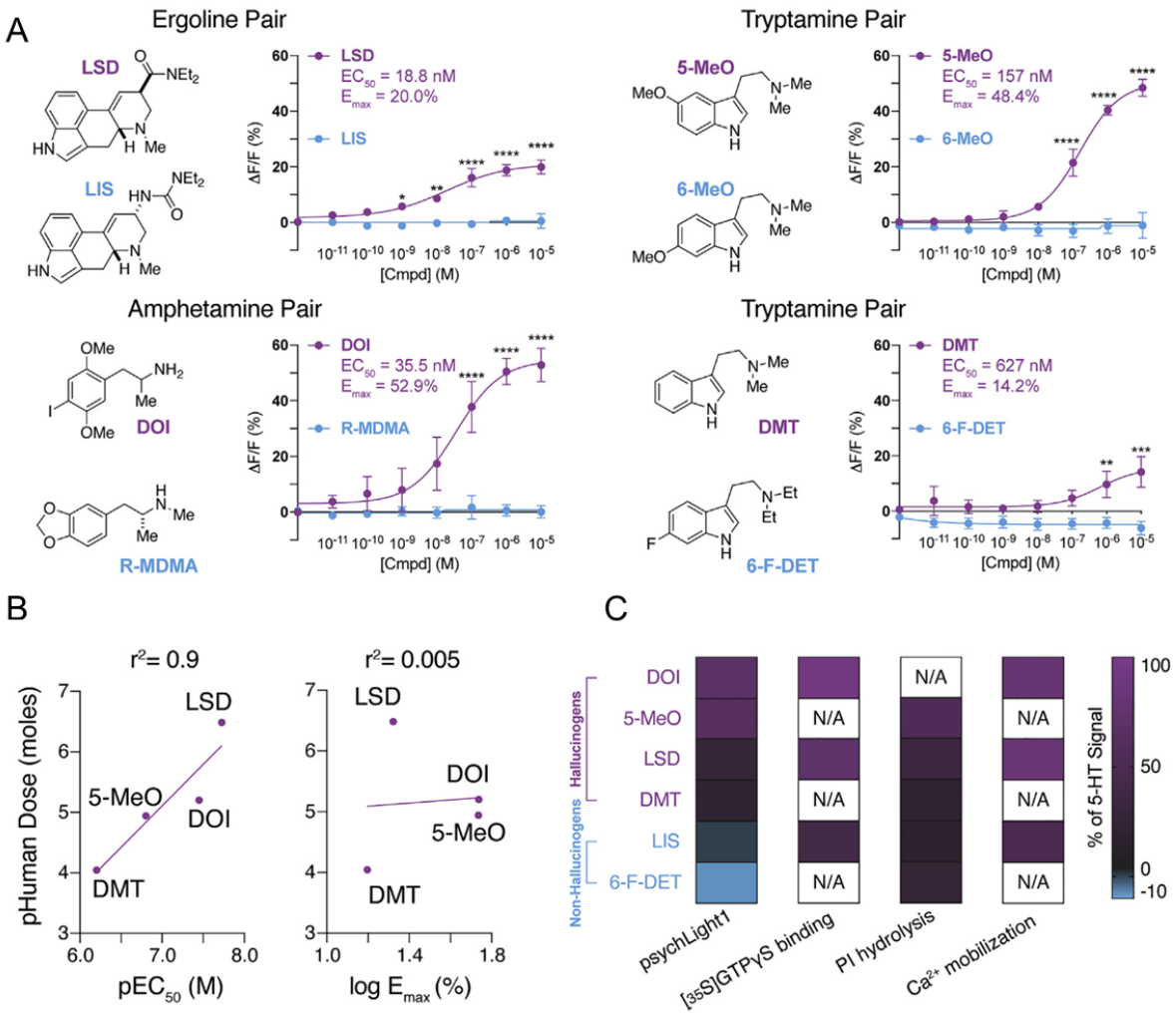

Figure 4.2. (A) Concentration-response studies using HEK293T cells transiently expressing psychLight1. Hallucinogens (magenta) were tested along with their non-hallucinogenic analogs (blue). Hallucinogens activated psychLight1 while their non-hallucinogenic congeners did not. n = 3 cells from 3 different cell passages; Error bars represent SEM, ∗p < 0.05, ∗∗p < 0.01, ∗∗∗p < 0.001, ∗∗∗∗p < 0.0001, compared to the non-psychedelic drug, two-way ANOVA. **(B)** PsychLight1 EC_{50} values, but not Emax values, correlate with hallucinogen potencies in humans. **(C)** PsychLight1 Emax values differentiate hallucinogens and non-hallucinogens, but other measures of 5-HT2AR activation (e.g., phosphoinositide [PI] hydrolysis, Ca2+ mobilization, [35S]GTPγS binding) do not. Data are normalized to 5-HT values within each experiment. Data for PI hydrolysis, calcium mobilization, and [^{35}S]GTPγS binding were obtained from previous reports.[9,10] PI hydrolysis data for 6-F-DET were estimated based on graphical data presented previously.[10] N/A indicates that data was unavailable.

We have demonstrated that psychLight can distinguish between hallucinogenic and structurally similar non-hallucinogenic analogs. Next, we wanted to assess if psychLight could be used to determine the binding of non-hallucinogenic 5-HT2A ligands. Several of the non-hallucinogenic compounds tested did not active psychLight but are known to have a potent affinity for 5-HT2ARs. By applying 5-HT before test compounds, we found that we could also measure the activity of antagonists like lisuride and 6-MeO-DMT using psychLight **(FIG. 4.3)**.

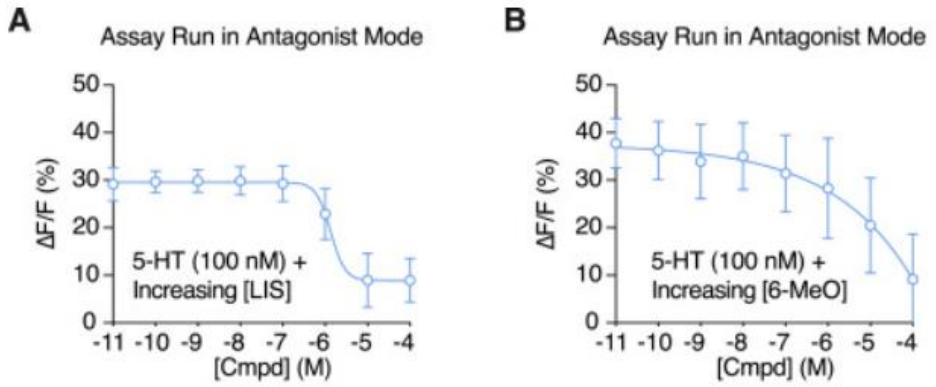

Figure 4.3. The non-hallucinogenic ligands lisuride **(A)** and 6-MeO-DMT **(B)** can compete off 5-HT resulting in a concentration-dependent reduction in psychLight fluorescence.

We further correlated the results of psychLight activation with hallucinogenic effects by using an *in vivo* model of hallucinogenic potential. We chose to use the head twitch response (HTR) assay due to the high degree of correlation between HTR and human potencies.[21] We found that while psychLight1 was predominantly expressed on the cell surface in HEK293T cells, in neurons psychLight1 was predominantly expressed intracellularly. The addition of the EF1α promoter to psychLight1, which we deemed psychLight2, shifted the expression of psychLight in neurons from the intracellular space to the cell surface (**FIG. 4.4A**). Three weeks after animals were injected with AAV9.hSynapsin1.psychlight2, we administered 5-MeO-DMT (50 mg/kg, intraperitoneal [i.p.]), saline, or KETSN (4 mg/kg [i.p]) and measured psychLight2 response using fiber photometry (**FIG 4.4C**). The hallucinogen 5-MeO-DMT gave an immediate increase in fluorescence which mirrored the increase in HTR. In contrast, mice receiving KETSN had a slower but

steady decrease in fluorescence and saline remained unchanged. These data suggest that psychLight can reliably detect conformational changes induced by agonists and antagonists both *in vitro* and *in vivo*.

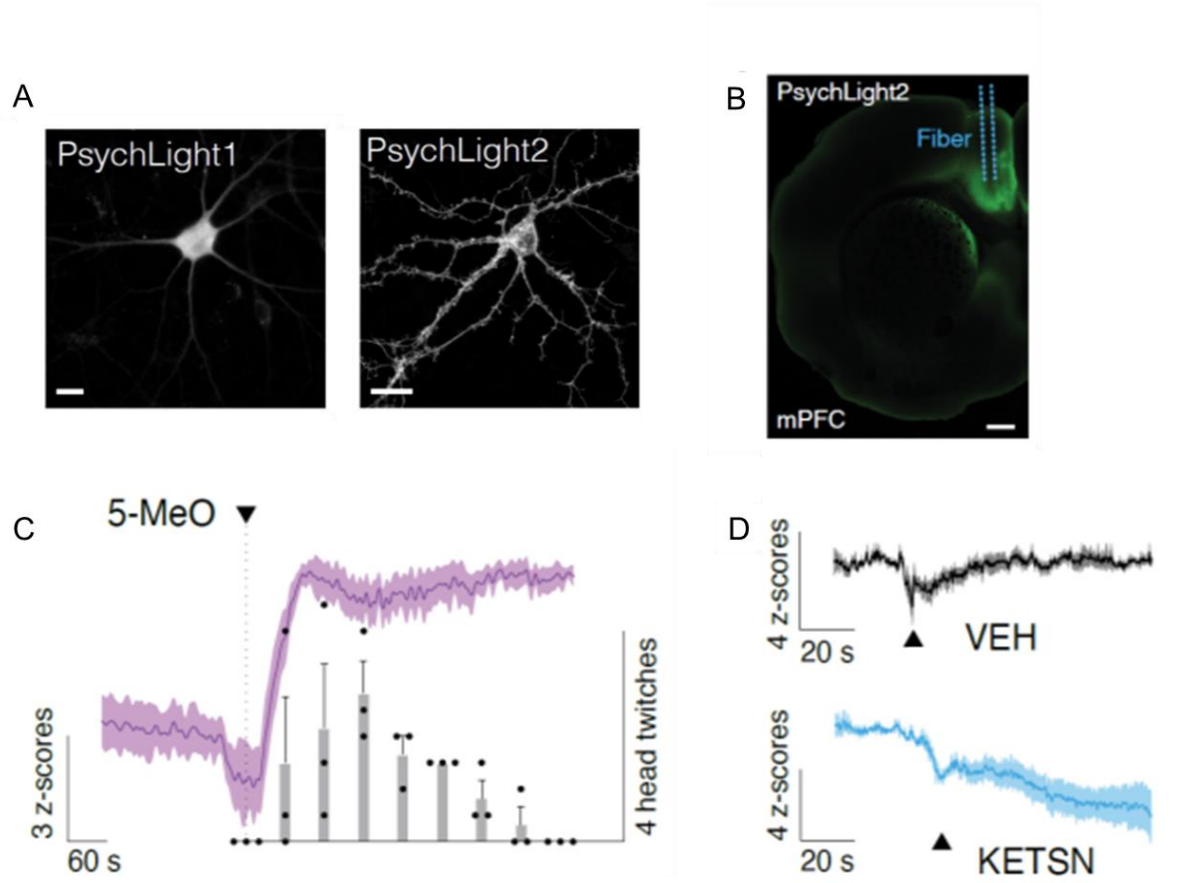

Figure 4.4. (A) Representative images of cultured dissociated hippocampal neurons transiently expressing psychLight1 and psychLight2. Scale bar, 20 μm. **(B)** Expression of psychLight2 in the prelimbic cortex near the site of fiber implantation. Scale bar, 500 μm. **(C)** Averaged-trial traces of psychLight2 responses shown as Z score following injection of 50 mg/kg 5-MeO (magenta, i.p.), the shaded area represents SEM. The number of head-twitch responses (bars) was also recorded and binned into 1-min intervals (n = 3 animals). **(D)** Averaged-trial traces of psychLight2 responses following the injection either of saline (VEH; top black) or an antagonist (4 mg/kg KETSN, bottom blue, i.p.) (n = 3 animals). Average traces indicated by solid lines; shaded area represents SEM.

Chapter 4.3 PsychLight as a Medium Throughput Screen

To utilize psychLight as a medium-throughput screen we first developed a HEK293T cell line stably expressing psychLight2 (PSYLI2 cell line). We validated the PSYLI2 cells using a widefield high-content imager (**FIG 4.5A**). We found that PSYLI2 cells were able to reliably differentiate hallucinogens from non-hallucinogens and gave comparable results to those obtained using psychLight1 on a confocal microscope. While the PSYLI2 cells had a slightly lower response on the high-content imager we found that this method was able to distinguish small changes made to the tryptamine scaffold (**FIG 4.5B**). Notably, changes such as increased methylation on the basic amine of the tryptamine scaffold produced significant changes in PSYLI2 response.

While tryptamine and serotonin are generally considered not to produce hallucinations, likely due to poor brain penetrance, there is evidence to suggest that both compounds are capable of eliciting hallucinogenic responses in animal models.[25] When injected Intracerebroventricularly, serotonin (40 µg) caused a pronounced increase in the number of head twitches in mice.[26] Further, 5-hydroxytryptophan (5-HTP), serotonin precursor, causes an increase in the number of head twitches in mice which correlated with increased levels of serotonin in the brain stem.[27,28] Whether or not these biogenic amines produce hallucinations in humans has not been fully investigated, however, hallucinations have been reported as a side effect of selective serotonin reuptake inhibitors (SSRIs).[29] A possible explanation for why serotonin does not produce hallucinations at basal levels is that serotonin is not able to reach the intracellularly expressed 5-HT2ARs.[30]

[25] Yamada, J.; Sugimoto, Y.; Horisaka, K. Pharmacological analysis of the variation in behavioural responses to tryptamine in five strains of mice. *Eur. J Pharmacol*. **1987**, 140, 323-330.
[26] Bohn, L. M.; Schmid, C. L. Serotonin receptor signaling and regulation via β-arrestins. *Crit Rev Biochem Mol Biol.* **2010**, 45, 555–566.
[27] Corne, S. J.; Pickering, R. W.; Warner, B. T. A method for assessing the effects of drugs on the central actions of 5-hydroxytryptamine. *Br J Pharmacol Chemother*. **1963**, 20, 106-20.
[28] Backstrom, J. R.; Chang, M. S.; Chu, H.; Niswender, C. M.; Sanders-Bush, E. Agonist-Directed Signaling of Serotonin 5-HT2C Receptors: Differences Between Serotonin and Lysergic Acid Diethylamide (LSD). *Neuropsychopharmacology* **1999**, 21, 77–81.
[29] Cancelli, I.; Marcon, G.; Balestrieri, M. Factors associated with complex visual hallucinations during antidepressant treatment. *Hum Psychopharmacol*. **2004**, 19, 577-584.
[30] For more information on this see chapter 2.

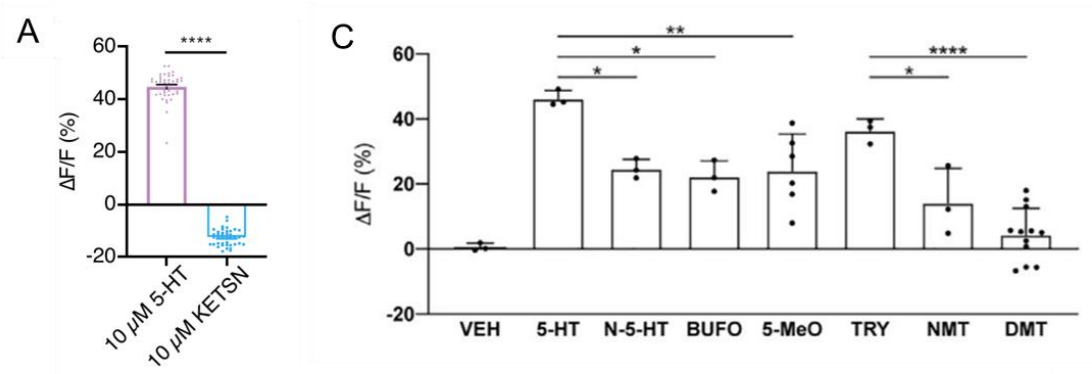

B

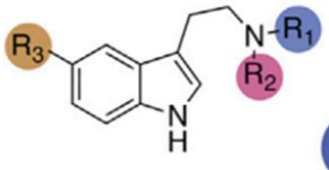

Compound	R_1	R_2	R_3
5-MeO-DMT (5-MeO)	Me	Me	OMe
N,N-Dimethyltryptamine (DMT)	Me	Me	H
N-Methyltryptamine (NMT)	Me	H	H
Tryptamine (TRY)	H	H	H
N,N-Dimethylserotonin (BUFO)	Me	Me	OH
N-Methylserotonin (N-5-HT)	Me	H	OH
Serotonin (5-HT)	H	H	OH

Figure 4.5. PSYLI2 cells can differentiate small changes in chemical structures. **(A)** Bar graph showing PSYLI2 response to 10 μM 5-HT (44.8 ± 0.8%) and 10 μM KETSN (−12.7 ± 0.5%). **(B)** Structures of compounds. **(C)** PSYLI2 fluorescence in response to compound treatments (10 μM). Data are represented by mean ± SEM, ∗∗∗∗p < 0.0001, ∗∗p < 0.01 and ∗p < 0.05, one-way ANOVA multiple comparison with Tukey's test.

Having demonstrated that PSYLI2 cells can accurately differentiate minor structural changes we screened a series of 83 compounds (**FIG 4.6**). This library consisted of compounds known to be hallucinogens, or non-hallucinogens, as well as known non-2A ligands, and compounds with unknown 5-HT2A affinity and hallucinogenic potential. We screened these compounds in both agonist mode to determine hallucinogenic potential and antagonist mode to determine 5-HT2A activity (**FIG 4.7A, B**). In agonist mode, hallucinogens reliably gave a response of 1 standard deviation above the vehicle control.

Compounds that caused a decrease in fluorescence in antagonist mode are likely to be non-hallucinogenic 5-HT2A ligands. It is worth noting the high degree of selectivity that psychLight has for serotonergic hallucinogens. Dissociative compounds like ketamine, salvinorin A, and Phencyclidine (PCP) failed to elicit a response in psychLight.

Using the results from the agonist and antagonist mode screen we were able to develop a ligand score to help predict 5-HT2AR binding (**FIG 4.7C**). Hallucinogenic ligands of 5-HT2A have a positive (red) score while non-hallucinogenic ligands have a negative ligand score (blue). Compounds that showed no activity at 5-HT2A had a ligand score of 0 (black). When plotted on a cartesian coordinate (agonist mode = x-axis, antagonist mode = y-axis) serotonergic hallucinogens, non-hallucinogenic 5-HT2A ligands, and non-binders of 5-HT2A clustered in well-defined groups (**FIG 4.8A**).

While we observed that psychLight was reliably able to predict the hallucinogenic potential of compounds we did find two compounds that gave unexpected results. Both 2-bromolysergic acid diethylamide (BOL-148) and bromocriptine produced an increase in fluorescence signal when screened at 10 μM in agonist mode. As both BOL-148 and bromocriptine are believed to be non-hallucinogenic we reasoned that the resulting increased signal may come from the inherent fluorescence of these molecules resulting in false positive signals. We performed a counter-screen by running a concentration-response with the two drugs in psychLight on a high content imager and in the absence of psychLight on a fluorescence plate reader (**FIG 4.8B**). In psychLight, only the 10 μM concentration resulted in an increased fluorescence signal which was consistent with our findings from the plate reader thus confirming that the fluorescence signal found using PSYLI2 cells resulted from the fluorescent nature of the molecule.

Chapter 4.4 PsychLight Predicts Hallucinogenic Potential

To confirm the findings from our medium library screen, we performed a 3-point dose-response in the HTR assay using compounds with previously unreported hallucinogenic potential **(FIG 4.9A)**. It had previously been established that ring fluorination diminishes hallucinogenic potential**.**[31] To our surprise though, 5-F-DMT, as well as 5-Cl-DMT, gave a positive result in psychLight agonist mode and caused a

[31] Blair, J. B.; Kurrasch-Orbaugh, D.; Marona-Lewicka, D.; Cumbay, M. G.; Watts, V. J.; Barker, E. L.; Nichols, D. E. Effect of ring fluorination on the pharmacology of hallucinogenic tryptamines. *J. Med. Chem*. **2000**, 43, 4701-4710.

robust increase in the HTR **(FIG 4.9B, C).** In contrast, 5-Br-DMT did not elicit a response in psychLight and produced no HTR. This is likely due to steric interactions caused by the bromine in the binding domain of the 5-HT2AR. All drugs caused a concentration-dependent decrease in locomotion suggesting that HTR and locomotion are not correlated **(FIG 4.9D)**. These results further validate that psychLight cannot only predict hallucinogenic activity but also detect small changes in signal resulting from minor modifications to a target scaffold.

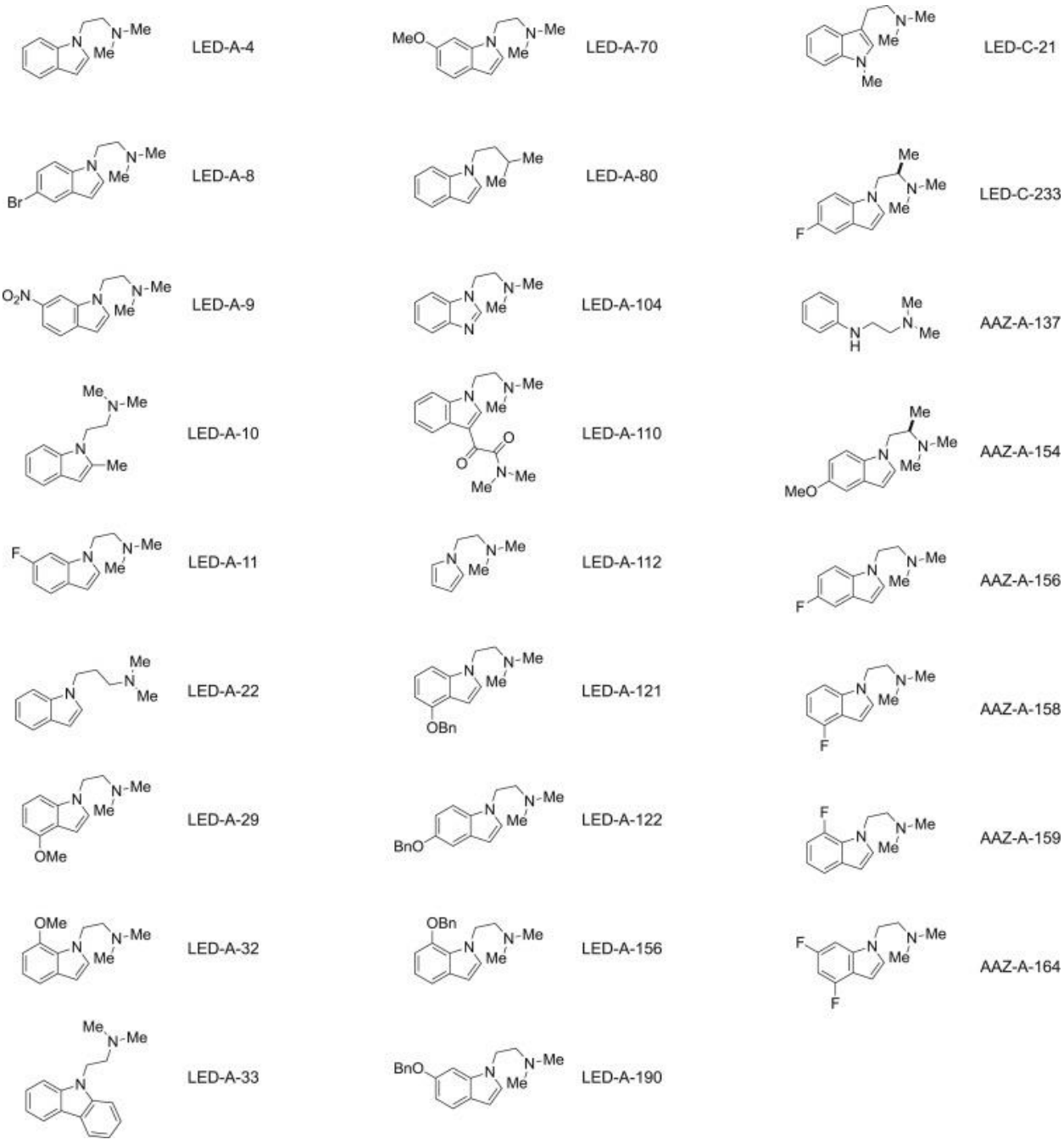

Figure 4.6. Structures of compounds synthesized in-house screened in **(FIG. 4.7)**.

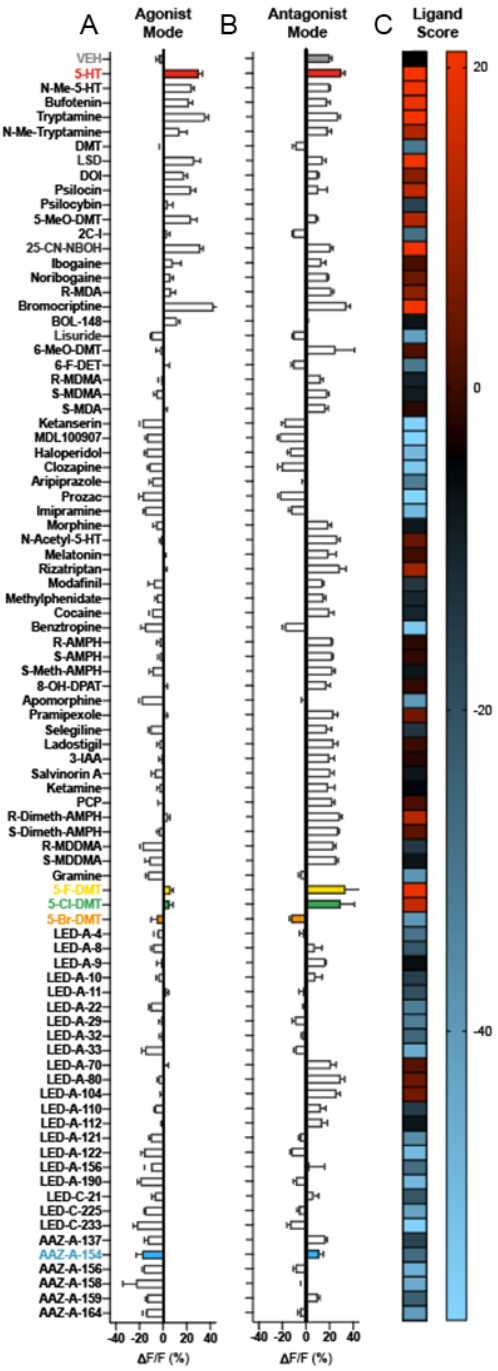

Figure 4.7..PSYLI2 cells as a screen for 5-HT2A activity. **(A)** Agonist mode screen of a medium compound library in PSYLI2 cells. **(B)** Antagonist mode screen of a medium compound library in PSYLI2 cells. **(C)** Ligand scores greater than 0 indicate a compound is more likely to be hallucinogenic. Scores less than 0 indicate compounds that are likely to be non-hallucinogenic ligands of the 5-HT2AR. Scores of 0 indicate compounds likely to be non-ligands of 5-HT2A.

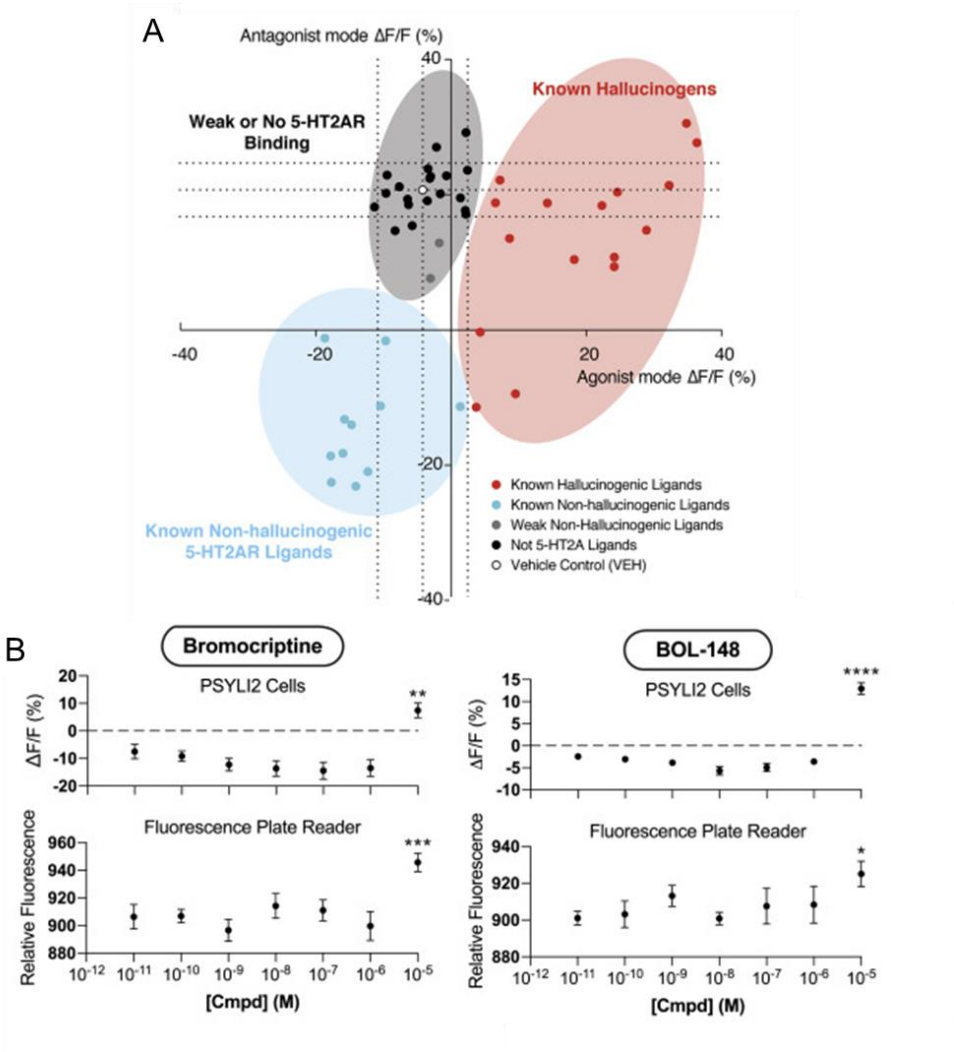

Figure 4.8. (A) Cartesian coordinate system of agonist and antagonist mode of psychLight. Responses from **(FIG 4.7 A, B)** were found to cluster into hallucinogenic, non-hallucinogenic 5-HT2AR ligands, and weak non-hallucinogenic ligands. respectively. Compounds with weak affinity for the 5-HT2AR (~1–10 μM) are shown in gray, whereas compounds that are known to not bind to the 5-HT2AR are shown in black. Dots indicate averaged ΔF/F values (n = 3 replicates from 3 passages of cells). **(B)** Concentration-response studies using PSYL2 cells (top) and a cell-free wells (bottom) reveal that BOL-148 and bromocriptine produce fluorescence artifacts at 10 μM (∗∗∗∗p < 0.0001, ∗∗∗p < 0.001, ∗∗p < 0.01 and ∗p < 0.05, one-way ANOVA compares to parent variant within the group with Dunnett's test). Data are represented as mean ± SEM 5-HT = 5-hydroxytryptamine; KETSN = ketanserin; BOL-148 = 2-bromolysergic acid diethylamide.

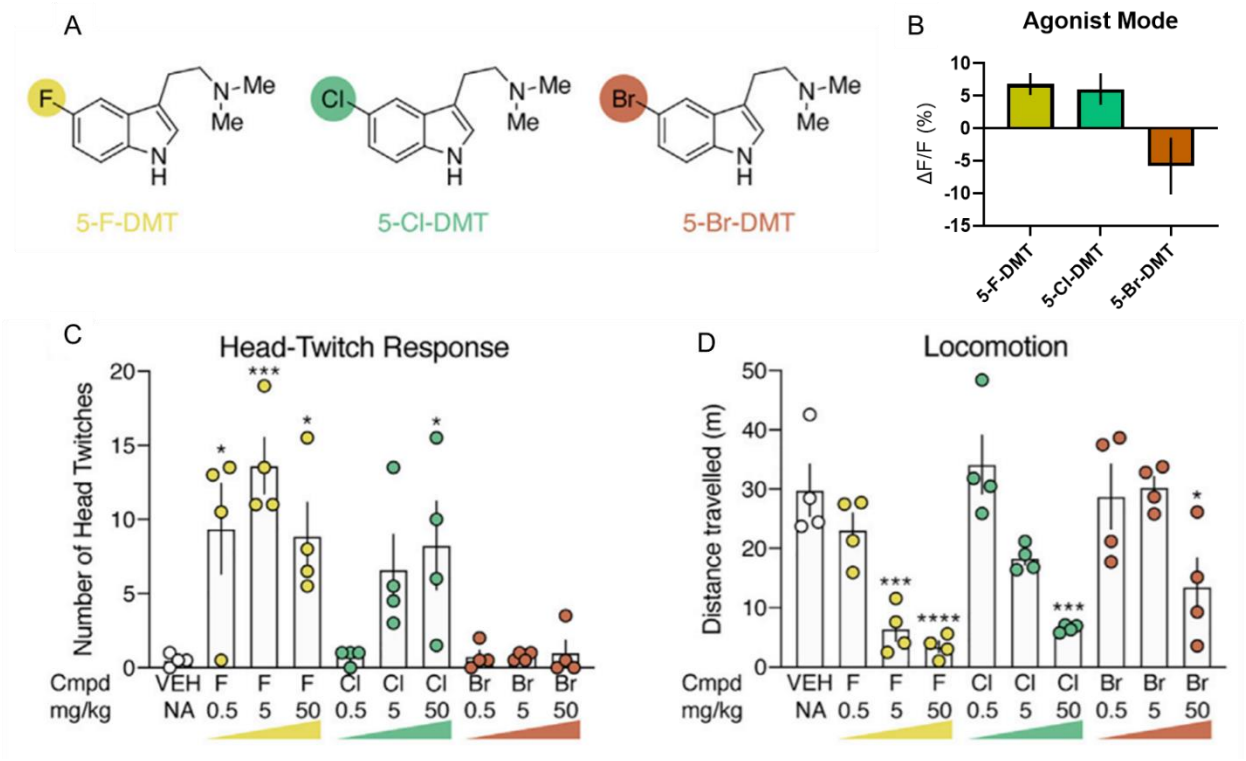

Figure 4.9. (A) Structure of 5-halo-DMT derivatives. **(B)** Agonist mode of the 5-halo substituted DMTs (n = 3 wells). **(C)** 5-F-DMT and 5-Cl-DMT produce head twitches whereas 5-Br-DMT does not (n = 4 mice). **(D)** All 5-halo-DMT produce a concentration-dependent decrease in locomotion (n = 4 mice). Data are represented as mean ± SEM., ****p<0.0001, ***p<0.001, and *p<0.05, vs. the vehicle control. For **(C–D)**, a one-way ANOVA with a Dunnett's post hoc test.

Chapter 4.5 PsychLight as a Pharmacological Tool for Drug Discovery

We have demonstrated the ability of psychLight to predict the hallucinogenic activity of novel compounds. Next, we wanted to use psychLight to aid in the discovery of novel non-hallucinogenic 5-HT2R ligands. These compounds are of particular interest to us as our previous work has shown that the hallucinogenic properties of 5-HT2A ligands are not necessary for their therapeutic effect.[7,8] From our medium compound screen we identified a previously unreported compound, AAZ-A-154 (AAZ) that gave a favorable ligand score(non-hallucinogenic binder of 5-HT2A). A key feature of entactogens like MDMA is a methyl group alpha to the basic amine resulting in a stereocenter. This is also a key feature of the scaffold

of ergolines like LSD. We designed AAZ in an attempt to take advantage of the diminished hallucinogenic effects of isoDMTs while incorporating features of the LSD and MDMA scaffolds (**FIG 4.10A**). Substitution of isoDMTs at the 5 position was previously shown not to dimmish the psychoplastogenic properties while removing any potential hallucinogenic side effects.[7]

Synthesis of AAZ and related analogs was accomplished via alkylation of indole with the respective chiral alkyl chloride. Alkylation of *R*-alaninol and subsequent conversion to the alkyl chloride proceeded in decent yields. It is worth noting issues with the alkylation step to afford **1**. Due to the small and hydrophilic nature of this compound when doing aqueous work ups the amino alcohol was inseparable from the water layer. Attempts to purify the compound via traditional techniques without an aqueous workup also proved futile. We found, however, that the addition of glycerol to the crude product allowed for efficient vacuum distillation to afford the desired product. Alkylation of the respective indoles with the chloride intermediate **2** proceeded smoothly to afford the desired products in moderate yields.

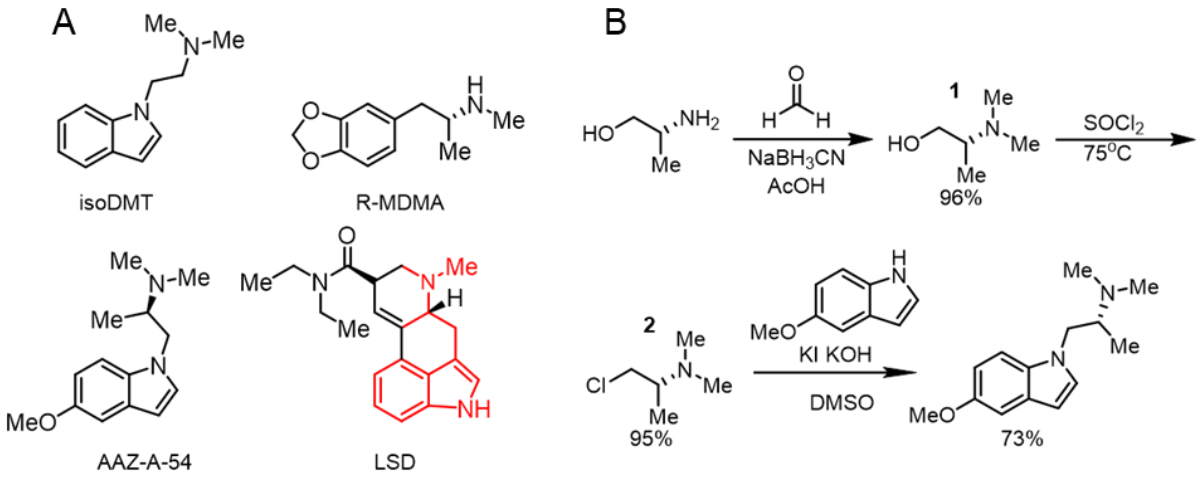

Figure 4.10. (A) Structures of isoDMT, LSD, R-MDMA, and AAZ. **(B)** Synthetic scheme of AAZ.

To characterize the interaction between AAZ and 5-HT2AR, we used psychLight to perform a Schild regression analysis revealing that AAZ is a competitive antagonist of 5-HT2A (**FIG 4.11A**). We next used a series of other GPCR sensors in agonist mode and antagonist mode to determine any off-target effects of AAZ (**FIG 4.11B**). We found that AAZ is selective for 5-HT2Rs showing no activity at other receptors including dopamine and norepinephrine receptors. To confirm that AAZ lacked hallucinogenic potential in

vivo, we tested multiple doses of AAZ using the HTR assay. As expected based on the psychLight screen AAZ produced no HTR and only caused a decrease in locomotion at the highest dose of 100 mg/kg (**FIG 4.11 C, D**).

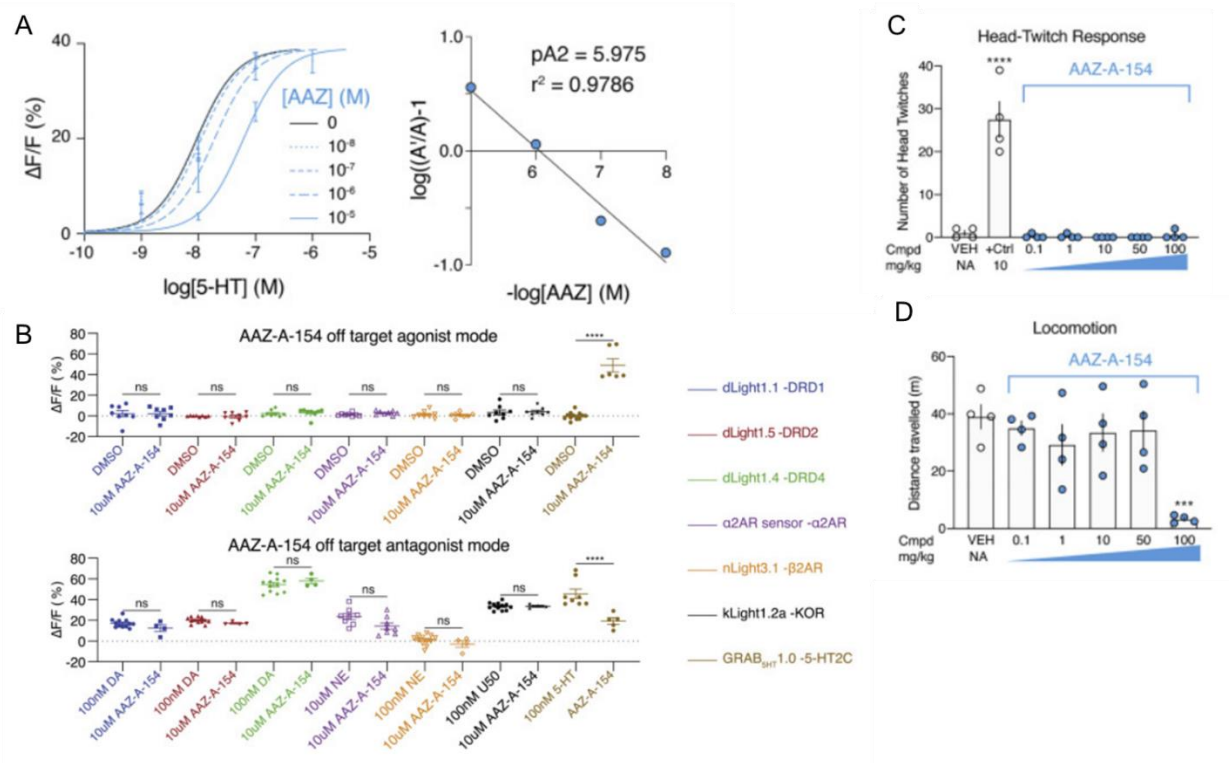

Figure 4.11. (**A**) Schild regression analysis reveals that AAZ is a psychLight competitive antagonist (n = 3 replicates from 1 passage of cells). (**B**) Data from agonist and antagonist mode of 7 receptor-based sensors (Agonist mode: 0.1% DMSO or 10 μM AAZ was added; Antagonist mode: 0.1% DMSO or 10uM AAZ-A-154 was added in the presence of 100 nM dopamine (DA), norepinephrine (NE), U-50488 (U50) or serotonin(5-HT)). ∗∗∗∗p < 0.0001, ns p > 0.05. One-way ANOVA. Tukey's multiple comparisons test. (**C**) AAZ does not trigger a HTR at any dose compared to that triggered by 5-MeO-DMT (n = 4 mice). (**D**) AAZ only decreases locomotion at the highest dose (100 mg/kg) (n = 4 mice). Data are represented as mean ± SEM. ∗∗∗∗p < 0.0001, ∗∗∗p < 0.001, and ∗p < 0.05, versus the vehicle control, one-way ANOVA with Dunnett's test.

We have previously reported that ligands of the 5-HT2AR are potent psychoplatogens.[4] Due to AAZ's activity at 5-HT2ARs, we theorized that it would be a potent psychoplastogen so we tested AAZ's ability to promote neuritogenesis. AAZ increased dendritic arbor complexity to a comparable extent to the fast-acting antidepressant ketamine (KET) (**FIG 4.12 A, B**). The psychoplastogenic effects were blocked by the 5-HT2R antagonist ketanserin (KETSN) suggesting that it, like other non-hallucinogenic psychoplastogens, is working via a 5-HT2R mediated mechanism (**FIG 4.12C**).[7,8] We used two behavioral assays—the forced swim test (FST), and the sucrose preference test—to assess the effects of AAZ on stress-coping strategies and anhedonia respectively.

In the FST, AAZ decreased the amount of time spent immobile, a behavioral response common in other psychoplastogens and fast-acting antidepressants (**FIG 4.12D**).[8][32] We utilized C57BL/6J mice in these studies because this strain does not respond robustly to traditional antidepressants such as selective serotonin reuptake inhibitors (SSRIs) or tricyclics.[33] AAZ had produced both rapid (30 min) and long-lasting (1week) effects in the FST.

To determine if AAZ could ameliorate anhedonia, we used VMAT2 heterozygous (VMAT2-HET) mice. Inhibition of VMAT2 precipitates depressive-like behaviors in humans, and VMAT2-HET mice display several depressive phenotypes including a reduced preference for a 1% sucrose solution over water alone.[34] Immediately following injection with AAZ, the VMAT2 mice exhibited a strong preference for sucrose water indistinguishable from the wild type (WT) (**FIG 4.12E**). These effects persisted for up to 12 days before VMAT2 mice started to exhibit a reduced sucrose preference. Further, these effects on sucrose preference were not attributed to increased fluid consumption (**FIG 4.12F**) or increased sucrose palatability as AAZ did not increase sucrose consumption in WT animals. Taken together this data suggests that psychLight can be a useful tool for not only predicting the hallucinogenic potential but also in the discovery of psychoplastogenic 5-HT2A ligands.

---

[32] Li, B.; Lee, B.; Liu, R. J.; Banasr, M.; Dwyer,J. M.; Iwata, M.; Li, X. Y.; Li, Y.; Aghajanian, G.; Duman, R. S. MTOR-dependent synapse formation underlies the rapid antidepressant effects of NMDA antagonists. *Science* **2010**, 329, 959-964.

[33] Hascoet, M.; Bourin, M. The Forced Swimming Test in Mice: A Suitable Model to Study Antidepressants. Mood and Anxiety Related Phenotypes in Mice. *Springer* **2009**, 85-118.

[34] Fukui, M.; Rodriguiz, R. M.; Zhou, J.; Jiang, S. X.; Philips, L. E.; Caron, M. G.; Wetsel, W. C. Vmat2 heterozygous mutant mice display a depressive-like phenotype. *J Neurosci.* **2007**, 27, 10520-10529.

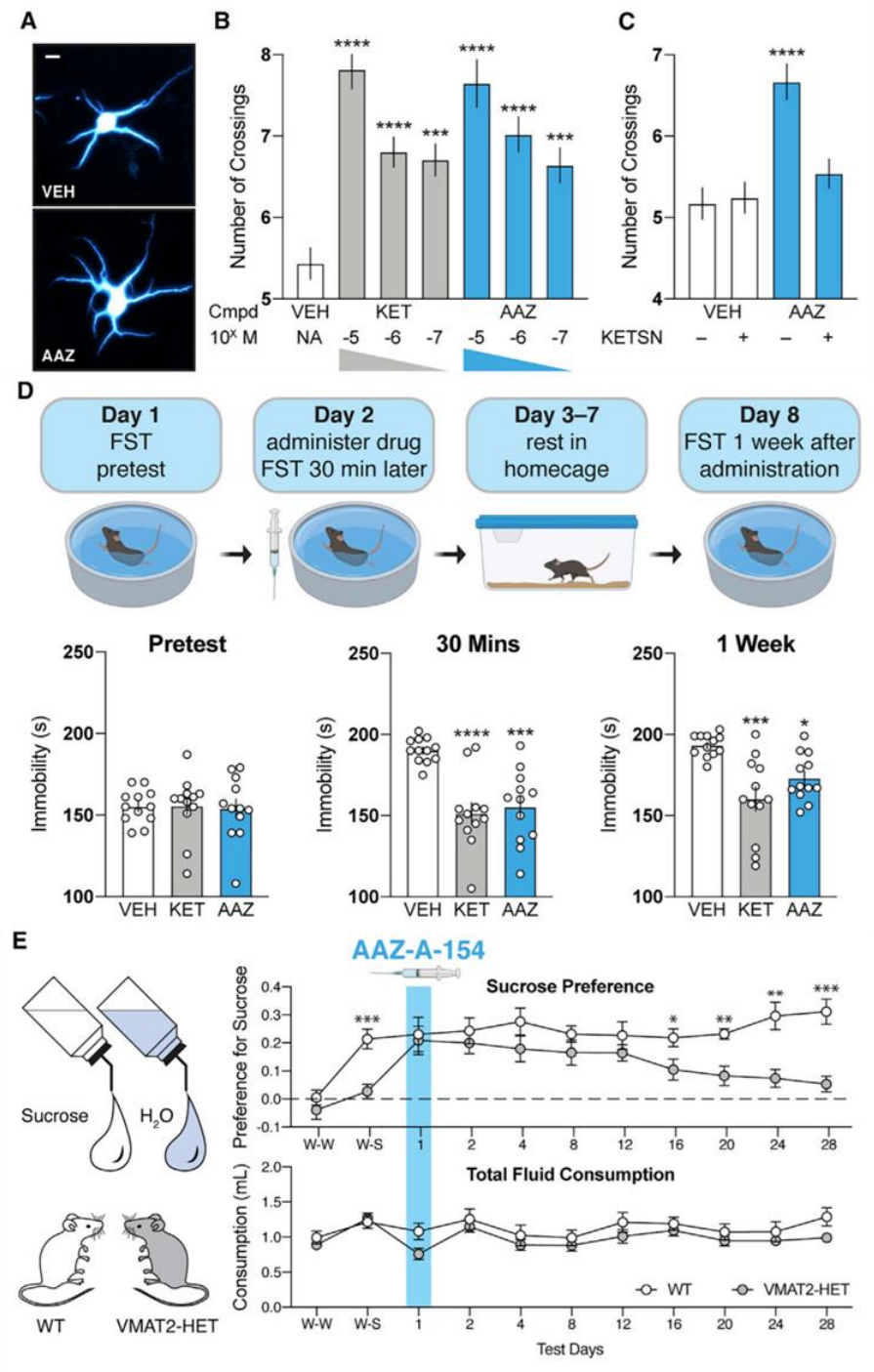

Figure 4.12. Characterization of the therapeutic effects of AAZ. **(A)** Representative images demonstrate that AAZ promotes dendritic branching. Scale bar, 20 μm. **(B)** The maximal number of crossings (Nmax) from Sholl plots (n = 51–60 neurons). ****p < 0.0001, ***p < 0.001, one-way ANOVA with Dunnett's test. **(C)** The effects of AAZ (100 nM) on dendritic growth can be blocked by the 5-HT2R antagonist ketanserin (KETSN, 1 μM, n = 39–58 neurons). ****p < 0.0001, one-way ANOVA with Dunnett's test. **(D)** Schematic

of the forced swim test design. AAZ (20 mg/kg) produces fast (30 min) and long-lasting (1 week) antidepressant-like effects comparable to ketamine (KET) (n = 12). ∗∗∗∗p < 0.0001, ∗∗∗p < 0.001, and ∗p < 0.05, one-way ANOVA with Dunnett's test. **(E)** At baseline, only WT mice exhibit a sucrose preference when given a 1% sucrose solution (W-S). AAZ (15 mg/kg) reduces anhedonia in VMAT2-HET mice for at least 12 days in the sucrose preference test. W-W, water-water pairing; W-S, water-sucrose (1%) pairing. Total fluid consumption was not different between genotypes at any time point. n = 11 mice/genotype; data are represented as means and SEMs, ∗∗p < 0.01 and ∗p < 0.05, WT versus VMAT2-HET, repeated-measures ANOVA with Bonferroni corrected pairwise comparisons.

Chapter 4.6 Conclusion

We have developed psychLight, the first cell-based assay capable of predicting the hallucinogenic potential of novel designer drugs. Unlike other serotonin-based sensors, psychLight is a modified 5-HT2A selective to the conformational states adopted by hallucinogenic compounds.[35] We have correlated the responses provided by psychLight *in vivo* with a behavioral response caused by hallucinogens, the HTR. We were also able to use psychLight to identify two 5-halo-DMTs with previously unknown hallucinogenic effects and validate the effects in the HTR assay.

In addition to being a powerful tool for predicting hallucinogenic potential, psychLight also has the potential as a powerful tool for studying 5-HT2R=based therapeutics. Unlike other assays based on GPCR downstream signaling of the 5-HT2A receptor, psychLight can easily distinguish between hallucinogenic and non-hallucinogenic ligands. PsychLight could prove to be a useful tool for understanding and determining the downstream pathways that correlate to the hallucinogenic and therapeutic effects of 5-HT2A ligands.

Using both the agonist and antagonist mode screens we were able to generate a ligand score to help characterize ligand properties at 5-HT2A receptors. Using these ligand scores, we were able to identify

[35] Unger, E. K.; Keller, J. P.; Altermatt, M.; Liang, R.; Yao, Z.; Sun, J.; Matsui, A.; Dong, C. E.; Hon, O. J.; Yao, Z.; Sun, J.; Banala, S.; Flanigan, M. E.; Jaffe, D. A.; Hartanto, S.; Carlen, J.; Mizuno, G. O.; Borden, P. M.; Shivange, A. V.; Cameron, L. P.; Sinning, S.; Underhill, S. M.; Olson, D. E.; Amara, S. G.; Lang, D. T.; Rudnick, G.; Marvin, J.; Lavis, L. D.; Lester, H. A.; Alvarez, V. A.; Fisher, A. J.; Prescher, J. A.; Kash, T. L.; Yarov-Yarovoy, V.; Gradinaru, V.; Looger, L. L.; Tian, L. Directed Evolution of a Selective and Sensitive Serotonin Sensor Via Machine Learning. *Cell* **2020**, 183, 1986–2002

AAZ, a previously unreported compound that showed a promising ligand score. We were able to show that AAZ produces psychoplastogenic effects via a 5-HT2R mediated mechanism. We also reported that AAZ produces anti-depressive like behaviors comparable to the fast-acting antidepressant ketamine in the forced swim test. We also found that AAZ has anti-anhedonic like effects in the sucrose preference test. All of this together demonstrates the power of psychLight as an important screen for the discovery of novel 5-HT2R based therapeutics.

ACKNOWLEDGEMENTS

I would like to acknowledge the Tian lab, in particular, Chunyang Dong for the design and development of psychLight. In addition, I wish to acknowledge the work of Chunyang Dong and Calvin Ly for their work performing the psychLight screens of compounds presented in this chapter. I would also like to acknowledge RJ Tombari and Arya Azinfar for synthesizing AAZ and related compounds, William Wetsel for performing the sucrose preference tests, and Max Vargas for performing the FST.

Chapter 4.7 Methods

Compounds

The NIH Drug Supply Program provided lysergic acid diethylamide hemitartrate, psilocin, psilocybin, 2-(4-Iodo-2,5-dimethoxyphenyl)ethan-1-amine hydrochloride (2C-I 2-bromo-lysergic acid diethylamide tartrate (BOL-148), ibogaine hydrochloride, noribogaine, cocaine hydrochloride, salvinorin A, and phencyclidine hydrochloride (PCP). Other chemicals were purchased from commercial sources such as serotonin hydrochloride (5-HT, Fisher, 50-120-7920), ketanserin (KETSN, ApexBio, 50-190-5332), ketamine hydrochloride (KET, Fagron, 803647), morphine sulfate (Mallinckrodt, Inc., 0406-1521-53), lisuride maleate (LIS, Tocris, 40-5210), bromocriptine mesylate (Tocris, 04-275-0), (±)-2,5-dimethoxy-4-iodoamphetamine hydrochloride (DOI, Cayman, 13885), imipramine hydrochloride (Cayman, 15890), modafinil (Cayman, 15417), (±)-threo-methylphenidate hydrochloride (Cayman, 11639), indole 3-aceitic acid (3-IAA, ACROS, AC12216-0250), gramine (ACROS, AC12018-0100), N-acetylserotonin (ACROS, AC22693-1000), melatonin (ACROS, AC12536-2500), tryptamine (TRY, ACROS, AC15798-0050), N-methyltryptamine (NMT, ACROS, AC151751000), MDL 100907 (MDL, Sigma, M3324-5MG), haloperidol (Sigma, H1512),

clozapine (Sigma, C6305), aripiprazole (Sigma, SML0935), fluoxetine hydrochloride (Sigma, F132-10MG), rizatriptan benzoate (Sigma, SML0247-10MG), benztropine mesylate (Sigma, SML0847-500MG), (±)-8-hydroxy-2-(dipropylamino)tetralin hydrobromide (8-OH-DPAT, Sigma, H8520-25MG), R-(-)-apomorphine hydrochloride hemihydrate (Sigma, A4393-100MG), pramipexole hydrochloride (Sigma, PHR1598-500MG), selegiline hydrochloride (Sigma, M003-250MG), ladostigil tartrate (Sigma, SML2263-5MG), RuBi-5-HT (Tocris, 3856) escitalopram oxalate (ESC, Tocris, 4796), L-glutamic acid (GLU, Sigma, G1251-500G), γ-aminobutyric acid (GABA, A5835-25G), dopamine hydrochloride (DA, Sigma, H8502-25G), and norepinephrine bitartrate (NE, 1468501). For cellular experiments, the VEH is dimethyl sulfoxide (DMSO, ACROS, AC327182500). For *in vivo* experiments, VEH = USP grade saline (0.9%, VWR, 68099-103). The remaining compounds used in these studies were synthesized in-house and judged to be pure based on NMR and UHPLC-MS. Compounds of the DMT, IsoDMT families (LED-A-4 − LED-C-21), and Tabernanthalog (TBG) were prepared as described previously.[7,8] All enantiopure amphetamines (i.e., amphetamine, methamphetamine, dimethamphetamine) and methylenedioxymethamphetamines (i.e., MDA, MDMA, MDDMA) were prepared using the methodology described by Nenajdenko.[36] The key step involved the regioselective ring-opening of enantiopure Boc-protected aziridines derived from *R*- and *S*-alaninol, respectively. The Boc-protected amphetamines and methylenedioxymethamphetamines were determined to be enantiomerically pure (>99 % ee) by chiral HPLC. The methylated amphetamines and methylated methylenedioxyamphetamines were readily prepared using known methods (Dunlap et al., 2020; Talluri and Sudalai, 2007).[7,37] All amphetamine and methylenedioxyamphetamine derivatives were prepared as the 1:1 fumarate salts with the exception of *R*- and *S*-MDMA, which were prepared as the 2:1 fumarate salts (i.e., hemifumarates). Lastly, *N*-Me-5-HT, *N*-Me-5-MeO-tryptamine hemifumarate, 6-fluorodiethyltryptamine (6-F-DET hemifumarate), 5-bromo-DMT hemifumarate, 5-chloro-DMT hemifumarate, 5-fluoro-DMT hemifumarate, and AAZ-A-137 hemifumarate were prepared using previously

[36] (Huot et al Nenajdenko, V.G.; Karpov, A.S.; Balenkova, E.S. A new convenient approach to chiral b aryl(heteroaryl)alkylamines. *Tetrahedron Asymmetry* **2001**, 12, 2517–2527.., 2011; Nenajdenko et al., 2001)
[37] Talluri S.K. Sudalai A. An organo-catalytic approach to the enantioselective synthesis of (R)-selegiline. *Tetrahedron* **2007**, 63, 9758-9763.

reported methods.[31,38,39,40]. Synthetic procedures and characterization data for AAZ-A-154 and LED-C-233 are reported below.

Animals

All experimental procedures involving animals were approved by the Institutional Animal Care and Use Committee (IACUC) at the University of California, Davis, the University of Colorado School of Medicine, or Duke University, and adhered to principles described in the National Institutes of Health Guide for the Care and Use of Laboratory Animals. The University of California, Davis, the University of Colorado School of Medicine, and Duke University are accredited by the Association for Assessment and Accreditation of Laboratory Animal Care International (AAALAC).

Abbreviations

β2AR = beta-2 adrenergic receptor; (S)-Meth-AMPH = (S)-methamphetamine; +Ctrl = positive control; µm = micrometer; 25-CN-NBOH = 4-(2-(2-Hydroxybenzylamino)ethyl)-2,5-dimethoxybenzonitrile hydrochloride; 2C-I = 2-(4-Iodo-2,5-dimethoxyphenyl)ethan-1-amine; 2P = 2-photon; 3-IAA = indole-3-acetic acid; 5-Br-DMT = 5-bromo-N,N-dimethyltryptamine; 5-Cl-DMT = 5-chloro-N,N-dimethyltryptamine; 5-F-DMT = 5-flouo-N,N-dimethyltryptamine; 5-HT = serotonin; 5-HT2AR = serotonin 2A receptor; 5-MeO = 5-methoxy-N,N-dimethyltrytamine; 6-F-DET = 6-flouro-N,N-diethyltrytamine; 6-MeO = 6-methoxy-N,N-dimethyltryptamine; 8-OH-DPAT = (±)-8-hydroxy-2-(dipropylamino)tetralin; AAV = adeno-associated virus; AAZ = AAZ-A-154; BLA = basolateral amygdala; BOL-148 = 2-bromo- lysergic acid diethylamide; BUFO = bufotenin, N,N-dimethyltryptamine; cpGFP = circularly permuted green fluorescent protein; D1R = dopamine receptor D1; DA = dopamine; DMSO = dimethyl sulfoxide; DMT = N,N-dimethyltrytamine; DOI = 2,5-dimethoxy-4-iodoamphetamine; DRN = dorsal raphe nucleus; EC50 = half maximal effective

[38] Marzaro, G.; Guiotto, A.; Chilin, A. Microwave-promoted mono-N-alkylation of aromatic amines in water: A new efficient and green method for an old and problematic reaction. *Green Chem.* **2009**, 11, 774-776.
[39] Somei, M.; Yamada, F.; Kurauchi, T.; Nagahama, Y.; Hasegawa, M.; Yamada, K.; Teranishi, S.; Sato, H., Kaneko, C. The chemistry of indoles. CIII. Simple syntheses of serotonin, N methylserotonin, bufotenine, 5-methoxy-N-methyltryptamine, bufobutanoic acid, N-(indol-3-yl)methyl-5-methoxy-N-methyltryptamine, and lespedamine based on 1-hydroxyindole chemistry. *Chem. Pharm. Bull*. **2001**, 49, 87–96.
[40] Tombari, R. J.; Saunders, C. M.; Wu, C.-Y.; Dunlap, L. E.; Tantillo, D. J.; Olson, D. E. Ex Vivo Analysis of Tryptophan Metabolism Using 19F NMR. *ACS Chem. Biol.* **2019**, 14, 1866-1873.

concentration; EF1α = human elongation factor-1 alpha; Emax = maximum efficacy; ESC = escitalopram oxalate; FST = forced swim test; GABA = γ-aminobutyric acid; GLU = glutamate; HEK293T = human embryonic kidney 293 cells with SV40 T-antigen; HTR = head-twitch response; IL3 = third intracellular loop; KET = ketamine; KETSN = ketanserin; LIS = lisuride; LSD = lysergic acid diethylamide; LTR = long terminal repeat; MDL = MDL 100907; N-5-HT = N-methylserotonin; N-acetyl-5-HT = N-acetylserotonin; NA = not available; NE = norepinephrine; NMT = N-methyltryptamine; OFC = orbitofrontal cortex; PCP = Phencyclidine; PCP = phencyclidine; R-AMPH = (R)-amphetamine; R-dimeth-AMPH = (R)-dimethamphetamine; R-MDA = (R)-3,4-methylenedioxyamphetamine; R-MDDMA = (R)-3,4-methylenedioxydimethylamphetamine; R-MDMA = (R)-3,4-methylenedioxy-methamphetamine; ROI = region of interest; S-AMPH = (S)-amphetamine; S-dimeth-AMPH = (S)-dimethamphetamine; S-MDA = (S)-3,4-methylenedioxyamphetamine; S-MDDMA = (S)-3,4-methylenedioxydimethylamphetamine; S-MDMA = (S)-3,4-methylenedioxy-methamphetamine; SEM = standard error mean; STD = standard deviation; TRY = tryptamine; VEH = vehicle; VMAT2-HET = vesicular monoamine transporter 2 heterozygous; W-S = water and 1% sucrose solution; W-W = water and water; WT = wild type; TBG = Tabernanthalog; ΔF/F = change in fluorescence over initial fluorescence.

Development of PsychLight1 and PsychLight2

All constructs were designed using circular polymerase extension cloning (CPEC), restriction cloning, and gBlock gene fragments (Integrated DNA Technologies).[41] Sequences coding for a FLAG epitope were placed at the 5′-end of the construct as previously described.[42] *HindIII* and *NotI* cut sites were placed at the 5′- and 3′-ends, respectively, for cloning into pCMV (Addgene) to generate all pCMV constructs. *BamHI* and *HindIII* sites were introduced via PCR for final subcloning onto pAAV.hSynapsin1 vectors (Addgene). To maximize coupling between conformational changes and chromophore fluorescence, we chose to use a cpGFP module (LSS-LE-cpGFP-LP-DQL) from GCaMP6 (Chen et al., 2013) for insertion into the human 5-HT2AR using circular polymerase extension cloning (CPEC).

[41] Quan, J.;Tian, J. Circular polymerase extension cloning for highthroughput cloning of complex and combinatorial DNA libraries. *Nat. Protoc.* **2011**, 6, 242–251.
[42] Irannejad, R.; Tomshine, J. C.; Tomshine, J. R.; Chevalier, M.; Mahoney, J. P.; Steyaert, J.; Rasmussen, S. G.; Sunahara, R. K.; El-Samad, H.; Huang, B.; von Zastrow, M. Conformational biosensors reveal GPCR signalling from endosomes. *Nature* **2013**, 495, 534–538.

For screening linker variants, we generated linker libraries by first creating an insert DNA carrying a randomized 2 amino acid linker on each side of cpGFP (LSS-xx-cpGFP-xx-DQL). Cloned constructs were amplified and purified with the Qiagen PCR purification kit prior to NEB® 5-α competent *E. coli* transformation. Competent cells were plated onto kanamycin-containing agar plates. After allowing for 24-hour of growth at 37 °C, single colonies were manually picked and grown overnight as described previously (Tian et al., 2009). Plasmids from the colonies were with purified using the Qiagen miniprep kit. Top variants were sequenced by Genewiz. For conversion of psychLight1 to psychLight2, an ER2 tag was added to the C-terminus of the protein, as described previously (Stockklausner et al., 2001), and the two original amino acids from the cpGFP sequence (i.e., F511 and N512, numbering based on psychLight2) were inserted into the N-terminal side of linker 2 to increase the baseline fluorescence. NEB® stable competent cells were transformed with PAAV_hSynapsin_psychLight2. After growth on an agar plate at 30°C, a single colony was selected. After sequencing confirmed the presence of the psychLight2 gene, the cells were expanded at 30°C in 100 mL of growth medium (2xYT), and purified with a Qiagen Endo-free Plasmid Maxi kit and send to the UC DAVIS Virus Packaging Core for virus production. Sequence information for psychLight1 and psychLight2.

Tissue Culture

HEK293T cells were grown in DMEM, supplemented with fetal bovine serum (FBS) and penicillin-streptomycin. Cells were transfected with Effectene according to the manufacturer's instructions. Before imaging, cells were washed with Hank's Balanced Salt Solution (HBSS) supplemented with 2 mM $MgCl_2$ and 2 mM $CaCl_2$. All images were collected in HBSS containing Mg^{2+} and Ca^{2+}.

Transient Transfection of PsychLight1

HEK293T cells were plated and transfected concurrently 24 h prior to each experiment using the Qiagen Effectene Transfection Reagent kit according to the manufacturer's protocol.

Confocal Microscopy Experiments

Dose-response experiments were performed using an Automate Perfusion System. Cells (HEK293T) were grown on 12 mm coverslips and transfected with psychLight1. The coverslips were then placed into a coverslip holder and washed with 5 mL of HBSS containing 2 mM $MgCl_2$ and 2 mM $CaCl_2$. Cells were perfused first with 5 mL of 0.1% DMSO, then drugs in ascending concentrations from 1 pM to 10 µM were added, with the concentration of DMSO being held constant at 0.1%. Images were recorded using a 465 nm laser and a 40x oil objection (0.55 N.A.) on a Zeiss 710 confocal microscope. For the competition studies described in Figure S3, HEK293T cells were prepared as described above; however, the cells were first exposed to 5 mL of 0.2% DMSO. Next, 100 nM 5-HT in 0.2% DMSO was introduced to the cells followed by ascending concentrations of the drug (from 1 pM to 10 µM) in a solution of 100 nM 5-HT, with the concentration of DMSO kept constant at 0.2%. Analysis was performed by taking 3 ROIs on the cell membrane using ImageJ and calculating the mean intensity for each ROI across the time points. Finally, the ΔF/F was calculated using the average of the baseline (0.1 or 0.2% DMSO) and the average intensity between each dosage over the average of the baseline.

***In vivo* PsychLight Recordings**

At the beginning of surgery, mice were anesthetized with 5% isoflurane for induction and later 1% isoflurane was used for maintenance. After induction of anesthesia, Carprofen (5 mg/kg) and Buprenorphine (1 mg/kg) were subcutaneously injected. The mouse was mounted on a stereotaxic frame. During surgery, body temperature was maintained with a heating pad. Before a sterile scalpel was used to make an incision, the hair covering the skin above the skull was removed. To have a consistent horizontal alignment of the skull, bregma and lambda were leveled to be on the same z-axis while two points on the surface of the skull 1.5 mm to either side of lambda were used to level the skull with regard to the y-axis. Following viral injection, optical fiber was implanted and secured with metabond and dental cement. Mice were monitored up to 14 days after surgery.

Viral Injection

To inject virus and implant optical fibers for fiber photometry experiments, craniotomy holes were made over the DRN, BNST, BLA, and OFC (DRN, inject with 20° angle, AP: -4.3 mm, ML: 1.1, DV: -2.85 mm; BNST, AP: 0.3 mm, ML: 1 mm, DV: -4.35 mm; BLA, AP: -1.35 mm, ML: 3mm, DV: -4.5 mm; and OFC, AP: 2.5 mm, ML: 1.5 mm, DV: -2.5 mm). Mice were injected with 300 nL of AAV9.*hSynapsin1*.psychLight2 (BNST, BLA, OFC) or AAV8.*hSynapsin1*.psychLight2 (DRN). Virus was injected using the Sub-Microliter Injection System with nanofil needles. The injection needle was lowered into the brain regions indicated above and infused per site at a rate of 100 nL per min. The injection volume was controlled by a microsyringe pump, which was connected to a controller. Following injection, the virus was allowed to diffuse into the tissue for an additional 10 min before the needle was withdrawn.

Optical Fiber Implantation

After viral injection, optical fibers were mounted into a stereotaxic holder and inserted into tissue targeting 50 μm above the brain regions mentioned above. A layer of Metabond was applied to the surface of the skull around the optical fiber followed by a layer of dental cement to secure the optical fiber.

.

Head-twitch Response with Fiber Photometry

Three animals were used for experiments measuring sensor activity in the prelimbic cortex. A 10 min baseline was recorded prior to compound administration (50 mg/kg 5-MeO or 4 mg/kg KETSN, i.p.) in a 5 mL/kg volume using 0.9% saline as the vehicle. To calculate the ΔF/F time series, a linear fit was applied to the 405 nm signals and aligned to the 465 nm signals. The fitted 405 nm signal was subtracted from 465 nm channels, and then divided by the fitted 405 nm signal to yield ΔF/F values. The number of head twitches were counted in 1 min intervals by 2 observers blinded to the treatment conditions and the results were averaged (interpersonnel kappas, Pearson's correlation coefficient = 0.96)

Creation of PSYLI2 Cell Line Stably Expressing PsychLight2

The psychLight2 gene was cloned into a pLVX plasmid with the EF1α promotor. The plasmid was transfected into HEK293T cells together with pCMV_delta8.2 and pCMV_VSV_G in a ratio of 10:7:3 using the Qiagen Effectene Transfection kit. After 14 h of incubation, the medium was exchanged for fresh DMEM. After an additional 48 h of incubation, the lentivirus-containing medium was collected, filtered through a 0.45 μm Durapore low-protein binding filter, concentrated using a Centricon-70 ultra filtration unit at 3,500 g for 50 min, and stored at -80ºC. Next, confluent HEK293T cells that had been grown in 24-well plates were infected with 20 μL of concentrated lentivirus for 48 h. Puromycin selection was performed as described by Tandon and co-workers (Tandon et al., 2018). Expression was assessed via fluorescence microscopy, and a single cell was selected for expansion. The new cell line, named PSYLI2, was frozen in 10% DMSO at -80ºC and then transferred to a liquid nitrogen dewar.

High-Content Imaging Experiments

Glass bottom 96-well plates (P96-1.5H-N, Cellvis) were coated with 50 μg/mL of poly-D-lysine (Sigma, P6407-5MG) and 10 μg/mL of laminin (Sigma, L2020) overnight in an incubator (37°C, 5% CO_2). Plates were washed with Dulbecco's PBS (ThermoFisher, 14190-250) and PSYLI2 cells were suspended in DMEM (Fisher, 11995073) containing 10% FBS (Fisher, 26-140-079) with 5% penicillin-streptomycin (Fisher, 15140-163) and plated at a density of 40,000 cells/well 24 h prior to each experiment. Immediately before an experiment, stock solutions of drugs in DMSO (10 mM) were diluted 1:100 in imaging media distributed across an empty 96-well plate (treatment plate) in triplicate following a randomized plate map. The imaging media consisted of 1 x HBSS (Fisher, 14175103) containing 0.5 M $MgCl_2$ (Sigma, M8266-1KG) and 0.5 M $CaCl_2$ (Sigma, C5670-50G). Cells grown in a separate 96-well plate (assay plate) were gently washed 3x with imaging media, and the wells were filled with an appropriate volume of imaging media for the respective experiment (*vide infra*).

Agonist Mode

For agonist mode experiments, 180 μL of imaging media were added to each well of the assay plate. Wells were then imaged on a Lecia DMi8 using Leica Application Suite X (V3.6.0.20104) at 40x (N.A.

= 0.6) with 5 regions of interest (ROI) taken per well using the default 5 ROI pattern for each well with no bias to location and no overlap of the ROIs (exposure = 350 ms, LED power = 80%). Next, 20 µL from the treatment plate was transferred to the assay plate containing a 1:1000 dilution of drug (10 µM as the final concentration in 0.1% DMSO). As positive, negative, and neutral controls, 5-HT (10 µM), ketanserin (10 µM), and DMSO (0.1%) were used, respectively. All final concentrations of drugs were 10 µM (0.1% DMSO) in agonist mode unless stated otherwise. After 5 min of incubation, the same sites were re-imaged using the same settings.

Once imaging was complete, the images were exported, and analyzed using a self-written MATLAB script. In short, segmentation was performed on individual images, and a mask highlighting the membrane of the HEK293T cells was generated. Pixel intensities were obtained from the mask-highlighted area and exported into Excel. The ΔF/F values for each well were calculated using the following equation:

$$\frac{(average\ after\ drug - average\ before\ drug)}{average\ before\ drug\ (baseline)}$$

These values were then used to obtain the triplicate mean (N = 3).

Antagonist Mode

For antagonist mode experiments, 160 µL of imaging media was added to each well of the assay plate. Wells were imaged on a Lecia DMi8 using Leica Application Suite X (V3.6.0.20104) at 40x (N.A. = 0.6) with 5 regions of interest (ROI) taken per well using the default 5 ROI pattern for each well with no bias to location and no overlap of the ROIs (exposure = 350 ms, LED power = 80%). A 100 µM 5-HT stock solution in DMSO was diluted 1:100 in imaging buffer. Next, 20 µL of this solution was added to the assay plate for a final concentration of 111 nM 5-HT (0.1% DMSO). The same 5 ROIs were imaged after 5 min of incubation. Next, 20 µL from the treatment plate was transferred to the assay plate for a final 1:1000 dilution of drug (10 µM drug, 100 nM 5-HT, 0.2% DMSO). All final concentrations of drugs were 10 µM with 100 nM 5-HT (0.2% DMSO) in antagonist mode unless stated otherwise. After 5 min of incubation, the same sites were re-imaged using the same settings.

Once imaging was complete, the images were exported, and analyzed using a self-written MATLAB script. In short, segmentation was performed on individual images, and a mask highlighting the membrane of the HEK23T cells was generated. Pixel intensities were obtained from the mask highlighted area and exported into Excel. Then the ΔF/F values for each well were calculated using the following equation:

$$\frac{(average\ after\ drug - average\ after\ 5{-}HT\ )}{average\ after\ 5{-}HT\ (baseline)}$$

These values were then used to obtain the triplicate average (N = 3). All imaging and incubation (both agonist and antagonist mode) were performed at ambient atmosphere and temperature.

Calculation of the Ligand Score

Compounds unlikely to bind to the sensor should produce minimal to no response in either agonist or antagonist mode. Therefore, a ligand score was calculated as:

$$\Delta(F/F)_{\text{Compound Agonist Mode}} - [(\Delta F/F)_{\text{VEH Antagonist Mode}} - (\Delta F/F)_{\text{Compound Antagonist Mode}}]$$

The black heatmap value indicating no effect was set to the value calculated for the vehicle control (i.e., -4.2). The maximal red and blue values were set to those calculated for a prototypical agonist (i.e., LSD, Ligand Score = 21) and antagonist (i.e., MDL100907, Ligand Score = -58), respectively.

Schild Regression Analysis

A treatment plate was prepared by pre-mixing various concentrations of a non-hallucinogenic compound with increasing concentrations of 5-HT. During imaging, 180 µL of imaging media were added to each well of the assay plate. Wells were then imaged on a Lecia DMi8 using Leica Application Suite X (V3.6.0.20104) at 40x (N.A. = 0.6) with 5 regions of interest (ROI) taken per well using the default 5 ROI pattern for each well with no bias to location and no overlap of the ROIs (exposure = 350 ms, LED power

= 80%). Next, 20 µL from the treatment plate was transferred to the assay plate for a final 1:1000 dilution of drug. All final drug treatments contained 0.1% DMSO. After 5 min of incubation, the same sites were re-imaged using the same settings. The data analysis method was the same as in agonist and antagonist mode.

Plate reader screening for compound fluorescence

A 96-well plate (UV transparent) was prepared with 100 µL of increasing concentration of BOL-148 and bromocriptine from 10^{-12} to 10^{-5} M together with vehicle control. The plate was read by Tecan Microplate Reader Spark® with excitation wavelength 465 nm (bandwidth 20 nm), emission wavelength 518 nm (bandwidth 20 nm), gain of 120, 5 ROI per well, total 30 flashes per well, and read at z-position 30000 µm from the bottom of the plate. All settings controlled by SparkControl software, V2.3.

Dendritogenesis Experiments

For the dendritogenesis experiments conducted using cultured E18 cortical neurons, timed-pregnant Sprague Dawley rats were obtained from Charles River Laboratories (Wilmington, MA). Full culturing, staining, and analysis details were performed as previously described.[7]

Forced Swim Test (FST)

Male and female C57BL/6J mice (9–10 weeks old at the time of the experiment, n = 6 of each sex per condition) were obtained from The Jackson Laboratory and housed 4–5 mice of the same sex/cage in a UCD vivarium following an IACUC approved protocol. After 1 week in the vivarium, each mouse was handled for approximately 1 min by a male experimenter for 3 consecutive days prior to the first FST. All experiments were conducted by the same male experimenter who performed the initial handling. During the FST, mice underwent a 6 min swim session in a clear Plexiglas cylinder (40 cm tall, 20 cm in diameter) filled with 30 cm of 24 ± 1ºC water. Fresh water was used for every mouse. After handling and habituation to the experimenter, drug-naïve mice first underwent a pretest swim to more reliably induce a depressive-like phenotype in subsequent FST sessions. Immobility scores for all mice were determined after the pre-test and mice were assigned to treatment groups to generate groups with similar mean immobility scores

used in the following two FST sessions. The next day, the animals received injections (i.p.) of AAZ-A-154 (20 mg/kg), ketamine (3 mg/kg) as the positive control, or vehicle (saline). After 30 min, the animals were subjected to the FST, dried with a towel, and then returned to their home cages. One week later, the FST was performed to assess the sustained effects of the drugs. All FSTs were performed between the hours of 0800 and 1300 h. The experiments were divided into two cohorts either of all males or females and conducted on different days. Experiments were video-recorded and manually scored offline by an experimenter blinded to treatment conditions. Immobility time—defined as passive floating or remaining motionless with no activity other than that needed to keep the mouse's head above water—was scored for the last 4 min of the 6 min trial.

Head-Twitch Response (HTR) and Locomotion Assays

The HTR assay was performed as described previously using both male and female C57BL/6J mice (2 male and 2 female = 4 total per treatment).[7] The mice were obtained from The Jackson Laboratory (Sacramento, C.A.) and were approximately 8-weeks old at the time of the experiments. Compounds were administered (5 mL/kg, i.p.) using 0.9% saline as the vehicle. After injection, animals were placed into an empty cage (8" x 13" x 5") and HTRs were videotaped, scored later by two blinded observers, and the results were averaged (interpersonnel kappas, Pearson correlation coefficient > 0.91). Locomotion was assessed using AnyMaze automated tracking software.

Sucrose Preference

Adult male and female wild-type (WT) and VMAT2 heterozygous (VMAT2-HET) mice were used for these experiments and they were housed in a humidity- and temperature-controlled room on a 14:10 h light:dark cycle.[34] Mice were housed individually 48 h prior to the experiment with *ad libitum* access to chow and water. For each day's experiment, bottles were prepared with water or a 1% sucrose solution and these were weighed just prior to the test. Two h prior to the beginning of the dark cycle, the home-cage water bottle was removed. One h after onset of the dark cycle, a pair of bottles was placed into the home cage. The mouse was given 2 h to drink, after which the bottles were removed and weighed immediately. Approximately 1 h later, the home-cage water bottle was returned. This procedure was

repeated daily with the water-water (W-W) pairing until the mouse showed stable drinking volumes over 3 consecutive days without any side-bias. Once criterion was achieved, the mouse was presented with the water-sucrose (W-S) pairing. The next day (day 1), mice were administered an acute injection of AAZ-A-154 (15 mg/kg, i.p.) and 5 min later were given the W-S pairing (i.e., day 1). Subsequent W-S pairings were presented on days 2 and 4, and then at 4-day intervals. Preference for the sucrose bottle was calculated as the volume of sucrose consumed minus the volume of water consumed, divided by the total volume of liquid consumed. Preference scores approaching "0" indicated no preference for sucrose or water, whereas positive scores signified a preference for sucrose and negative scores denoted a preference for water.

Compound Synthesis

The syntheses and characterization of most compounds used in this study have been reported previously. Here, we provide synthetic procedures and characterization data for AAZ-A-154 and LED-C-233, as they have not been previously described.

(R)-2-(dimethylamino)propan-1-ol. To an ice-cold solution of R-alaninol (4.93 g, 65.6 mmol) and glacial acetic acid (18.9 mL, 328 mmol, 5.0 equiv) in MeOH (328 mL) was added sodium cyanoborohydride (9.075 g, 144 mmol, 2.2 equiv) followed by 37% formaldehyde$_{(aq)}$ (13.8 mL, 171 mmol, 2.6 equiv). The reaction was stirred at room temperature for 12 h before being concentrated under reduced pressure. The residue was diluted with glycerol (100 mL) and distilled under reduced pressure to yield the pure compound as a colorless oil (6.5 g, 96%), which was used without further purification.

(R)-1-chloro-*N,N*-dimethylpropan-2-amine hydrochloride. To an ice-cold solution of $SOCl_2$ (2.1 mL, 29 mmol, 1.1 equiv) was added (R)-2-(dimethylamino)propan-1-ol (2.7 g, 26 mmol). The mixture was heated to reflux for 4 h before being concentrated under reduced pressure to yield the desired product as a white solid (3.92 g, 95%), which was used without further purification.

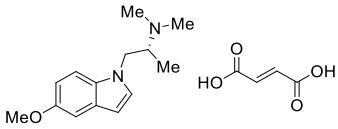

AAZ-A-154. To a solution of 5-methoxyindole (441 mg, 3.00 mmol) in DMSO (7.5 mL) was added (R)-1-chloro-*N,N*-dimethylpropan-2-amine hydrochloride (664 mg, 4.20 mmol, 1.4 equiv), potassium iodide (697 mg, 4.2 mmol, 1.4 equiv), and potassium tert-butoxide (0943 mg, 8.40 mmol, 2.8 equiv). The reaction mixture was stirred for 24 h, before being diluted with 1.0 M $NaOH_{(aq)}$ (750 mL). The aqueous phase was extracted with DCM (3 x 100mL). The organic extracts were combined, dried over Na_2SO_4, filtered, and concentrated under reduced pressure to yield a colorless oil, which was purified by flash chromatography (9:1 DCM/MeOH with 1% ammonium $hydroxide_{(aq)}$). The purified oil was dissolved in $CHCl_3$ (3 mL) and added dropwise to a boiling solution of fumaric acid (253 mg, 2.18 mmol, 1.0 equiv) in THF (10 mL). The mixture was concentrated under reduced pressure to yield the desired product as the 1:1 fumarate salt (758 mg, 73%). ^{1}H NMR (600 MHz, DMSO-d_6) δ 7.37 (d, 1H, *J* = 8.8 Hz), 7.30 (s, 1H), 7.03 (s, 1H, *J* = 3.1 Hz), 6.76 (d, 1H, *J* = 8.8 Hz), 6.61 (s, 2H), 6.32 (s, 1H), 4.25 (dd, 1H *J* = 6.3, 7.8 Hz), 4.02 (dd, 1H, *J* = 6.3, 7.8 Hz), 3.74 (s, 3H,) 3.11 (q, 1H, *J* = 6.3, 6.6, Hz), 2.30 (s, 6H), 0.84 (d, 3H, *J* = 6.6 Hz). ^{13}C NMR (100 MHz, CD_3OD) δ 171.0, 155.8, 136.1, 132.8, 130.9, 129.7, 113.3, 111.2, 103.8, 103.3, 61.6, 56.2, 47.5, 39.9, 11.7 ppm.

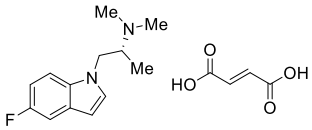

LED-C-233*.* To a solution of 5-fluoroindole (100 mg, 0.739 mmol) in DMSO (1.90 mL) was added (R)-1-chloro-*N,N*-dimethylpropan-2-amine hydrochloride (128 mg, 0.814 mmol, 1.1 equiv), potassium iodide (135 mg, 0.814 mmol, 1.1 equiv), and potassium hydroxide (166 mg, 15.8 mmol, 5.0 equiv). The reaction mixture was stirred for 24 h, before being diluted with 1.0 M $NaOH_{(aq)}$ (100mL). The aqueous phase was extracted with DCM (3 x 25 mL). The organic extracts were combined, dried over Na_2SO_4, filtered, and concentrated under reduced pressure to yield a colorless oil, which was purified by flash chromatography (9:1 DCM/MeOH with 1% ammonium $hydroxide_{(aq)}$). The purified oil was dissolved in acetone (2 mL) and added dropwise to a boiling solution of fumaric acid (48.1 mg, 0.409 mmol, 1.0 equiv) in acetone (5 mL). The

mixture was concentrated under reduced pressure to yield the desired product as the 1:1 fumarate salt (111 mg, 54%). ^{1}H NMR (600 MHz, CD_3OD) δ 7.49 (m, 1H,), 7.34 (d, 1H, *J* = 3.2 Hz), 7.25 (dd, 1H, *J* = 2.5, 9.3 Hz), 6.98 (td, 1H, *J* = 2.5. 9.3 Hz), 6.72 (s, 2H), 6.53 (d, 1H, *J* = 3.2 Hz), 4.63 (dd, 1H *J* = 5.7, 8.9 Hz), 4.35 (dd, 1H, *J* = 5.7, 8.9 Hz), 3.86 (m, 1H,) 2.84 (s, 6H), 1.21 (d, 3H, *J* = 6.7 Hz). ^{13}C NMR (100 MHz, CD_3OD) δ 171.0, 160.2, 158.7, 136.1, 134.2, 131.1, 130.8, 130.7, 111.5, 111.4, 111.3, 111.1, 106.7, 106.5, 103.6, 103.5, 61.5, 47.6, 40.0, 11.6ppm.

STATISTICAL ANALYSIS

Treatments were randomized, and the data were analyzed by experimenters blinded to the treatment conditions. Statistical analyses were performed using GraphPad Prism (version 8.1.2) unless noted otherwise. All comparisons were planned prior to performing each experiment. The sucrose preference and the volume of liquid consumed in the anhedonia test were analyzed separately by repeated measures ANOVA using a within subjects' effects of days and a between subjects' effects of genotype with SPSS 27 programs (IBM SPSS Statistics, Chicago, IL). *Post-hoc* analyses were by Bonferroni corrected pair-wise comparisons. A $p<0.05$ was considered significant. Data are represented as mean ± SEM, unless otherwise noted, with asterisks indicating *$p < 0.05$, **$p < 0.01$, ***$p < 0.001$, and ****$p < 0.0001$.

Chapter 5. An Analog of LSD With Antipsychotic Potential

Chapter 5.1 Introduction

Schizophrenia has a major impact on the global disease burden effecting almost 1% of the population world wide.[1,2] Schizophrenia is characterized by 3 distinct types of symptoms: positive, such as hallucinations; negative symptoms, such as anhedonia; and cognitive impairments and has a high prevalence of comorbidity with other psychiatric conditions like depression and addiction.[3] Traditional treatments for schizophrenia have primarily focused on treating the positive symptoms via blockade of dopamine receptors.[4]

More recent advances have led to the development of atypical antipsychotics which also work via blockade of dopamine receptors. However, unlike traditional antipsychotics, atypical antipsychotics also have inverse agonist properties at 5-HT2A receptors, which are believed to modulate dopamine release in the ventral tegmental area (VTA). In the prefrontal cortex (PFC), 5-HT2A receptors are primarily found on pyramidal cells which exert top-down control on dopaminergic neurons in the ventral tegmental and regulate mesocortical dopamine (DA) release.[5,6,7] There is also evidence to suggest that atypical antipsychotics have effects treating the cognitive deficits in schizophrenia which could result from

[1] Chant, D.; Welham, J.; McGrath, J. A systematic review of the prevalence of schizophrenia. *PLoS Med*. **2005**, 2, e141.
[2] Moreno-Küstner, B.; Martin, C.; Pastor, L. . Prevalence of psychotic disorders and its association with methodological issues. A systematic review and meta-analyses. *PLoS One* **2018**, 13, e0195687.
[3] Rosenheck, R. A.; Tsai, J. Psychiatric comorbidity among adults with schizophrenia: a latent class analysis *Psychiatry Res* . **2013**, 210, 16-20.
[4] Stankovic, S.; Abbs, B.; Liu, I. Y.; Nasrallah, H.; Fava, M.; Arango, C.; Bugarski-Kirola, D. Pimavanserin for negative symptoms of schizophrenia: results from the ADVANCE phase 2 randomised, placebo-controlled trial in North America and Europe. *Lancet Psychiatry* . **2022**, 9, 46-58.
[5] Cornea-Hebert, V.; Riad, M.; Wu, C.; Singh, S. K.; Descarries, L. Cellular and subcellular distribution of the serotonin 5-HT2A receptor in the central nervous system of adult rat. *J Comp Neurol*. **1999**, 409, 187-209.
[6] Vazquez-Borsetti, P.; Cortes, R.; Artigas, F. Pyramidal neurons in rat prefrontal cortex projecting to ventral tegmental area and dorsal raphe nucleus express 5-HT2A receptors. *Cereb Cortex* **2009**, 19, 1678-1686.
[7] Bortolozzi, A.; Diaz-Mataix, L.; Scorza, C. M.; Celada, P.; Artigas, F. The activation of 5-HT receptors in prefrontal cortex enhances dopaminergic activity. *J Neurochem*. **2005,** 95, 1597-1607.

interactions at 5-HT2ARs.[8,9,10] Working memory and processing of executive functions are some of the key areas impacted by schizophrenia.[11] As neuroplasticity plays a key role in memory and cognition, compounds able to promote neuroplasticity in key brain regions may prove to be beneficial in treating the cognitive deficits of schizophrenia.[12] We have reported on a class of drugs, psychoplastogens, which are capable of rapidly promoting increases in structural and functional neuroplasticity in the PFC via a 5-HT2AR dependent mechanism.[13,14]

While antipsychotic medications have efficacy for treating the positive symptoms, they provide little relief from the negative symptoms of schizophrenia such as anhedonia.[15] The most common treatment for the negative symptoms of schizophrenia involves antidepressants in combination with antipsychotics.[16] These results seem to be highly dependent on the antidepressant used, as bupropion, a norepinephrine–dopamine reuptake inhibitor (NDRI), failed to improve the negative symptoms.[17] Understanding the impact of antidepressants on the negative symptoms is convoluted by multiple drug interactions arising from the antipsychotic being used in addition to the antidepressant being examined in clinical trials. These complications suggest a need for therapeutics that can treat all the symptoms of schizophrenia to negate unwanted drug interactions.

---

[8] Desamericq, G.; Schurhoff, F.; Meary, A.; Szoke, A.; Macquin-Mavier, I.; Bachoud-Levi, A. C.; Maison, P. Long-term neurocognitive effects of antipsychotics in schizophrenia: a network meta-analysis. *Eur J Clin Pharmacol*. **2014**, 70, 127-134.

[9] Opler, L. A.; Medalia, A.; Opler, M. G.; Stahl, S. M. Pharmacotherapy of cognitive deficits in schizophrenia. *CNS Spectr.* **2014**, 19, 142-156.

[10] Poyurovsky, M.; Koren, D.; Gonopolsky, I.; chneidman, M.; Fuch, C.; Weizman, A.; Weizman, R. Effect of the 5-HT2 antagonist mianserin on cognitive dysfunction in chronic schizophrenia patients: an add-on, double-blind placebo-controlled study. *Eur Neuropsychopharmacol*. **2003,** 13, 123-128.

[11] Guo, J. Y. Ragland, J. D. Carter, C. S. Memory and cognition in schizophrenia. *Molecular Psychiatry*, **2019**, 24, 633–642.

[12] Lee, Y. S.; Silva, A. J. The molecular and cellular biology of enhanced cognition. *Nature Reviews Neuroscience* **2009**, 10, 126–140.

[13] Olson, D. E. Psychoplastogens: A Promising Class of Plasticity-Promoting Neurotherapeutics. *J Exp Neurosci.* **2018**. doi: 10.1177/1179069518800508

[14] Ly, C.; Greb, C. A.; Vargas, M. V.; Duim, W. C.; Grodzki, A. C. G.; Lein, P. J.; Olson, D. E. Transient Stimulation with Psychoplastogens is Sufficient to Initiate Neuronal Growth. *ACS Pharmacol. Transl. Sci.* **2020**, 4, 452–460.

[15] Harvey, R. C.; James, A. C.; Shields, G. E. A Systematic Review and Network Meta-Analysis to Assess the Relative Efficacy of Antipsychotics for the Treatment of Positive and Negative Symptoms in Early-Onset Schizophrenia. *CNS Drugs* **2016** 30, 27-39.

[16] Singh, S. P.; Singh, V.; Kar, N.; Chan, K. Efficacy of antidepressants in treating the negative symptoms of chronic schizophrenia: meta-analysis. *Br J Psychiatry* **2010**, 197, 174-179..

[17] Harvey, R. C.; James, A. C.; Shields, G. E. A Systematic Review and Network Meta-Analysis to Assess the Relative Efficacy of Antipsychotics for the Treatment of Positive and Negative Symptoms in Early-Onset Schizophrenia. *CNS Drugs* **2016**, 30, 27-39.

We have recently reported on a novel psychoplastogen, AAZ, which produced long-lasting effects in a mouse model of anhedonia.[18,19] In addition, the ability of psychoplastogens to promote plasticity in pyramidal neurons in the PFC suggests that these drugs may be efficacious for treating the cognitive and negative symptoms of schizophrenia. One of the most potent psychoplastogens is the serotonergic psychedelic lysergic acid diethylamide (LSD). LSD is capable of robustly increasing the number of dendritic spines in cortical neurons and has shown remarkable results for treating neurological disorders like depression.[20] However, the acute, hallucinogenic effects of LSD have been proposed to induce psychosis and impair working memory.[21] Therefore, we sought to develop a non-hallucinogenic analog of LSD that retained the psychoplastogenic and anti-depressant-like effects without the hallucinogenic or acute cognitive effects.

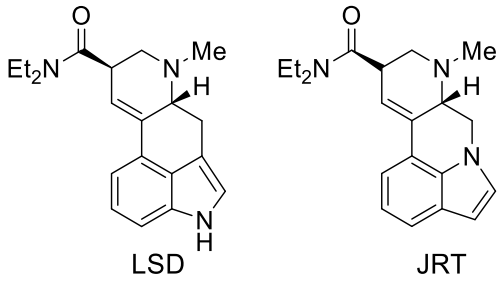

Figure 5.1 Structures of LSD and JRT.

Chapter 5.2 Development of JRT

We have recently reported that inversion of the indole in hallucinogenic tryptamines diminishes the hallucinogenic effects of psychedelics without altering the psychoplastogenic effects.[22] The NH bond of the

[18] For more details about AAZ see chapter 4.
[19] Dong, C.; Ly, C.; Dunlap, L. E.; Vargas, M. V.; Sun, J.; Hwang, I.-W.; Azinfar, A.; Oh, W. C.; Wetsel, W. C.; Olson, D. E.; Tian, L. Psychedelic-Inspired Drug Discovery Using an Engineered Biosensor. *Cell* **2021,** 10, 2779-2792.e18.
[20] Schimmel, N.; Breeksema, J. J.; Smith-Apeldoom, S. Y.; Veraart, J. van den Brink, W.; Schoevers, R. A. Psychedelics for the treatment of depression, anxiety, and existential distress in patients with a terminal illness: a systematic review. *Psychopharmacology (Berl)* **2022,** 239, 15-33.
[21] Pokorny, T.; Duerler, P.; Seifritz, E.; Vollenweider, F. X.; Preller, K. H. LSD acutely impairs working memory, executive functions, and cognitive flexibility, but not risk-based decision-making. *Psychol Med*. **2020**, 50, 2255-2264.
[22] For more details see chapter 2 or Dunlap L. E., Azinfar A., Ly C., Cameron L. P., Viswanathan J., Tombari R.J., Myers-Turnbull D., Taylor J.C., Grodzki A.C., Lein P.J., Kokel D., Olson, D.E. Identification of Psychoplastogenic N,N-Dimethylaminoisotryptamine (isoDMT) Analogues through Structure-Activity Relationship Studies. J. Med. Chem. 2020; 63: 1142-1155.

indole moiety of LSD interacts with a key serine residue (S 2.42) which is crucial for binding in the orthosteric binding pocket.[23] Non-hallucinogenic ligands primarily occupy the extended binding pocket.[24] It could be that removal of this interaction with the key serine residue shifts the binding pose of isoDMTs to favor the extended binding pocket. Inversion of the indole in LSD yielded an analog which we deemed JRT. The structure of JRT can be broken down into both a northern hemisphere, a substituted tetrahydropyridine, and a southern hemisphere, indole. These two hemispheres could be connected via a Suzuki coupling and subsequent S_N2 displacement of a leaving group. The northern hemisphere could be prepared via alkylation of the C6 position of a 5-substituted nicotinic acid and conversion of the carboxylic acid to a diethylamide.

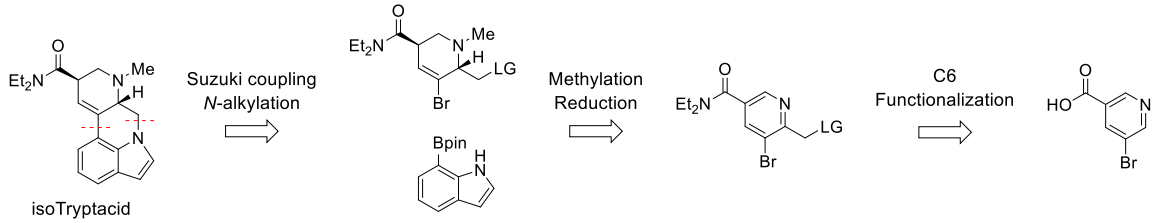

Figure 5.2. Proposed retrosynthesis of JRT.

We began our synthesis using commercially available 5-Bromo-nicotinic acid **1**. Treatment with oxalyl chloride followed by the addition of diethylamine afforded the desired 5-Bromo-nicotinamide **2**. The resulting nicotinamide was oxidized to the subsequent N-oxide using MCPBA. With *N*-oxide **3** in hand, we were able to selectively chlorinate C6 and reduce the pyridine using oxalyl chloride to afford **4**. Initial attempts at the nucleophilic aromatic substitution of the aryl chloride using diethyl malonate did produce **6**, however, the harsh conditions required resulted in significant decomposition. We, therefore, subjected the aryl chloride **4** to halogen exchange using a mixture of trimethylsilyl chloride and sodium iodide to afford compound **5**. Treatment of **5** with copper(I) iodide and diethyl malonate afforded **6** in moderate yields over 2 steps. We found that **6** underwent monodecarboxylation smoothly in the presence of a base, however,

[23] Kim, K.; Che, T.; Panova, O.; DiBerto, J. F.; Lyu, J.; Krumm, B. E.; Wacker, D.; Robertson, M. J.; Seven, A. B.; Nichols, D. E.; Shoichet, B. K.; Skiniotis, G.; Rother, B. L. Structure of a Hallucinogen-Activated Gq-Coupled 5-HT 2A Serotonin Receptor. *Cell*. **2020**, 182,1574-1588.
[24] Cao, D.; Yu, J.; Wang, H.; Luo, Z.; Liu, X.; He, L.; Qi, J.; Fan, L.; Tang, L.; Chen, Z.; Li, J.;Cheng. J.; Wang. S. Structure-based discovery of nonhallucinogenic psychedelic analogs. *Science* **2022**, 375, 403-411.

the decarboxylation of the remaining acid proved unsuccessful. We found that we were able to fully decarboxylate **6** by adjusting the pH after the first decarboxylation to furnish **7**.

Oxidation of **7** using MCPBA afforded **8** in high yields over 2 steps. Using a Boekelheide rearrangement we were able to convert **9** to the respective TFA protected alcohol using trifluoroacetic anhydride (TFAA), which upon hydrolysis afforded us the primary alcohol **10**. Subsequent methylation and reduction of the pyridine yielded the tetrahydropyridine as an inseparable mixture of diastereomers **10** (anti) and **11** (syn). We anticipated the anti-configuration would be the favored product based on NMR data of similar tetrahydropyridines, such as that of LSD itself.[25] We obtained a 5:2 mixture of the anti/syn diastereomers **10** and **11** respectively, which we were able to couple with a 7-Bpin-indole providing **12** and **13**. Surprisingly, treatment of alcohols **12** and **13** with tosyl chloride and triethylamine did not yield the corresponding tosylate but rather the alkyl chloride which proved prone to decomposition in attempts to alkylate the indole nitrogen. However, we found that tosylation of the alcohol with sodium hydroxide in chloroform followed by addition of DMSO as a cosolvent facilitated the tosylation and corresponding N-alkylation in one step to afford JRT-E-074 and JRT-E-120 as the major and minor products, respectively. As JRT-E-074 was the diastereomer that shared the same relative stereochemistry as LSD, we separated the enantiomers via chiral prep-HPLC to afford (+)-JRT-E-074 and (-)-JRT-E-074, (+)JRT and (-)JRT respectively, which we are currently in the process of obtaining crystal structures of to confirm absolute stereochemistry.

[25] Salamone, S. J.; Li, Z.; McNally, A. J.; Vitone, S.; Wu, R. S. Epimerization Studies of LSD Using 1H Nuclear Magnetic Resonance (NMR) Spectroscopy. *J. Anal. Toxicol.* **1997**, 21, 492–497.

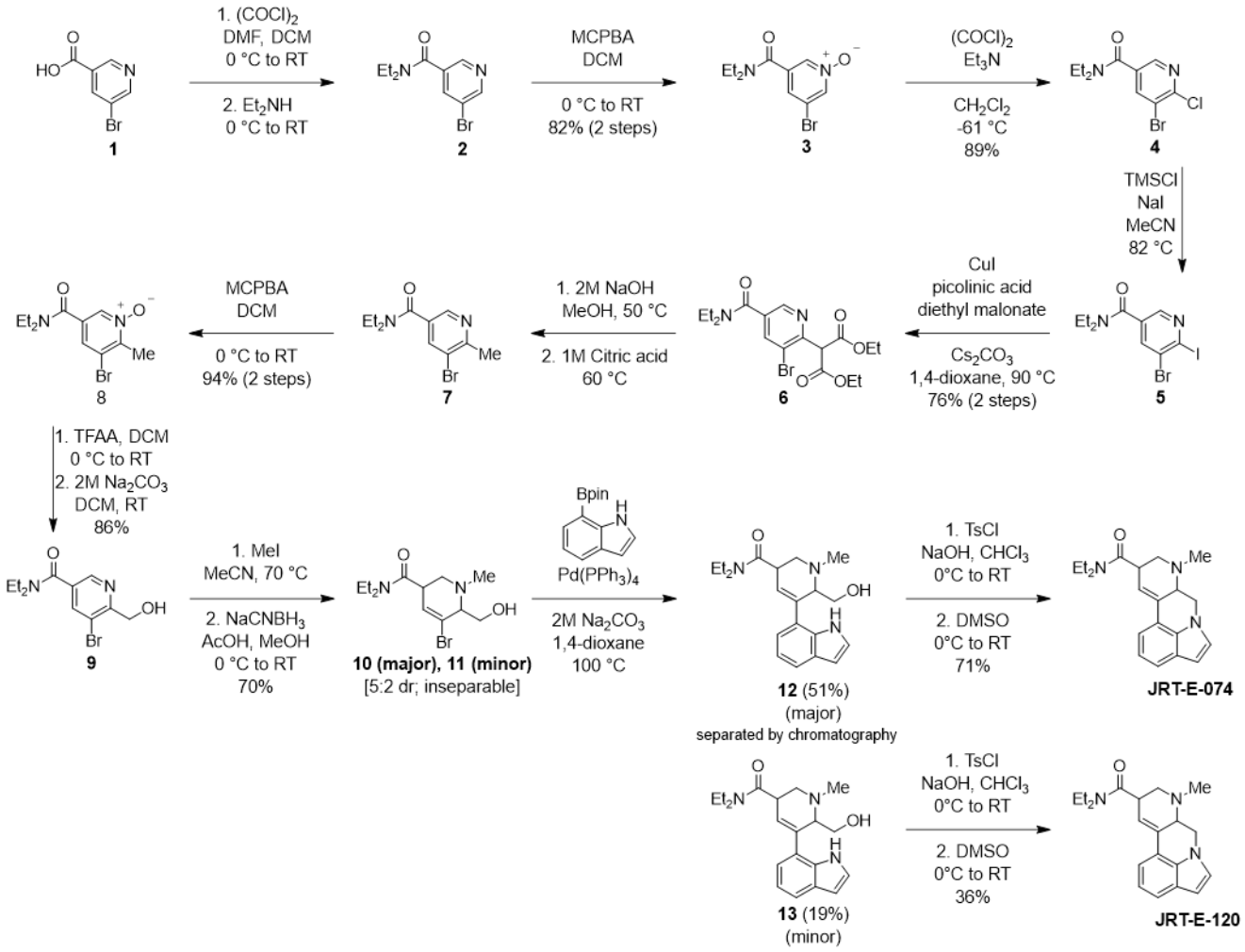

Figure 5.3 Synthetic scheme of JRT-E-074 and JRT-E-120.

Chapter 5.3 JRT is a Highly Selective 5-HT2R Ligand

As LSD has a high affinity for 5-HT2Rs we screened both (+)JRT and (-)JRT in radioligand binding assays at the 5-HT2A and 5-HT2C receptors. We found that (+)JRT has nanomolar affinity for 5-HT2A and 5-HT2C with (-)JRT showing an order of magnitude decreased affinity (**Table 5.1**). Next, we screened both compounds for agonist activity by measuring inositol phosphate accumulation. Both compounds were found to be agonists, with (+)JRT being the more potent compound at 5-HT2 activation **(Table 5.1).** The affinity

of (+)JRT for 5-HT2CRs may prove beneficial as agonists of 5-HT2CRs have been reported to have antipsychotic-like activity.[26]

	5-HT2A		5-HT2C	
	RLB	**IPOne**	**RLB**	**IPOne**
Ligand	IC50 (nM)	EC50 (nM)	IC50 (nM)	EC50 (nM)
(+)JRT	35.7 ± 3.6	17.6 ± 1.9	75.6 ± 12	33.9 ± 4.3
(-)JRT	399 ± 44	241 ± 49	709 ± 160	555 ± 79
5-HT	22.9 ± 4.7	N/D	3.17 ± 0.5	N/D
α-Me-5-HT	N/D	7.62 ± 0.2	N/D	5.5 ± 0.2

Table 5.1. RadioLigand Binding and Inositol Phosphate Assays. [3H]-DOI was used as the hot ligand in both the 5-HT2A and 5-HT2C radioligand binding assays (N = 2). Values represent mean ± SE. N/D = not determined. 5-HT = serotonin, α-Me-5-HT = alpha-methyltryptamine.

Chapter 5.4. JRT Blocks LSD-Induced HTR.

As LSD is a potent hallucinogen, we wanted to assess the effects of the JRT compounds in a phenotypic model of hallucinations in vivo. We used the head twitch response assay (HTR) as it has been shown to correlate well with human potencies for hallucinogenic compounds.[27] We compared (+)JRT and (-)JRT to LSD in a 3-point dose-response in the HTR assay in mice. Only LSD at 0.2mg/kg caused a significant increase in the number of head twitches suggesting that both (+)JRT and (-)JRT are non-hallucinogenic **(FIG 5.4A)**. Psychedelics like LSD cause alterations in behavioral responses similar to those found in patients with schizophrenia including alterations to perception.[28,29] Thus we tested the ability of JRT to block the HTR caused by LSD. We found that (+)JRT at 1mg/kg was able to block the HTR caused

[26] Pogorelov, V. M.; Rodriguiz, R. M.; Cheng, J.; Huang, M.; Schmerberg, C. M.; Meltzer, H. Y.; Roth, B. L.; Kozikowski, A. P.; Wetsel, W. C. 5-HT 2C Agonists Modulate Schizophrenia-Like Behaviors in Mice. *Neuropsychopharmacology* **2017**, 42, 2163-2177..

[27] Halberstadt, A. L.; Chatha, M.; Klein, A. K.; Wallach, J.; Brandt, S. D. Correlation between the potency of hallucinogens in the mouse head-twitch response assay and their behavioral and subjective effects in other species *Neuropharmacology*. **2020** .167, 107933.

[28] Marona-Lewicka, D.; Nichols, C. D.; Nichols, D. E. An animal model of schizophrenia based on chronic LSD administration: old idea, new results. *Neuropharmacology* **2011**, 61, 503-512.

by LSD at 0.2mg/kg **(FIG 5.4B)**. As (+)JRT was able to block the HTR caused by LSD, we used it as our lead candidate for further screenings.

Another in vivo measure of the positive symptoms of schizophrenia is amphetamine-induced locomotion. As the positive symptoms are thought to arise from hyperfunction in the mesolimbic dopamine system, administration of dopamine releasers, like amphetamine, are used to mimic the positive symptoms of schizophrenia. Antipsychotics like aripiprazole and clozapine can block the amphetamine-induced hyperlocomotion in mice **(FIG 5.4C).**[30,31] We found that (+)JRT produced no changes to locomotion in mice and pretreatment of (+)JRT (1mg/kg) blocked amphetamine (3mg/kg) induced locomotion **(FIG 5.5D)**.

[30] Leite, J. V.; Guimarae, F. S.; Moreira, F. A. Aripiprazole, an atypical antipsychotic, prevents the motor hyperactivity induced by psychotomimetics and psychostimulants in mice*. Eur J Pharmacol*. **2008,** 578, 222-227.
[31] Hideshima, K. S.; Hojati, A.; Saunders, J. M.; On, D. M.; Revenga, M. F.; Shin, J. M.; Sanchez-Gonzalez, A.; Dunn, C. M.; Pais, A. B.; Pais, A. C.; Miles, M. F.; Wolstenholme, J. T.; Gonzalez-Maeso, J. Role of mGlu2 in the 5-HT 2A receptor-dependent antipsychotic activity of clozapine in mice. *J. Psychopharmacology (Berl).* **2018,** 235, 3149-3165.

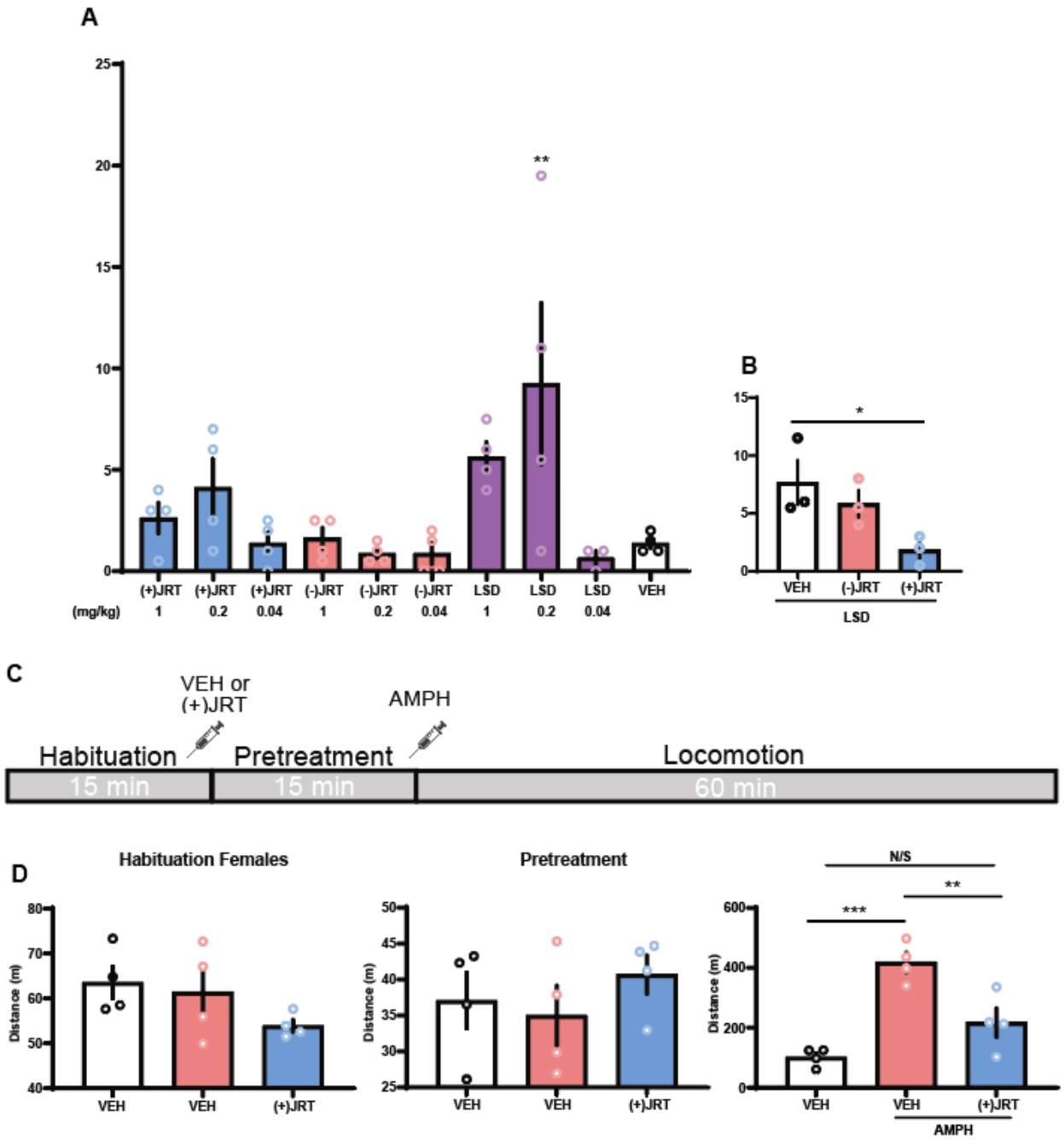

Figure 5.4 JRT Blocks the Positive Symptoms of Schizophrenia. **(A)** Neither (+)JRT nor (-)JRT cause a significant increase in the number of HTR. (N = 3–4 mice). **(B)** (+)JRT but not JRT (1 mg/kg) blocks the LSD (0.2 mg/kg) induced HTR. (C) Schematic depicting the amphetamine-induced locomotion design. (D) (+)JRT (1 mg/kg) produced no changes to locomotion. Pretreatment of (+)JRT (1 mg/kg) decreases amphetamine-induced locomotion. (N = 4) data are represented as means and SEMs, ∗∗∗p < 0.001, ∗∗p < 0.01 and ∗p < 0.05.

Chapter 5.5 Conclusion

We have developed (+)JRT, an analog of LSD with reduced hallucinogenic potential, with an overall yield of 11% over 11 steps. The key step in the synthesis of (+)JRT involves the coupling of the northern (tetrahydropyridine) and southern (indole) hemispheres. We designed this route to not only afford an expedient synthesis of (+)JRT but also minimize the need for extensive purification steps.

We have gathered preliminary data to suggest that (+)JRT may have antipsychotic-like effects in treating the positive symptoms of schizophrenia. A major challenge in schizophrenia research is a lack of behavioral models, however some drugs, like LSD and amphetamine, have been shown to mimic the positive symptoms.[30] Due to the ability of LSD to cause hallucinations it was argued that LSD-induced psychosis mimics schizophrenia.[32] We theorized that blocking the effects of LSD-induced hallucinations may prove to be a useful tool in the determination of antipsychotic-like activity. We found that (+)JRT had reduced effects in an in vivo model of hallucinations, and that (+)JRT was able to block the HTR caused by LSD in mice. We also screened (+)JRT using a more traditional measure of the positive symptoms of schizophrenia, amphetamine-induced hyperlocomotion. (+)JRT had no effects on locomotion however animals pretreated with (+)JRT showed reduced changes to locomotion following treatment with amphetamine

A lot of work remains to elucidate the therapeutic potential of (+)JRT, however, we believe that the data presented here show promising results towards the development of a non-hallucinogenic analog of a classic psychedelic for treating schizophrenia. We are currently in the process of screening (+)JRT in models of both the cognitive deficits and negative symptoms of schizophrenia.

ACKNOWLEDGEMENTS

I would like to thank Jeremy Tuck for his work synthesizing JRT and Delix Therapeutics for performing the chiral separation and receptor screening. I would also like to thank David Favela for his help determining the optical rotation of JRT.

[32] Vardy, M. M.; Kay, S. R. LSD psychosis or LSD-induced schizophrenia? A multimethod inquiry. *Arch Gen Psychiatry*. **1983**, 40, 877-883.

Chapter 5.6 Methods

Drugs

The NIH Drug Supply Program provided LSD and D-amphetamine sulfate was purchased from Sigma Aldrich. (+)JRT and (-)JRT were synthesized in-house and deemed to be >95% pure by HPLC.

Animals

All experimental procedures involving animals were approved by the Institutional Animal Care and Use Committee (IACUC) at the University of California, Davis, and adhered to principles described in the National Institutes of Health Guide for the Care and Use of Laboratory Animals. The University of California, Davis is accredited by the Association for Assessment and Accreditation of Laboratory Animal Care International (AAALAC).

Radioligand Binding and IP-1 Assays.

Radioligand binding assays were performed by Neurofit and Delix Therapeutics using [3H]-DOI as the hot ligand.

Head-Twitch Response Assay

The HTR assay was performed as described previously using a total of 12 female C57BL/6J mice (N = 3–4).[22] The mice were obtained from The Jackson Laboratory (Sacramento, C.A.) and were approximately 8–12 weeks old at the time of the experiments. Compounds were administered (5 mL/kg, i.p.) using 0.9% saline as the vehicle. After injection, animals were placed into an empty cage (40cm x 40cm) and HTRs were videotaped. Animals were given a one-week washout period before being tested again. All drug treatments were randomized and no animal received the same drug and dose twice.[33] Videos were scored later by two blinded observers, and the results were averaged (interpersonal kappas, Pearson correlation coefficient > 0.91). For the blocking experiments, animals were injected with (+)JRT (1

[33] Smith, D. A.; Bailey, J. M.; Williams, D.; Fantegrossi, W. E. Tolerance and Cross-Tolerance to Head Twitch Behavior Elicited by Phenethylamine- and Tryptamine-Derived Hallucinogens in Mice. *J Pharmacol Exp Ther*. **2014**, 351, 485–491.

mg/kg), (-)JRT (1 mg/kg), or saline (5 ml/kg, i.p) and placed in an empty cage. After 15 minutes animals were removed and injected with LSD (0.2 mg/kg, 5 ml/kg, ip) and placed in the test arena and filmed for 20 minutes.

Amphetamine Induced Locomotion

The amphetamine-induced locomotion assay was done using female C57BL/6J mice (N = 4). The mice were obtained from The Jackson Laboratory (Sacramento, C.A.) and were approximately 8 weeks old at the time of the experiments. Animals were placed in the test arena to get a basal reading of locomotion and habituate them to the testing arena for 15 minutes. Animals were removed and injected with (+)JRT (1 mg/kg) or saline (2.5 mL/kg, i.p) using 0.9% saline as the vehicle and placed back in the test arena for 15 minutes. Animals were then removed and injected with amphetamine (3 mg/kg) or saline (2.5 mL/kg) and placed back in the test arena for 60 minutes. Locomotion was assessed using AnyMaze automated tracking software.

Chemistry (General)

All reagents were obtained from commercial sources and were used without purification unless otherwise noted. DMSO was purified by passage under 12 psi N_2 through activated alumina columns. Reactions were performed using glassware that was flame-dried under reduced pressure (~1 Torr). Chromatography was performed using Fisher Chemical Silica Gel Sorbent (230−400 mesh, grade 60). Compounds purified by chromatography were dissolved in a minimal amount of chloroform for loading. Thin-layer chromatography (TLC) was performed on Millipore silica gel 60 F254 plates. Visualization of the developed chromatogram was accomplished by fluorescence quenching or by staining with ninhydrin.

Nuclear magnetic resonance (NMR) spectra were acquired on either a Bruker 400 operating at 400 and 100 MHz or a Varian 600 operating at 600 and 150 MHz for 1H and 13C respectively, and are referenced internally according to residual solvent signals. Data for ^{1}H NMR are recorded as follows: chemical shift (δ, ppm), multiplicity (s, singlet; d, doublet; t, triplet; q, quartet; m, multiplet), integration, coupling constants (Hz). Data for ^{13}C NMR are reported in terms of chemical shift (δ, ppm). Infrared spectra were recorded using a Thermo Nicolet iS10 Fourier transform infrared (FT-IR) spectrometer with a Smart

iTX Accessory [diamond attenuated total reflection (ATR)] and are reported in the frequency of absorption (v, cm^{-1}). Liquid chromatography−mass spectrometry (LC−MS) was performed using a Waters LC−MS with an ACQUITY Arc QDa detector. Stock solutions for behavioral assays were prepared fresh before their use. Specific rotations were obtained on a AUTOPOL IV Automatic Digital Polarimeter.

Synthesis of isoTryptacid

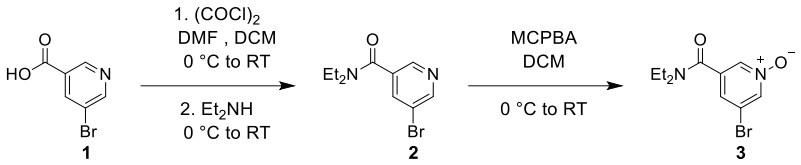

5-bromo-*N,N*-diethylnicotinamide 4. To a 0°C cooled mixture of 5-bromonicotinic acid (10.000 g, 49.503 mmol, 1.0 equiv) in DCM (250 mL) was added oxalyl chloride (6.37 mL, 74.2 mmol, 1.5 equiv) slowly. To the suspension was added DMF (0.5 mL) dropwise, and the mixture was warmed to ambient temperature and stirred for 1 h. The mixture was cooled to 0 °C and a solution of diethylamine (25.61 mL, 247.5 mmol, 5.0 equiv) in DCM (250 mL) was added slowly via cannula. The mixture was warmed to ambient temperature and stirred for 30 min. H_2O (500 mL) was added, followed by 2M HCl (40 mL) until the pH = 1 to 2. The layers were separated, and the aqueous layer was further extracted with DCM (3 x 200 mL). The organic extracts were combined and sequentially washed with saturated aqueous $NaHCO_3$ (1 x 250 mL) and brine (1 x 250 mL). The organic extract was dried over Na_2SO_4, and concentrated under reduced pressure.

3-bromo-5-(diethylcarbamoyl)pyridine 1-oxide 5.To a 0°C cooled solution of the resulting brown oil in DCM (200 mL) was added MCPBA (70-75% balance) (22.781 g, 99.006 mmol, 2.0 equiv). The mixture was warmed to ambient temperature and stirred for 18 h. To the solution was added saturated aqueous $NaHCO_3$ (500 mL) and then 1M NaOH (500 mL). The layers were separated, and the aqueous layer was further extracted with 10% IPA in DCM (3 x 200 mL). The organic layers were combined, dried over Na_2SO_4, filtered, and concentrated under reduced pressure. The residue was purified via chromatography on silica gel (EtOAc then 12% MeOH in EtOAc) and concentrated under reduced pressure. The resulting pale yellow oil was dissolved in DCM (50 mL), and to the solution was added hexanes (500 mL) slowly with vigorous

stirring. The suspension was cooled to 0 °C, filtered, and washed with 100 mL cold hexanes to afford **3** (11.041 g, 82%) as a white solid. ^{1}H NMR (400 MHz, $CDCl_3$) δ = 8.32 (t, *J* = 1.5 Hz, 1H), 8.09 (t, *J* = 1.3 Hz, 1H), 7.35 (t, *J* = 1.3 Hz, 1H), 3.54 – 3.46 (m, 2H), 3.29 – 3.21 (m, 2H), 1.24 – 1.12 (m, 6H) ppm. ^{13}C NMR (100 MHz, $CDCl_3$) δ = 164.3, 141.0, 136.3, 135.9, 126.4, 120.7, 43.5, 39.9, 14.4, 12.8 ppm. LRMS (ES^+) *m/z* $[M + H]^+$ calcd for $C_{10}H_{14}BrN_2O_2^+$ 273.02; Found 273.12. IR (diamond, ATR) v 3445, 3068, 2973, 2934, 1633 cm^{-1}.

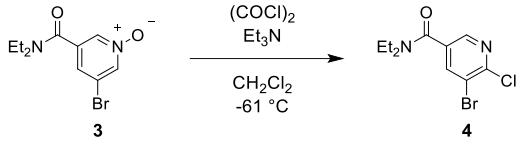

5-bromo-6-chloro-*N,N*-diethylnicotinamide 6. To a -61°C cooled ($CHCl_3$/dry ice) solution of **3** (9.900 g, 36.395 mmol, 1.0 equiv) and Et_3N (10.15 mL, 72.79 mmol, 2.0 equiv) in DCM (180 mL) was added oxalyl chloride (6.24 mL, 72.8 mmol, 2.0 equiv) slowly dropwise. The mixture was stirred for 30 minutes, then MeOH (5 mL) was added slowly before warming to ambient temperature, then saturated aqueous $NaHCO_3$ (25 mL) was added. The solution was poured into 1M NaOH (600 mL) and the layers were separated. The aqueous layer was further extracted with DCM (3 x 150 mL). The organic extracts were combined, washed with brine (250 mL), dried over Na_2SO_4, and concentrated under reduced pressure. The residue was purified by chromatography on silica gel (25% EtOAc in hexanes) to afford 4 (9.442 g, 89%) as a crystalline white solid. ^{1}H NMR (400 MHz, $CDCl_3$) δ = 8.34 (s, 1H), 7.96 (s, 1H), 3.59 – 3.42 (m, 2H), 3.36 – 3.18 (m, 2H), 1.28 – 1.10 (m, 6H) ppm. ^{13}C NMR (100 MHz, $CDCl_3$) δ = 166.0, 151.5, 145.3, 140.7, 133.0, 120.5, 43.6, 39.9, 14.4, 12.9 ppm. LRMS (ES^+) *m/z* $[M + H]^+$ calcd for $C_{10}H_{13}BrClN_2O^+$ 290.99; Found 291.00. IR (diamond, ATR) v 2974, 2935, 1627, 1574 cm^{-1}.

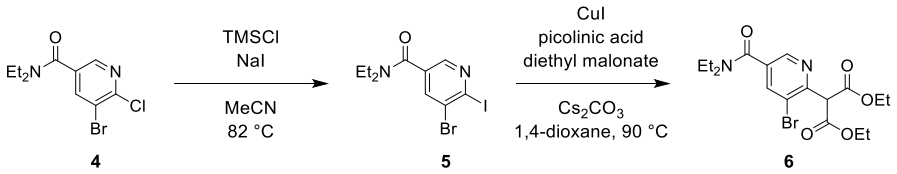

5-bromo-*N, N*-diethyl-6-iodonicotinamide 7. [0001] To a vigorously stirred mixture of **4** (5.000 g, 17.243 mmol, 1.0 equiv) and NaI (20.676 g, 137.94 mmol, 8.0 equiv) in acetonitrile (40 mL) was added

TMSCl (3.28 mL, 25.86 mmol, 1.5 equiv) slowly. The mixture was stirred at ambient temperature for 30 min, then heated at reflux for 1 hour, with ¼ of the reaction volume removed and collected in a Dean-Stark receiver during this time period. The resulting yellow suspension was cooled to ambient temperature, diluted with DCM (150 mL), and added to a saturated aqueous $NaHCO_3$ solution (250 mL). With vigorous stirring, a saturated aqueous $Na_2S_2O_8$ solution (100 mL) was added, followed by 1M NaOH (80 mL). The resultant clear solution was transferred to a separatory funnel and the layers were separated. The aqueous layer was further extracted with DCM (3 x 100 mL). The organic extracts were combined, washed with brine (200 mL), dried over Na_2SO_4, and concentrated under reduced pressure.

Diethyl 2-(3-bromo-5-(diethylcarbamoyl)pyridin-2-yl)malonate 8. The resulting pale orange solid was added to a sealable screw cap flask along with copper(I) iodide (0.164 g, 0.861 mmol. 0.05 equiv), picolinic acid (0.212 g, 1.72 mmol, 0.1 equiv), and Cs_2CO_3 (16.854 g, 51.729 mmol, 3.0 equiv). 1,4-dioxane (43 mL) and diethyl malonate (5.26 mL, 34.5 mmol, 2.0 equiv) were added, and the flask capped. The mixture was stirred and heated at 90 °C for 16 h. The mixture was cooled to ambient temperature and filtered over celite, and the filter cake was washed with EtOAc (200 mL). The filtrate was added to H_2O (500 mL), then 1M HCl (10 mL) was added and the layers were separated. The aqueous layer was further extracted with EtOAc (2 x 200 mL). The organic extracts were combined, washed with brine (250 mL), dried over Na_2SO_4, and concentrated under reduced pressure. The residue was purified by chromatography on silica gel (20% EtOAc in hexanes to 50% EtOAc in hexanes) to afford 6 (5.461 g, 76%) as a pale yellow oil. ^{1}H NMR (400 MHz, $CDCl_3$) δ = 8.52 (d, *J* = 1.8 Hz, 1H), 7.92 (d, *J* = 1.8 Hz, 1H), 5.22 (s, 1H), 4.34 – 4.23 (m, 4H), 3.62 – 3.44 (m, 2H), 3.38 – 3.19 (m, 2H), 1.32 – 1.10 (m, 12H) ppm. ^{13}C NMR (100 MHz, $CDCl_3$) δ = 166.62, 166.58, 152.5, 142.2, 138.9, 133.5, 121.9, 62.3, 59.9, 43.6, 39.8, 14.5, 14.1, 12.9 ppm. LRMS (ES^+) *m/z* $[M + H]^+$ calcd for $C_{17}H_{24}BrN_2O_5^+$ 415.09; Found 415.19. IR (diamond, ATR) v 2980, 2937, 1735, 1631 cm^{-1}.

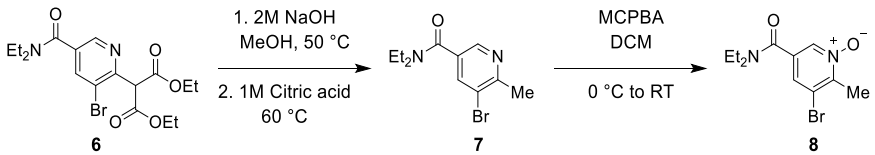

5-bromo-*N,N*-diethyl-6-methylnicotinamide 9. To a solution of **6** (5.350 g, 12.92 mmol, 1.0 equiv) in MeOH (130 mL) was added 2M aq. NaOH (32 mL), and the solution was stirred and heated at 50°C for 16 h. To the resulting suspension, 1M aq. Citric acid (45 mL) was added to adjust the pH to 4, and the solution was stirred and heated at 60°C for 24 h. The solution was cooled to ambient temperature and the MeOH was removed by concentration under reduced pressure. The solution was added to H_2O (250 mL) and extracted with DCM (3 x 200 mL). The organic layers were combined, washed with brine (250 mL), dried over Na_2SO_4, and concentrated under reduced pressure.

3-bromo-5-(diethylcarbamoyl)-2-methylpyridine 1-oxide 10. To a 0°C cooled solution of the resulting residue in DCM (50 mL) was added MCPBA (70-75% balance) (5.946 g, 25.84 mmol, 2.0 equiv) slowly. The solution was warmed to ambient temperature and stirred for 22 h. The solution was added to 150 mL 1M NaOH and the layers were separated. The aqueous layer was further extracted with 10% isopropyl alcohol in DCM (3 x 100 mL). The organic extracts were combined, dried over Na_2SO_4, filtered, and concentrated under reduced pressure. The residue was purified by column chromatography on silica gel (EtOAc then 10% MeOH in EtOAc) to afford 8 (3.469 g, 94%) as a white solid. ^{1}H NMR (400 MHz, $CDCl_3$) δ = 8.19 (d, *J* = 0.9 Hz, 1H), 7.4 (d, *J* = 0.9 Hz, 1H), 3.58 – 3.39 (m, 2H), 3.36 – 3.18 (m, 2H), 2.66 (s, 3H), 1.24 – 1.10 (m, 6H) ppm. ^{13}C NMR (100 MHz, $CDCl_3$) δ = 164.6, 150.2, 136.2, 133.0, 127.0, 122.1, 43.5, 39.9, 17.4, 14.4, 12.8 ppm. LRMS (ES^+) *m/z* $[M + H]^+$ calcd for $C_{11}H_{16}BrN_2O_2^+$ 287.04; Found 287.12. IR (diamond, ATR) v 3455, 2972, 2935, 1632 cm^{-1}.

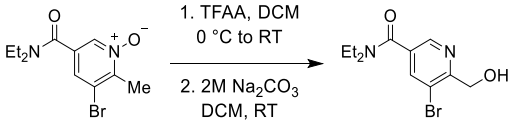

5-bromo-*N,N*-diethyl-6-(hydroxymethyl)nicotinamide 11. To a 0°C cooled solution of **8** (1.301 g, 4.531 mmol, 1.0 equiv) in DCM (22.6 mL) was added trifluoroacetic anhydride (1.57 mL, 11.3 mmol, 2.5 equiv) dropwise. The solution was warmed to ambient temperature and stirred for 4 h before concentrating under reduced pressure. The residue was re-dissolved in DCM (22.6 mL) and 2M aq. Na_2CO_3 (45.2 mL) was added. The biphasic solution was stirred vigorously at ambient temperature for 18 h, then poured into H_2O

(100 mL). The layers were separated and the aqueous layer was further extracted with DCM (3 x 50 mL). The organic extracts were combined, washed with brine (100 mL), dried over Na_2SO_4, and concentrated under reduced pressure. The residue was purified by column chromatography on silica gel (EtOAc) to afford 9 (1.119 g, 86%) as a yellow oil. ^{1}H NMR (400 MHz, $CDCl_3$) δ = 8.53 (d, *J* = 1.7 Hz, 1H), 7.90 (d, *J* = 1.7 Hz, 1H), 4.77 (d, *J* = 4.7 Hz, 2H), 4.23 (t, *J* = 4.7 Hz, 1H), 3.64 – 3.46 (m, 2H), 3.38 – 3.18 (m, 2H), 1.32 – 1.08 (m, 6H) ppm. ^{13}C NMR (100 MHz, $CDCl_3$) δ = 166.8, 157.6, 144.1, 138.6, 133.2, 118.7, 63.4, 43.6, 39.9, 14.5, 12.9 ppm. LRMS (ES$^+$) *m/z* $[M + H]^+$ calcd for $C_{11}H_{16}BrN_2O_2$ 287.04; Found 287.12. IR (diamond, ATR) v 3412, 2972, 2934, 1624, 1588 cm^{-1}.

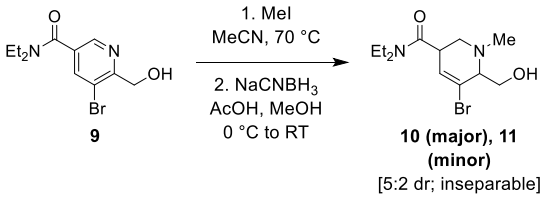

5-bromo-*N,N*-diethyl-6-(hydroxymethyl)-1-methyl-1,2,3,6-tetrahydropyridine-3-carboxamide 12,13. To a solution of **9** (0.980 g, 3.413 mmol, 1.0 equiv) in MeCN (4.25 mL) in a vial was added MeI (1.28 mL, 20.5 mmol, 6.0 equiv). The vial was capped and the solution was heated with stirring at 70°C for 24 h then subsequently cooled to ambient temperature. To the mixture was added EtOAc (8.5 mL) followed by hexanes (8.5 mL) with vigorous stirring. The suspension was cooled to 0°C, filtered, and washed with hexanes (2 x 5 mL). The resulting yellow solid was dried under reduced pressure and used directly in the next step.

To a 0°C cooled solution of the resulting methyl pyridinium salt (1.285 g, 2.995 mmol, 1.0 equiv) in MeOH (30 mL) was added AcOH (0.51 mL, 8.9 mmol, 3.0 equiv) followed by the dropwise addition of $NaCNBH_3$ (0.565 g, 8.98 mmol, 3.0 equiv) in MeOH (6 mL). The solution was warmed to ambient temperature and stirred for 16 h, then concentrated under reduced pressure. The residue was dissolved in EtOAc (100 mL) and added to 1M NaOH (200 mL). The layers were separated, and the aqueous layer was further extracted with EtOAc (3 x 100 mL). The organic extracts were combined and washed with brine (150 mL), dried over Na_2SO_4, and concentrated under reduced pressure. The residue was purified by column chromatography on silica gel (3% MeOH in DCM) to afford an inseparable mixture of diastereomers 12 (major diastereomer)

and 13 (minor diastereomer) (0.726 g, 70%), 5:2 dr) as a pale yellow oil. ^{1}H NMR (400 MHz, $CDCl_3$) δ = 6.21† (s, 1H), 6.11* (d, *J* = 2.8 Hz, 0.4H), 3.94† (dd, *J* = 2.0 Hz, 1H), 3.88 – 3.78 (m, 1.4H), 3.70 – 3.64* (m, 0.4H), 3.59* (dd, *J* = 8.8, 11.6 Hz, 0.4H), 3.54 – 3.47† (m, 1H), 3.34 (quint, *J* = 7.3 Hz, 5.6H), 3.21* (dd, *J* = 9.4, 13.6 Hz, 0.4H), 3.14 – 3.08* (m, 0.4H), 3.02 – 2.92† (m, 2H), 2.88 – 2.80† (m, 1H), 2.76* (dd, *J* = 5.1, 14 Hz, 0.4H), 2.55* (s, 1.2H), 2.45† (s, 3H), 2.24 – 2.14 (m, 4.2H), 1.09 (t, *J* = 7.1 Hz, 4.2H) ppm. ^{13}C NMR (100 MHz, $CDCl_3$) δ = 170.22, 170.15, 130.4, 127.6, 123.3, 122.9, 68.6, 67.6, 60.9, 59.6, 53.6, 47.0, 43.5, 42.9, 42.2, 42.1, 41.3, 40.7, 40.4, 36.7, 15.1, 14.9, 13.2, 13.1 ppm. LRMS (ES^+) *m/z* $[M + H]^+$ calcd for $C_{12}H_{22}BrN_2O_2^+$ 305.09; Found 305.14. IR (diamond, ATR) v 3418, 2970, 2934, 2799, 1629 cm^{-1}. †denotes ^{1}H NMR signal arising exclusively from the major diastereomer; *denotes ^{1}H NMR signal arising exclusively from the minor diastereomer; undesignated signals arise from a mixture of both.

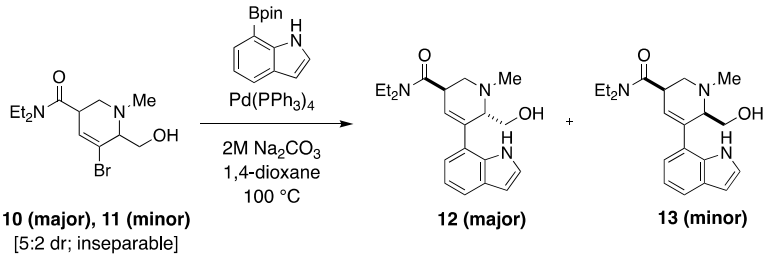

***N,N*-diethyl-6-(hydroxymethyl)-5-(1H-indol-7-yl)-1-methyl-1,2,3,6-tetrahydropyridine-3-carboxamide 14,15**. A mixture of diastereomers **10** and **11** (5:2 dr) (0.698 g, 2.29 mmol, 1.0 equiv), 1,4-dioxane (22.9 mL), indole-7-boronic acid pinacol ester (0.834 g, 3.43 mmol, 1.5 equiv), and 2M aq. Na_2CO_3 (2.29 mL) were added to a vial and the solution was sparged with N_2 for 10 min before the addition of $Pd(PPh_3)_4$ (0.132 g, 0.114 mmol, 0.05 equiv). The vial was capped and the mixture was heated with stirring at 100°C in a preheated oil bath for 4 h. The mixture was cooled to ambient temperature, added to H_2O (400 mL), and extracted with EtOAc (3 x 150 mL). The organic extracts were combined, washed with brine (200 mL), dried over Na_2SO_4, and concentrated under reduced pressure. The residue was purified by column chromatography on silica gel (2% MeOH in DCM to 10% MeOH in DCM) to afford 14 (major diastereomer) (0.398 g, 51%) and 15 (minor diastereomer) (0.148 g, 19%) as off white semi-solids. Major Diastereomer, 12. ^{1}H NMR (400 MHz, $CDCl_3$) δ = 9.46 (s, 1H), 7.56 (d, *J* = 7.8 Hz, 1H), 7.22 (t, *J* = 2.8 Hz, 1H), 7.06 (t, *J*

= 7.3 Hz, 1H), 7.00 (dd, *J* = 0.9, 8.4 Hz, 1H), 6.53 (dd, *J* = 2.1, 3.2 Hz, 1H), 5.92 (s, 1H), 3.79 (dd, *J* = 3.0, 11.2 Hz, 1H), 3.74 – 3.66 (m, 1H), 3.50 – 3.28 (m, 5H), 3.26 – 3.08 (m, 3H), 3.07 – 2.96 (m, 1H), 2.52 (s, 2H), 1.23 (t, *J* = 7.1 Hz, 3H), 1.10 (t, *J* = 7.1 Hz, 3H) ppm. ^{13}C NMR (100 MHz, $CDCl_3$) δ = 171.7, 137.3, 135.4, 128.11, 128.05, 124,9, 124.1, 121.4, 119.9, 119.4, 102.4, 66.8, 59.1, 54.0, 43.2, 42.0, 40.3, 39.3, 14.9, 13.1 ppm. LRMS (ES^+) *m/z* $[M + H]^+$ calcd for $C_{20}H_{28}N_3O_2^+$ 342.22; Found 342.32. IR (diamond, ATR) v 3267, 2970, 2932, 1615 cm^{-1}. Minor Diastereomer, 13. ^{1}H NMR (400 MHz, $CDCl_3$) δ = 9.86 (s, 1H), 7.55 (d, *J* = 7.8 Hz, 1H), 7.29 – 7.24 (m, 1H), 7.07 (t, *J* = 7.4 Hz, 1H), 6.98 (dd, *J* = 0.6, 7.6 Hz, 1H), 6.51 (dd, *J* = 2.1 Hz, 3.2 Hz, 1H), 6.08 – 6.04 (m, 1H0, 3.76 – 3.68 (m, 1H), 3.64 – 3.28 (m, 8H), 3.15 – 3.06 (m 1H), 2.99 (dd, *J* = 5.7, 13.2 Hz, 1H), 2.66 (s, 3H), 1.26 (t, *J* = 7.2 Hz, 3H), 1.17 (t, *J* = 7.1 Hz, 3H) ppm. ^{13}C NMR (100 MHz, $CDCl_3$) δ = 173.0, 135.7, 135.0, 128.4, 125.6, 125.4, 123.8, 120.0, 119.4, 119.0, 102.1, 64.8, 60.9, 48.6, 42.7, 42.3, 40.6, 34.8, 15.1, 13.3 ppm. LRMS (ES^+) *m/z* $[M + H]^+$ calcd for $C_{20}H_{28}N_3O_2^+$ 342.22; Found 342.32. IR (diamond, ATR) v 3270, 2973, 2934, 1613 cm^{-1}.

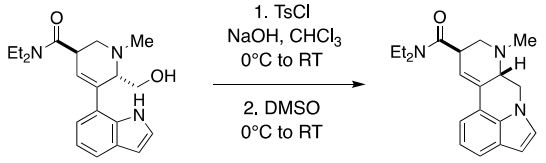

JRT-E-074. To a 0°C cooled solution of **15** (0.250 g, 0.732 mmol, 1.0 equiv) in $CHCl_3$ (7.3 mL) was added freshly crushed NaOH (0.234 g, 5.86 mmol, 8.0 equiv). A solution of TsCl (0.167 g, 0.878 mmol, 1.2 equiv) in $CHCl_3$ (1.5 mL) was added dropwise over 10 minutes. The mixture was warmed to ambient temperature and stirred for 1.5 h. The mixture was cooled to 0°C, and DMSO (3.7 mL) was added slowly before warming to ambient temperature and stirring for 1 h. The mixture was partitioned in H_2O (250 mL) and EtOAc (200 mL) and the layers were separated. The aqueous layer was further extracted with EtOAc (3 x 100 mL). The organic extracts were combined, washed with brine (250 mL), dried over Na_2SO_4, and concentrated under reduced pressure. The residue was purified by column chromatography on silica gel (8% MeOH in EtOAc to 12% MeOH in EtOAc) to afford 14 (0.168 g, 71 %) as an off white semi-solid. ^{1}H NMR (400 MHz, $CDCl_3$) δ = 7.5 (d, *J* = 7.9 Hz, 1H), 7.31 (d, *J* = 7.3 Hz, 1H), 7.08 – 7.04 (m, 2H), 6.46 (d, *J* = 3.0 Hz, 1H), 6.31 (s, 1H), 4.66 (dd, *J* = 5.4, 11.2 Hz, 1H), 3.90 – 3.82 (m, 1H), 3.80 (t, *J* = 11.1 Hz, 1H), 3.54 – 3.40 (m, 5H), 3.05 (dd, *J* = 5.0, 11.2 Hz, 1H), 2.95 (t, *J* = 10.7 Hz, 1H), 2.59 (s, 3H), 1.26 (t, *J* = 7.1Hz, 3H), 1.18 (t, *J* =

7.1Hz, 3H) ppm. ^{13}C NMR (100 MHz, CDCl) δ = 171.2, 133.2, 132.5, 126.3, 126.2, 120.3, 120.0, 118.91, 118.88, 114.9, 101.3, 60.5, 55.8, 48.0, 44.0, 42.1, 40.3, 39.9, 15.0, 13.2 ppm. LRMS (ES$^+$) *m/z* [M + H]$^+$ calcd for $C_{20}H_{26}N_3O^+$ 324.21; Found 324.29. IR (diamond, ATR) v 2972, 2869, 2798, 1636 cm^{-1}. Chiral Separation of the 2 enatiomers of JRT-E-074 were performed by SAI Life Sciences and Delix Therapeutics.

(+)-JRT-E-074 $[\alpha]_D^{20}$ +8.7 (c = 0.0011 in ethanol). (-)-JRT-E-074 $[\alpha]_D^{20}$ -9.9 (c = 0.0011 in ethanol).

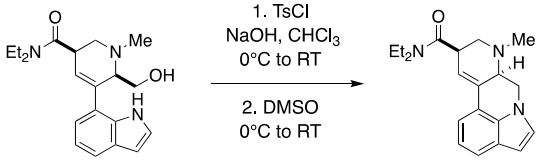

JRT-E-120. To a 0°C cooled solution of **16** (0.130 g, 0.381 mmol, 1.0 equiv) in $CHCl_3$ (3.8 mL) was added freshly crushed NaOH (0.122 g, 3.05 mmol, 8.0 equiv). A solution of TsCl (0.087 g, 0.46 mmol, 1.2 equiv) in $CHCl_3$ (0.76 mL) was added dropwise over 10 minutes. The mixture was warmed to ambient temperature and stirred for 1.5 h. The mixture was cooled to 0°C, and DMSO (1.9 mL) was added slowly before warming to ambient temperature and stirring for 3 h. The mixture was partitioned in H_2O (200 mL) and EtOAc (150 mL) and the layers were separated. The aqueous layer was further extracted with EtOAc (3 x 50 mL). The organic extracts were combined, washed with brine (100 mL), dried over Na_2SO_4, and concentrated under reduced pressure. The residue was purified by column chromatography on silica gel 8% MeOH in EtOAc to 12% MeOH in EtOAc) to afford 15 (0.044 g, 36%) as a brown semi-solid. ^{1}H NMR (400 MHz, $CDCl_3$) δ = 7.48 (d, *J* = 7.9 Hz, 1H), 7.22 (d, *J* = 7.2 Hz, 1H), 7.08 – 7.02 (m, 2H), 6.45 (d, *J* = 3.0 Hz, 1H), 6.37 (dd, *J* = 2.0, 3.6 Hz, 1H), 4.50 (dd, *J* = 5.5, 11.2 Hz, 1H), 4.02 (t, *J* = 11.2 Hz, 1H), 3.66 – 3.60 (m, 1H), 3.56 – 3.30 (m, 5H), 3.15 (dd, *J* = 5.7, 12.2 Hz, 1H), 2.83 (dd, *J* = 4.8, 12.2 Hz, 1H), 2.62 (s, 3H), 1.27 (t, *J* = 7.0 Hz, 3H), 1.13 (t, *J* = 7.0 Hz, 3H) ppm. ^{13}C NMR (100 MHz, CDCl) δ = 171.5, 133.4, 133.4, 126.5, 126.2, 120.4, 120.1, 119.9, 118.9, 114.2, 101.2, 58.6, 52.5, 47.9, 43.6, 42.0, 40.3, 37.4, 15.0, 13.2 ppm. LRMS (ES$^+$) *m/z* [M + H]$^+$ calcd for $C_{20}H_{26}N_3O^+$ 324.21; Found 324.29. IR (diamond, ATR) v 2969, 2932, 2871, 2791, 1634 cm^{-1}.

STATISTICAL ANALYSIS

Treatments were randomized, and the data were analyzed by experimenters blinded to the treatment conditions. Statistical analyses were performed using GraphPad Prism (version 8.1.2) unless noted otherwise. All comparisons were planned before performing each experiment. *Post-hoc* analyses were by Bonferroni corrected pairwise comparisons. A $p<0.05$ was considered significant. Data are represented as mean ± SEM, unless otherwise noted, with asterisks indicating *$p < 0.05$, **$p < 0.01$, ***$p < 0.001$, and ****$p < 0.0001$.